



National Library
of Canada

Acquisitions and
Bibliographic Services Branch

395 Wellington Street
Ottawa, Ontario
K1A 0N4

Bibliothèque nationale
du Canada

Direction des acquisitions et
des services bibliographiques

395, rue Wellington
Ottawa (Ontario)
K1A 0N4

Your file Votre référence

Our file Notre référence

NOTICE

The quality of this microform is heavily dependent upon the quality of the original thesis submitted for microfilming. Every effort has been made to ensure the highest quality of reproduction possible.

If pages are missing, contact the university which granted the degree.

Some pages may have indistinct print especially if the original pages were typed with a poor typewriter ribbon or if the university sent us an inferior photocopy.

Reproduction in full or in part of this microform is governed by the Canadian Copyright Act, R.S.C. 1970, c. C-30, and subsequent amendments.

AVIS

La qualité de cette microforme dépend grandement de la qualité de la thèse soumise au microfilmage. Nous avons tout fait pour assurer une qualité supérieure de reproduction.

S'il manque des pages, veuillez communiquer avec l'université qui a conféré le grade.

La qualité d'impression de certaines pages peut laisser à désirer, surtout si les pages originales ont été dactylographiées à l'aide d'un ruban usé ou si l'université nous a fait parvenir une photocopie de qualité inférieure.

La reproduction, même partielle, de cette microforme est soumise à la Loi canadienne sur le droit d'auteur, SRC 1970, c. C-30, et ses amendements subséquents.

Canada

UNIVERSITY OF ALBERTA

**A NOVEL BIOREACTOR
FOR CULTIVATION OF SHEAR-SENSITIVE CELLS**

by

GEORGE Z. LU



A thesis submitted to the Faculty of Graduate Studies and Research
in partial fulfillment of the requirements for the degree of

DOCTOR OF PHILOSOPHY

DEPARTMENT OF CHEMICAL ENGINEERING
EDMONTON, ALBERTA

FALL 1994



National Library
of Canada

Acquisitions and
Bibliographic Services Branch

395 Wellington Street
Ottawa, Ontario
K1A 0N4

Bibliothèque nationale
du Canada

Direction des acquisitions et
des services bibliographiques

395, rue Wellington
Ottawa (Ontario)
K1A 0N4

Your file - Votre référence

Our file - Notre référence

The author has granted an irrevocable non-exclusive licence allowing the National Library of Canada to reproduce, loan, distribute or sell copies of his/her thesis by any means and in any form or format, making this thesis available to interested persons.

L'auteur a accordé une licence irrévocable et non exclusive permettant à la Bibliothèque nationale du Canada de reproduire, prêter, distribuer ou vendre des copies de sa thèse de quelque manière et sous quelque forme que ce soit pour mettre des exemplaires de cette thèse à la disposition des personnes intéressées.

The author retains ownership of the copyright in his/her thesis. Neither the thesis nor substantial extracts from it may be printed or otherwise reproduced without his/her permission.

L'auteur conserve la propriété du droit d'auteur qui protège sa thèse. Ni la thèse ni des extraits substantiels de celle-ci ne doivent être imprimés ou autrement reproduits sans son autorisation.

ISBN 0-315-95220-2

Canada

UNIVERSITY OF ALBERTA
RELEASE FORM

NAME OF AUTHOR: **GEORGE Z. LU**

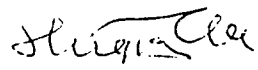
TITLE OF THESIS: **A NOVEL BIOREACTOR
FOR CULTIVATION OF
SHEAR-SENSITIVE CELLS**

DEGREE: **DOCTOR OF PHILOSOPHY**

YEAR THIS DEGREE GRANTED: **1994**

Permission is hereby granted to the **UNIVERSITY OF ALBERTA LIBRARY** to reproduce single copies of this thesis and to lend or sell such copies for private, scholarly, or scientific research purposes only.

The author reserves all other publication and other rights in association with the copyright in the thesis, and except as hereinbefore provided neither the thesis nor any substantial portion thereof may be printed or otherwise reproduced in any material form whatever without the author's prior written permission.

Signed: 

Permanent address:

Nearaway
750 Pears Road
R.R. 4, Victoria
BC V9B 5T8

DATE: April 29, 1994

UNIVERSITY OF ALBERTA

FACULTY OF GRADUATE STUDIES AND RESEARCH

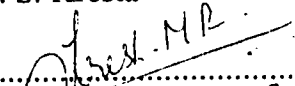
The undersigned certify that they have read, and recommend to the FACULTY OF GRADUATE STUDIES AND RESEARCH for acceptance, a thesis entitled A NOVEL BIOREACTOR FOR CULTIVATION OF SHEAR-SENSITIVE CELLS submitted by GEORGE Z. LU in partial fulfillment of the requirements for the degree of DOCTOR OF PHILOSOPHY.

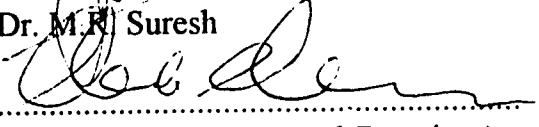

.....
Dr. M.R. Gray (Supervisor)


.....
Dr. B.G. Thompson (Co-Supervisor)


.....
Dr. J.H. Masliyah


.....
Dr. S. Kresta


.....
Dr. M.R. Suresh


.....
Dr. C. Chavarie (External Examiner)

Date:  April 28, 1994

TO

KIN

MURRAY

FLEMING AND AILEEN

MY PARENTS

ACKNOWLEDGMENT

I wish to express my sincere gratitude to Dr. Murray Gray and Dr. Brad Thompson for their enthusiastic supervision, constant help and encouragement during the course of my PhD program.

I would like to thank Dr. K. Nandakumar, Dr. J. Masliyah, and Dr. S. Kresta for many valuable discussions and suggestions pertinent to bioreactor hydrodynamics.

I would also like to thank Walter Boddez at the Instrument Shop for his help in setting up the experimental apparatus for flow visualization and mixing studies.

Thanks are due to the Biotechnology Department and Biotechnology Pilot Plant of Alberta Research Council (ARC), Biomira Inc. for use of their lab space and facilities. Technical assistance from Lez Witte at ARC, and Wilma Bowe at Biomira are specially acknowledged.

Thanks are also due to all faculty members and fellow graduate students in the Department of Chemical Engineering who have made my graduate study a most enjoyable experience.

Finally, I wish to acknowledge the financial support from the Natural Science and Engineering Research Council of Canada (NSERC), and from the Alberta Research Council.

ABSTRACT

Large-scale cultivation of animal cells is becoming very important as a wide range of products produced by or derived from animal cells near commercialization. These cells are vulnerable to hydrodynamic forces created by agitation and/or aeration which are frequently used to provide mixing and oxygen in bioreactors. In microcarrier culture for anchorage-dependent cells, forces generated by the interaction of microcarrier beads with each other and with small turbulent eddies cause cell damage. In suspension culture, however, cell damage is due to bubble bursting and liquid film draining on the gas-liquid interface.

Air sparging represents a simple and inexpensive way of supplying oxygen, but a critical question to be addressed in reactor design is how to provide sufficient mixing and oxygen, and at the same time cause minimal cell damage due to bursting bubbles and foam at the liquid surface. We have developed a unique bioreactor concept, i.e., use inclined plates to control the contact between cells and bubbles. This design minimizes collection of cells by rising bubbles, contact between cells and bursting bubbles at the gas-liquid interface, and therefore cell entrainment into a foam layer. The Inclined-plate Bioreactor has simple hydrodynamics which can be easily characterized by bubble rising, liquid and cell circulation patterns. Scale-up of this reactor design is, therefore, straightforward compared to conventional stirred tank, bubble column, and airlift bioreactors.

A prototype was built and used to grow a murine hybridoma cell line. Maximum viable cell count and exponential growth of the cells were not affected by inclination, but an inclination of 30° gave an antibody titer of 42 mg/L which more than doubled the yield of 17 mg/L in the vertical position. By comparison, the culture gave yields of 30 mg/L when grown in spinner flasks. The enhanced antibody production in the inclined bioreactor corresponded to a prolonged stationary phase.

As part of the design and scale-up, a rectangular bubble column was used for hydrodynamic and mixing studies. The hydrogen bubble technique and tracer injection were the respective methods used to experimentally determine the liquid

circulation velocity and mixing time for sparging rates of 0.001 to 0.06 vvm, and for inclination angles of 0 to 45°. Simulation of liquid circulation in the inclined bubble column was carried out using the FLOW3D package. A mixing model with one adjustable parameter was presented as a potential means for interpreting the experimental mixing data.

Table of Contents

Abstract	
Table of Contents	
List of Figures	
List of Tables	
Nomenclature	
Symbols	
1 Introduction	1
References	2
2 Background Literature	4
2.1 Cell damage in suspension culture	4
2.2 Cell damage in microcarrier culture	6
2.3 Considerations for bioreactor design	12
2.3.1 Oxygenation of animal cell culture	12
2.3.2 Bubble-free oxygenation	12
References	13
3 Physical Modeling of Animal Cell Damage by Hydrodynamic Forces in Suspension Cultures	17
3.1 Introduction	17
3.2 Materials and methods	19
3.2.1 Preparation of microcapsules	19
3.2.2 Dextran assay	21
3.2.3 Microcapsule breakage experiments	21
3.3 Results and discussion	23

3.3.1	Microcapsule breakage by stirring	23
3.3.2	Microcapsule breakage by sparging	27
3.4	Conclusions	33
	References	33
4	Cultivation of Hybridoma Cells in an Inclined Bioreactor	35
4.1	Introduction	35
4.2	Materials and methods	38
4.2.1	Cell line and culture medium	38
4.2.2	Inoculum preparation	38
4.2.3	Bioreactor cultures	39
4.2.4	Analytical methods	41
4.2.5	Flotation experiments	42
4.3	Results and discussion	43
4.3.1	Typical bioreactor culture and control experiments	44
4.3.2	Cell growth and antibody production as a function of inclination	50
4.3.3	LDH as an indicator of cell damage	53
4.3.4	Cell sedimentation	54
4.3.5	Reasons for increased antibody production in the inclined bioreactor	55
4.4	Conclusions	58
	References	58
5	Loss of Shear Sensitivity in Hybridoma Cells	61
5.1	Introduction	61
5.2	Materials and methods	62
5.3	Results and discussion	63
5.3.1	Cell line acclimatization in control experiments	63

5.3.2	Cell line acclimatization in bioreactor experiments	67
5.3.3	Effect of cell line acclimatization on bioreactor performance	69
5.3.4	LDH release	71
5.3.5	Glucose consumption	74
5.4	Conclusions	76
	References	76
6	Hydrodynamics and Mixing in an Inclined Bubble Column	78
6.1	Introduction	78
6.2	Materials and methods	80
6.2.1	Inclined bubble column	80
6.2.2	Flow visualization	81
6.2.3	Bubble size and rise velocity	83
6.2.4	Computational fluid dynamics (CFD) simulation	83
6.2.5	Mixing study	84
6.3	Results and discussion	86
6.3.1	Qualitative observations	86
6.3.2	Bubble size and rise velocity	87
6.3.3	Liquid velocity profile	91
6.3.4	CFD simulation	98
6.3.5	Mixing time	101
6.3.6	Mixing model	104
6.4	Conclusions	108
	References	109
7	Hydrodynamic Behavior of Microcarriers in an Inclined Bubble Column	111
7.1	Introduction	111
7.2	Materials and methods	112

7.2.1	Microcarriers and medium	112
7.2.2	Preparation of microcarrier suspension	112
7.2.3	Inclined bubble column	113
7.2.4	Sampling	114
7.3	Results and discussion	114
7.3.1	Sparging without antifoam	114
7.3.2	Sparging with antifoam	114
7.4	Conclusions	116
	References	117
8	Conclusions and Recommendations	118
A	ELISA Procedure for Determination of IgG Antibody	120
B	Command File Used for FLOW3D Simulation	124
C	Raw Data for Chapter 4	128
D	Raw Data for Chapter 5	144

List of Figures

3-1	A scanned image of the microcapsules prepared by the emulsion technique.	20
3-2	Cumulative volumetric distribution of the initial microcapsules.	21
3-3	Surface tension measured for a series of standard Tween solution.	22
3-4	Volumetric breakage of microcapsules at 500 rpm in 2L fermenter. Symbols show replicate experiments at high and medium Tween-20 concentrations. Curves are least-squares fits to Equation (2).	24
3-5	Cumulative number distribution of the microcapsules surviving 500 rpm stirring for 90 min in the 2-L fermenter. The 1-L microcapsule suspension used for the breakage study had a Tween concentration of 1000 ppm.	26
3-6	Volumetric breakage of microcapsules at $1 \text{ L}\cdot\text{min}^{-1}$ sparging in the bubble column. Symbols show replicate experiments, or otherwise noted on the plots. Curves are least-squares fits to Equation (2).	28
3-7	Cumulative number distribution of microcapsules surviving $1 \text{ L}\cdot\text{min}^{-1}$ sparging for 90 min in the bubble column. The 1-L microcapsule suspension used for the breakage study had a Tween concentration of 10 ppm.	29
4-1	Schematic diagram of inclined-plate bioreactor showing liquid circulation.	37
4-2	Schematic diagram of the experimental inclined-tube bioreactor.	40

4-3	Cell counts and antibody titer versus time for control culture grown in Petrie dishes from the same inoculum as bioreactor experiment #1 (vertical).	44
4-4	Cell counts and antibody titer versus time for control culture grown in spinner flasks from the same inoculum as bioreactor experiment #1 (vertical).	45
4-5	Cell growth and antibody formation as a function of time for bioreactor experiment #1 (vertical).	46
4-6	Foaming in bioreactor experiment #1 (vertical).	47
4-7	LDH release in bioreactor experiment #1 (vertical), compared with data from dish and spinner controls.	48
4-8	LDH release is linearly correlated with viability when cells enter the stationary phase.	49
4-9	Growth and antibody production in bioreactor experiment #4 with 30° inclination.	50
4-10	Comparison of growth and antibody production with time in the bioreactor at different angles of inclination.	52
4-11	Comparison the time course of LDH release in the bioreactor between experiment #1 (vertical) and experiment #4 with 30° inclination.	54
4-12	Growth and antibody production for bioreactor experiment #6 with 45° inclination and 0.18 to 0.24 vvm aeration rate.	56
4-13	Viable and dead cell concentrations in the bubble column during a batch flotation experiment. Sample 1 was taken from mid-exponential growth phase at 35 h, sample 2 from stationary phase at 50 h, and sample 3 from death phase at 75 h.	57

5-1	Viable cell count and antibody formation as a function of time in tissue culture dishes. Different symbols indicate that cells had been subcultured for different periods of time in tissue culture dishes prior to inoculating the dishes as control experiments for their respective bioreactor culture.	64
5-2	Viable cell count and antibody formation as a function of time in spinner flasks. Different symbols indicate that cells had been subcultured for different periods of time in tissue culture dishes prior to inoculating the spinners as control experiments for their respective bioreactor culture.	66
5-3	Effect of passage number of subculture on the final antibody titer in tissue culture dishes and in spinner flasks as control experiments for bioreactor cultures.	67
5-4	Viable cell count and antibody formation as a function of time from the vertical bioreactor. Different symbols show that cells had been subcultured in dishes for different periods of time prior to inoculum preparation for bioreactor cultures.	68
5-5	Viable cell count and antibody formation as a function of time from the bioreactor inclined at 45° from vertical. Different symbols show that cells had been subcultured in dishes for different periods of time prior to inoculum preparation for bioreactor cultures.	70
5-6	Plot of LDH vs. $\int X \cdot dt$ yields two distinct straight lines, slopes of which give the specific LDH release rates.	72
5-7	Time course of glucose consumption for two vertical bioreactor experiments, comparing the unacclimatized	

cells with the acclimatized cells.	75
6-1 Experimental set-up of the inclined bubble column.	82
6-2 Conductivity response curve recorded by the chart recorder for the experiment with superficial gas velocity of 0.02 cm/s and inclination angle of 30°.	85
6-3 Liquid circulation patterns in vertical and inclined bubble column.	86
6-4 Bubble size as a function of inclination angle for four different superficial gas velocities. Error bars represent 95% confidence interval.	88
6-5 Bubble rise velocity as a function of inclination angle for five different superficial gas velocities.	89
6-6 Air bubbles in this study were larger than those used by Masliyah et al. (1993), and Re was greater than 130 which was the upper limit for equation (1). Symbols represent the experimental data obtained from the inclined bubble column for a superficial gas velocity of 0.002 cm/s.	90
6-7 Velocity profiles were determined from the hydrogen bubble pictures from the experiment with a superficial gas velocity of 0.02 cm/s and an inclination angle of 30°. Different symbols represent profiles obtained from different pictures.	93
6-8 Average downward liquid velocity as a function of inclination angle for three different superficial gas velocities.	95
6-9 Downward liquid velocity estimated from the conductivity response curve.	96
6-10 Downward liquid velocity as a function of aspect ratio.	97
6-11 A comparison of the liquid velocity profiles between the	

simulation results and experimental data. The upward liquid velocity in the vicinity of rising bubbles were not available from the hydrogen bubble method.	100
6-12 Mixing time as a function of inclination angle for different superficial gas velocities.	102
6-13 Mixing time as a function of aspect ratio.	103
6-14 Recycle-cross-flow model.	104
7-1 Schematic diagram of the experimental bubble column.	113
7-2 Microcarrier concentration near the liquid surface as a function of the inclination angle for a constant sparging rate of 0.05 vvm. The straight line is from a linear regression of the data from 10° to 40° inclinations. Error bars represent 95% confidence interval.	116
A-1 A standard curve for ELISA assay from experiment #4.	121
A-2 Cell growth and antibody production for the repeated vertical experiment.	122
B-1 Bubble size as a function of the aspect ratio for a sparging rate of 33.7 mL/min and 30° inclination.	126
B-2 Bubble rise velocity as a function of the aspect ratio for a sparging rate of 33.7 mL/min and 30° inclination.	127
C-1 Ammonia formation in bioreactor experiment #1.	129
C-2 Lactate formation in bioreactor experiment #1.	130
C-3 Glucose consumption in bioreactor experiment #1.	131
C-4 Glucose consumption in bioreactor experiment #2.	132

C-5 Cell growth and antibody production for bioreactor experiment #3.	133
C-6 Glucose consumption in bioreactor experiment #3.	134
C-7 LDH release in bioreactor experiment #4.	135
C-8 Dish control for bioreactor experiment #5.	136
C-9 Spinner control for bioreactor experiment #5.	137
C-10 Cell growth and antibody production for bioreactor experiment #5.	138
C-11 Glucose consumption in bioreactor experiment #5.	139
C-12 LDH release in bioreactor experiment #5.	140
C-13 Glucose consumption in bioreactor experiment #6.	141
C-14 Cell growth and antibody production for bioreactor experiment #7.	142
C-15 Glucose consumption in bioreactor experiment #7.	143
D-1 Cell growth and antibody production in bioreactor experiment #1.	145
D-2 LDH release in bioreactor experiment #1.	146
D-3 Glucose consumption in bioreactor experiment #1.	147
D-4 Controls for bioreactor experiment #2.	148
D-5 Cell growth and antibody production in bioreactor experiment #2.	149
D-6 Glucose consumption in bioreactor experiment #2.	150
D-7 LDH release in bioreactor experiment #2.	151
D-8 Flotation study #2 used cells from the bioreactor culture (experiment #2). Sample 1 was taken at 50 hr, and sample 2 at 86.5 hr. The flotation study was discussed in Chapter 4.	152
D-9 Controls for bioreactor experiment #3.	153
D-10 Cell growth and antibody production in bioreactor experiment #3.	154
D-11 Glucose consumption in bioreactor experiment #3.	155
D-12 LDH release in bioreactor experiment #3.	156
D-13 Dish control for bioreactor experiment #4.	157

D-14Spinner control for bioreactor experiment #4.	158
D-15Cell growth and antibody production in bioreactor experiment #4.	159
D-16Glucose consumption in bioreactor experiment #4.	160
D-17LDH release in bioreactor experiment #4.	161

List of Tables

3-1	Kinetic constants for breakage of microcapsules in an agitated fermenter. 1 L of microcapsule suspension containing different Tween concentrations were stirred at 500 rpm in the 2-L New Brunswick fermenter.	25
3-2	Foam characteristics and kinetics of microcapsule breakage in a bubble column. 1 L of microcapsule suspension containing different Tween concentrations was sparged at $1 \text{ L} \cdot \text{min}^{-1}$ with air.	30
4-1	A comparison of the free gas-liquid interfacial area in different bioreactor types having the same working volume.	37
4-2	Organization of bioreactor experiments.	43
4-3	Duration of stationary phase and amount of antibody produced in bioreactor experiments.	53
5-1	Organization of bioreactor experiments.	63
5-2	Maximal viable cell count and antibody titer achieved for different inclination angles of the bioreactor: a comparison between unacclimatized and acclimatized cells.	71
5-3	LDH release in control experiments.	73
5-4	Specific LDH release rates for bioreactor experiments.	74
5-5	Specific glucose consumption rates for bioreactor experiments.	76
6-1	Maximum downward liquid velocity and the distance	

of the zero-velocity cross point from the lower wall of
the inclined bubble column.

94

A-1 Amino acid concentrations (μM) in the fresh medium
and in the spent medium at the end of experiment #1.

123

Nomenclature

A	area (m^2)
C	tracer concentration (M)
C_{Db}	drag coefficient for air bubbles
C_{LDH}	LDH concentration (IU/L)
c	viable cell concentration (cells/mL)
c_i	inert bead concentration (beads/mL)
c_m	microcarrier concentration (beads/mL)
D	vessel diameter (m)
D_i	impeller diameter (m)
d_c	survival microcapsule diameter (μm)
Eo_m	modified bubble Eotvos number
G	aeration rate (vvm)
H	liquid height (cm)
ISF	integrated shear factor
K	cross-flow coefficient
K_e	a constant depending on the cell and microcarrier properties
k_{LDH}	specific LDH release rate (hr^{-1})
k_d	cell death rate (hr^{-1})
L	microcarrier size (μm)
L_c	critical length for cell death (μm)
LDH	lactate dehydrogenase
N	impeller rotation speed (rpm)
OUR	oxygen uptake rate (mols/s/cell)
P	internal pressure (N/m^2)

q_1	specific death rate (hr^{-1})
q_2	specific death rate (hr^{-1})
Re_b	bubble Reynolds number
S	conductivity (μS)
T	tensile strength of microcapsule membrane (N/m)
t	time (hr)
$t_{5\%}$	time to reach 5% change on the conductivity response curve (min)
$t_{95\%}$	time to reach 95% change on the conductivity response curve (min)
t_m	mixing time (min)
U	velocity (m/s)
u_g	superficial gas velocity (cm/s)
V	total liquid volume (m^3)
$V_{b,t}$	volumetric breakage at time t (%)
$V_{b,\infty}$	maximum breakage when $t \rightarrow \infty$ (%)
vvm	volume of air per volume of liquid per min
X	viable cell concentration (cells/mL)
Y	extent of mixing (%)

Symbols

ν	kinematic viscosity (m^2/s)
ε	energy dissipation per unit mass (w/kg)
$\bar{\varepsilon}$	average power input per unit mass (w/kg)
μ	viscosity ($\text{Pa}\cdot\text{s}$)
μ_1	cell growth rate (hr^{-1})
μ_{obs}	observed growth rate (hr^{-1})
k	breakage rate constant (min^{-1})
α	inclination angle ($^\circ$)
α_{LDH}	LDH release per cell (IU/cell)
τ	residence time (s)
λ_K	Kolmogorov length scale (m)

Chapter 1

Introduction

Cell cultivation technology has been growing rapidly since the first virus vaccine was produced by animal tissue culture. A large number of valuable compounds of medical, pharmaceutical, and veterinary importance can be obtained from animal cell culture. The production of monoclonal antibodies by means of hybridoma cell culture and the production of insect-pathogenic baculoviruses by insect cell culture are probably the most important examples. With the advent of recombinant DNA technology, bacterial cells, due to their fast growth and inexpensive medium requirement, were pursued for producing products which had been previously derived from animal cells. However, it was soon found that bacteria lack the capability of the post-translational modifications which are necessary to obtain proper biological activity of the product. Interest in animal cell cultures was, therefore, renewed.

As compared to bacteria, animal cells have a slower growth rate, and more complex nutrient requirements. In addition, animal cells are much larger in size (approximately one order of magnitude larger than bacterial cells), and do not have a strong cell wall to protect them from any adverse environmental stimuli. As a result, when they are cultivated in bioreactors, these cells are exposed to and injured by hydrodynamic forces which are created by agitation and/or aeration. Bioreactor operation and scale-up require understanding of the mechanisms of cell damage.

In sparged bioreactors, animal cell damage was found to be associated with the free gas-liquid interface (Handa-Corrigan et al., 1987, 1989). Bubble bursting at the liquid surface and film drainage in the foam layer were mainly responsible for elevated cell death rates. For agitated bioreactors with surface aeration, gas bubbles were entrained into the bulk liquid through the instable vortex around the impeller shaft; these entrained bubbles were found to cause cell death in the agitated bioreactors (Kunas and Papoutsakis, 1990). When the head-space was eliminated in the bioreactors, hybridoma cells were not affected by stirring at 700

rpm with a Rushton turbine. Mechanisms of cell damage in bioreactors have recently been reviewed by Papoutsakis (1991) and Cherry (1993).

In bioreactor design and operation, cells must be prevented from contacting damaging bubbles. Strategies have included the use of mechanical separation by containing the gas bubbles in a wire cage (Brennan, 1987), and the use of silicone tubing within an agitated bioreactor (Su et al., 1992). These designs, however, have complex internals, and are difficult to scale up.

The overall objectives of this thesis were to first examine the mechanisms of cell damage in a stirred-tank bioreactor and in a bubble column bioreactor (Chapter 3). Nylon microcapsules were used as a physical model to mimic cell damage in suspension cultures. The investigation of physical damage of cells was completely uncoupled from any biological effects such as shift in metabolisms when using biological cells. Based on this investigation, a novel bioreactor concept, i.e. Inclined-plate Bioreactor, was proposed. A hybridoma cell line was grown in a prototype bioreactor to test the design (Chapter 4). The implications of cell line acclimatization on bioreactor performance are presented in Chapter 5. To gain some insight into design and scale-up of this novel bioreactor, hydrodynamics and mixing were characterized using an inclined rectangular bubble column (Chapter 6). As this bioreactor concept may find potential application for microcarrier systems, the hydrodynamic behavior of microcarriers was also studied (Chapter 7).

REFERENCES

- Brennan, A. 1987. A suspension culture perfusion system for production of monoclonal antibodies. *ProBioTech (Suppl. Process Biochem.)* **22**: 7-8.
- Cherry, R.S. 1993. Animal cells in turbulent fluids: details of the physical stimulus and the biological response. *Biotechnol. Adv.* **11**: 279-299.
- Handa-Corrigan, A., Emery, A.N., and Spier, R.E. 1989. Effect of gas-liquid interfaces on the growth of suspended mammalian cells: Mechanisms of cell damage by bubbles. *Enzyme Microb. Technol.* **11**: 230-235.

- Handa-Corrigan, A., Emery, A.N., and Spier, R.E. 1987. On the evaluation of gas-liquid interfacial effects on hybridoma viability in bubble column bioreactors. *Develop. Biol. Stand.* **6**: 241-253.
- Kunas, K.T. and Papoutsakis, E.T. 1990. Damage mechanisms of suspended animal cells in agitated bioreactors with and without bubble entrainment. *Biotechnol. Bioeng.* **36**: 476-483.
- Papoutsakis, E.T., 1991. Fluid-mechanical damage of animal cells in bioreactors. *Trends Biotechnol.* **9**: 427-437.
- Su, W.W., Caram, H.S., Humphrey, A.E. 1992. Optimal design of the tubular microporous membrane aerator for shear-sensitive cultures. *Biotechnol. Prog.* **8**: 19-24.

Chapter 2

Background Literature

2.1 CELL DAMAGE IN SUSPENSION CULTURE

Cell suspension culture has received increased attention due to its numerous advantages over other culture techniques (Leist et al., 1990). One major concern in scale-up, however, is the oxygen supply. Agitation and aeration provide mixing and oxygen, but can cause damage to animal cells which are vulnerable to hydrodynamic forces due to their relatively large size and lack of a protective cell wall.

Studies in viscometers (Abu-Reesh and Kargi, 1989; Smith et al., 1987; Tramper et al., 1986) and shear devices of the capillary-tube type (Augenstein et al., 1971) exposed cells to well-defined shear fields. Smith et al. (1987) showed that a murine hybridoma grew exponentially for 15 hours within a Couette viscometer at a constant shear rate of 420 s^{-1} . At a shear rate of 870 s^{-1} , however, cell damage occurred as evidenced by a reduction in live cell count and an increase in the intracellular lactate dehydrogenase (LDH) leakage to the culture medium. The corresponding damaging shear stress was $0.67 \text{ N}\cdot\text{m}^{-2}$. Tramper et al. (1986) reported a critical shear stress of $1 - 4 \text{ N}\cdot\text{m}^{-2}$ at which cell viability started to decrease progressively for insect cell lines tested in a Haake rotaviscometer. In other cell damage studies, suspensions of two strains of mammalian tissue cells, human HeLa S3 and mouse L929, were pumped through capillary tubes of various lengths and diameters (Augenstein et al., 1971). L929 cells were found to be more sensitive to shear forces; cell death began at a shear stress of $150 \text{ N}\cdot\text{m}^{-2}$.

Animal cells in bioreactor cultures, however, are seldom exposed to well-defined, constant levels of laminar shear stress. Rather, they experience long-term, transient shear forces from liquid turbulence (Cherry and Kwon, 1990), which results from the agitation and aeration required for mixing and oxygen supply. Turbulent shear caused a higher degree of damage than laminar shear at the same shear level and exposure time in a viscometer tested in both laminar and turbulent

flow regimes (Abu-Reesh and Kargi, 1989). Small scale bioreactors with turbulent mixing have been frequently used in cell damage studies (Dodge and Hu, 1986; Gardner et al., 1989; Lee et al., 1988; Passini and Goochee, 1989).

In agitated bioreactors, agitation rates around 200 rpm were found to be detrimental to hybridoma cells (Dodge and Hu, 1986; Lee et al., 1988). In microcarrier cell cultures, Kolmogorov's theory of isotropic turbulence was successfully applied to conclude that cell damage occurred when the smallest eddy size was comparable with the microcarrier bead size (Cherry and Papoutsakis, 1988; Croughan and Wang, 1989). For cells grown in free suspensions, however, the same damage mechanism could not apply because the cells are much smaller than microcarriers (Cherry and Kwon, 1990). Other reports showed that a high intensity of stirring did not seem to cause cell damage (Backer et al., 1987; Oh et al., 1989). Backer et al. (1987) used a 150-L tank stirred by a marine impeller at 520 rpm to study the shear effects on murine hybridoma growth, and observed no significant declines in cell viability and oxygen uptake. Oh et al. (1989) showed that agitation (450 rpm, Rushton turbine) alone was not harmful to the three murine hybridomas studied. Only when sparging of air was combined with stirring did the net cell growth rate and the maximum cell number fall markedly.

Kunas and Papoutsakis (1990a) then further investigated the cell damage mechanisms in surface-aerated stirred bioreactors. When the reactor was operated without a head space, therefore without vortex formation and bubble entrainment, cells could be damaged by shear forces in the turbulent bulk liquid only at agitation rates as high as 700 rpm. However, when air bubbles were entrained into the liquid through the unstable gas-liquid interface, low agitation rates such as 220 rpm gave a dramatic reduction in apparent growth rates. They concluded that cell damage was due to vortex formation at the free surface accompanied by bubble entrainment and breakup in the surface-aerated bioreactor. Smith et al. (1989) also claimed that increased cell damage was related to gas-liquid interaction associated with the vortex rather than the energy dissipation in the liquid.

Sparging provides an effective strategy to meet oxygen requirements and to keep cells in homogeneous suspension, but recent studies have shown that contacting bubbles with cell suspensions is detrimental to mammalian cells (Handa-Corrigan et al., 1989, 1987; Jobses et al. 1991) and insect cells (Tramper

et al., 1986). For example, the death rate of insect cells was found to be proportional to the air flow rate when a bubble column filled with a suspension of 10^6 cells·mL⁻¹ was sparged at different air flow rates (Tramper et al., 1986).

Recent work indicates that cell-bubble interactions most likely cause cell damage (Handa-Corrigan et al, 1989, 1987; Tramper and Vlak, 1988; Tramper et al., 1987). There are three zones in a bubble column where this interaction may occur; the sparger zone where bubbles are first formed, the bubble-rising zone where bubbles travel through the bulk liquid, and the gas-liquid interface zone where bubbles disengage from the medium. Tramper et al. (1987) estimated shear stresses experienced by the cells in the three different zones and concluded that the air injection zone was most likely the region for cell damage. These estimates were corrected in a later article by the same authors to show that the free surface zone may be as important as the air injection zone (Tramper and Vlak, 1988).

Handa-Corrigan et al. (1989, 1987) found that cell damage was due to bubble disengagement at the gas-liquid interface and identified three distinct mechanisms for cell damage; oscillatory disturbances caused by rapidly bursting bubbles in culture medium with antifoam, physical shearing in the draining liquid films (lamellae) around the bubble, and the actual loss of cells in the foam layer in the medium without antifoam. They also claimed that Pluronic F-68 formed a stable foam layer which the cells did not penetrate, and therefore protected cells from physical damage. Jobses et al. (1991) and Murhammer and Goochee (1990a), however, proposed that pluronic and other block copolymers protect cells from damage due to their direct interaction with cell membranes. A stable foam layer was neither necessary (Murhammer and Goochee, 1988) nor sufficient to protect cells (Murhammer and Goochee, 1990b). Another component frequently used in animal cell culture is serum, which can affect the growth kinetics of hybridoma cells (Low and Harbour, 1985) and protect them from shear damage (Kunas and Papoutsakis, 1990b; Ozturk and Palsson, 1991).

2.2 CELL DAMAGE IN MICROCARRIER CULTURE

Some cell types have to attach to a surface for growth. This anchorage dependent

characteristic of many animal cell lines led to a multitude of designs for cell propagators which include petrie-dishes, T-flasks, and roller bottles. The disadvantage in scaling-up these systems from laboratory to industrial capacity is that it involves the multiplication of the number of independent reactors. This is highly labor intensive and increases the problem of sterile control. A major innovation came in 1967 when van Wezel suggested the use of suspended microcarriers for mass cell culture (van Wezel, 1967). Cells are attached to and therefore grown on the microcarrier surface. Advantages in using microcarrier culture are:

- a. increase in available specific surface area for growth;
- b. easy suspension in media for a homogeneous environment which can be readily scaled up, controlled and monitored for reliable and reproducible operations;
- c. simplified cell/medium separation.

Animal cells on microcarriers, however, are especially susceptible to fluid-mechanical damage. In addition to the fragile nature of animal cells, this susceptibility is due to the lack of individual cell mobility, i.e. cell rotation and translation. One major hydrodynamic effect is the removal of cells from the microcarrier, which may be lethal to some cell lines such as diploid FS-4 cells (Croughan and Wang, 1989). For FS-4 cells grown on Cytodex microcarriers in 125 mL spinners, the removal of whole cells from the microcarriers increased with stirring speed (Croughan and Wang, 1989). With other cell lines, such as CHO cells, removal is reversible. Cells were able to reattach to the microcarriers after removal and secondary growth was possible. This phenomenon explained the resistance of CHO cells to agitation (Croughan and Wang, 1990).

A well-defined shear field has been used to quantify effects of shear on anchorage-dependent cells (Kretzmer and Schugerl, 1991; Stathopoulos and Hellums, 1985). Stathopoulos and Hellums (1985) used a flow chamber to study the effect of shear on human embryonic kidney cells grown as an attached, confluent monolayer on a microscope slide. Shear stress levels of $0.65 \text{ dyne}\cdot\text{cm}^{-2}$ or greater caused cell removal. Higher shear stress levels (greater than $2.6 \text{ dyne}\cdot\text{cm}^{-2}$) applied for 24 hr resulted in detachment of 75 - 85% of the cells and marked cell disruption. Other cell lines such as BHK cells were found to be more

resistant to shear created in a very similar piece of shear device (Kretzmer and Schugerl, 1991). Cells were able to withstand high shear stress levels (about 500 dyne·cm⁻²) at an exposure time of 1 hour. No significant cell morphology change was observed up to 200 dyne·cm⁻². Therefore, different cell lines can react to shear differently.

Microcarrier culture in agitated vessels, however, frequently experience a turbulent environment rather than a well-defined flow field. Besides shear stress, normal forces from pressure and velocity fluctuations can play an important role in cell damage (Croughan and Wang, 1991). Therefore, small-scale bioreactors have been extensively used to study the mechanisms of fluid-mechanical damage of microcarrier culture.

Croughan and Wang (1989) measured DNA release into the culture fluid to monitor the cell lysis and removal from the microcarrier. They proposed that a reduction in net cell growth could be due to growth inhibition, cell death, or a combination of both. Experimental data therein obtained were found to fit the model of growth and death without growth inhibition or growth stimulation.

Both Hu (1983) and Sinsky et al. (1981) found that cell growth did not correlate with the impeller tip speed. These authors proposed the concept of integrated shear factor (ISF) as given by

$$\text{ISF} = \frac{2\pi N D_i}{D - D_i} \quad (1)$$

where N is the impeller rotation speed, D_i the impeller diameter, and D the vessel diameter. It was then found that growth of FS-4 cells on microcarriers was well correlated with the integrated shear factor. Although this type of correlation may be potentially useful with respect to scale-up, it does not provide much insight into the fundamental fluid-mechanical mechanisms of cell damage in microcarrier cultures.

Extensive experimental studies combined with theoretical analysis have

shown that the primary mechanisms of cell damage in agitated reactors are (a) direct interaction between microcarriers and turbulent eddies, and (b) collisions between microcarriers in turbulent flow (Cherry and Papoutsakis, 1986; Croughan and Wang, 1991).

In turbulent flow fields, short term hydrodynamic forces arise through the motion of turbulent eddies. In conjunction with the cascade in energy transfer from large to small eddies, there exists a spectrum of eddy sizes down to the viscous dissipation regime. The large primary eddies have large velocity fluctuations of low frequency and are of a size comparable to the physical dimension of the system, for example, the impeller diameter. These eddies are anisotropic and contain the bulk of the kinetic energy. Interaction of the large eddies with slow-moving streams produces smaller eddies of high frequency which further disintegrate until finally they are dissipated into heat by viscous forces. Kolmogorov argued that, for large Reynolds numbers, e.g., the impeller Reynolds number, ND^2/μ , the smaller eddies are independent of the bulk motion and are isotropic. The properties of these eddies are firstly a function of the local energy dissipation rate per unit mass, ϵ . Below the eddy size, λ_K , at which viscous dissipation occurs, their properties also depend on viscosity. There is, therefore, an equilibrium established which contains a wide range of eddy sizes, the universal equilibrium range. An eddy Reynolds number, Re_K , defined as $Re_K = \lambda_K V_K / \nu$, conceptually represents the balance of inertial to viscous forces, and within the spectrum of sizes the Kolmogorov scale λ_K is the size where these two forces are in balance, or $Re_K = 1$. From dimensional analysis, the Kolmogorov length scale is defined as

$$\lambda_K = (\nu^3 / \epsilon)^{1/4} \quad (2)$$

Under conditions of isotropic equilibrium in the viscous dissipation regime, the size of the smallest eddies is roughly given as the Kolmogorov length scale, λ_K , for the eddies in the viscous dissipation regime.

Dilute microcarrier cultures of FS-4 cells in spinner vessels were carried out by Croughan et al. (1989). The power input per unit mass and medium viscosity were both varied to determine if hydrodynamic death correlates with the

Kolmogorov length scale for the smallest eddies. Cell death became apparent when the average Kolmogorov length scale fell below about 130 μm , or about two-thirds of the microcarrier diameter of 185 μm . Based on this correlation, an "eddy-length" model was developed to describe the kinetics of hydrodynamic damage in dilute microcarrier cultures (Croughan et al., 1989).

$$\frac{dc}{dt} = \mu_1 \cdot c \quad L > L_c \quad (3)$$

$$\frac{dc}{dt} = \mu_1 \cdot c - q_1 \cdot c \quad L \leq L_c \quad (4)$$

$$q_1 = K_e (\bar{\epsilon} / \nu^3)^{3/4} \quad (5)$$

where μ_1 is the intrinsic specific growth rate, q_1 is the specific death rate due to microcarrier-eddy interactions, $\bar{\epsilon}$ is the average power input per unit mass, ν is the kinematic fluid viscosity, K_e is a function of the cell and microcarrier properties, L is the microcarrier size, and L_c is the critical length of approximately 130 μm for cell death.

Besides damage due to microcarrier-eddy interactions, cell death could arise from microcarrier collision when microcarrier concentration is high (Croughan and Wang, 1991; Cherry and Papoutsakis, 1986). Inert microcarriers Sephadex G-50 beads were used to manipulate the microcarrier concentration in FS-4 culture on Cytodex 1. At a low agitation rate such as 35 rpm, there was no effect on growth from increasing the bead concentration; but at 150 rpm, detrimental effect was apparent when the inert bead concentration was increased from 0 to 10, 20, and 30 $\text{g} \cdot \text{L}^{-1}$ (Croughan et al., 1988). Their "eddy-length" model was then extended to include cell death from microcarrier collisions and the following kinetic model was proposed for cell growth:

$$\frac{dc}{dt} = \mu_1 c - q_1 c - q_2 c_m c - (q_2 / 2) c_i c \quad (6)$$

where c is the viable cell concentration, c_m is the microcarrier concentration, c_i is the inert bead concentration, q_1 and q_2 are the specific death rates. Equation (6)

was then rearranged as

$$\frac{dc}{dt} = b \cdot c - (q_2 / 2) c_i \cdot c \quad (7)$$

and therefore

$$\mu_{obs} = b - (q_2 / 2) c_i = \left(\frac{1}{c} \cdot \frac{dc}{dt} \right)_{avg} \quad (8)$$

where

$$b = \mu_1 - q_1 - q_2 c_m = \text{constant.}$$

μ_{obs} was plotted against c_i and a straight line was the verification of their proposed model (Croughan et al., 1988).

Cherry and Papoutsakis (1988) proposed that microcarrier collision with parts of the reactor was a major damage mechanism besides those of bead-eddy and bead-bead interactions. Microcarriers, however, are small and nearly neutrally buoyant. They probably do not rapidly penetrate the boundary layers surrounding the solid vessel parts (Croughan and Wang, 1991).

Direct sparging, as a simple and inexpensive method of supplying oxygen and mixing, has been routinely used in production of monoclonal antibodies. In contrast, all microcarrier cultures have been conducted in stirred-tank bioreactors. There is only one published study of microcarrier culture by sparging (Aunins et al., 1986). Without antifoam, microcarriers were rapidly collected into the foam layer through flotation. Many microcarriers were spattered through bubble bursts into distant regions of the vessel (Aunins et al., 1986). When antifoam was used to depress the foam formation, very mild sparging produced a detrimental effect on cell growth. Bliem et al. (1991) recognized the potential problem of cell damage by direct sparging microcarrier cultures in airlift bioreactors. Handa-Corrigan (1990) also suggested that studies of solid-liquid-gas interfaces would be necessary to understand foam flotation of animal cells cultivated on microcarriers. The difficulties in using direct sparging for microcarrier cultures seem to have been commonly known; yet fundamental understanding of microcarrier flotation

phenomena has not been pursued at all, at least according to published sources.

2.3 CONSIDERATIONS FOR BIOREACTOR DESIGN

Stirred-tank bioreactors are widely used in many microbial processes. With some modifications mainly in the geometries of the agitator, these reactors have been adapted for cultivation of animal cells (Brennan, 1987; Hu and Dodge, 1985; Shi et al., 1992; Kamen et al., 1991; Backer et al., 1988). To date, the largest stirred-tank bioreactors used for animal cells have working volumes of 5,000 to 10,000 litres (Bliem et al., 1991). The other type which has found successful industrial applications is airlift bioreactors. CellTech of the UK has up to 2,000 litres of airlift reactors in operation for the production of monoclonal antibodies from hybridoma cells (Griffiths, 1991). Compared to STR, airlift reactors are preferred due to their engineering simplicity, easy scale-up, and low shear characteristics.

For novel designs of animal cell bioreactors, there are two major chemical engineering considerations:

1. The availability of oxygen which is the least soluble, yet highly necessary nutrient.
2. The elimination of a damaging environment, since animal cells are generally delicate.

2.3.1 Oxygenation Of Animal Cell Cultures

The oxygen uptake rates (OUR) of animal cells fall into the range of $0.10 - 1.5 \times 10^{-16}$ mols·s⁻¹ per cell (Bliem et al., 1991). This is 1/100 or 1/1000 of the OUR of most microbial cells. Were it not for other problems associated with gassing, such as cellular damage and excessive foaming, this low oxygen requirement could be readily met by most existing oxygenation systems (Bliem et al., 1991).

2.3.2 Bubble-free Oxygenation

Based on the findings that bubble bursting at the gas-liquid interface is the major cell damaging mechanism, minimizing cellular flotation in the bulk liquid and

exposure to bursting bubbles at the free interface should be considered in novel bioreactor designs. Both STR and bubble column reactors have the entire free surface for bursting. In STR and bubble-column reactors, both bubbles and cells are homogeneously distributed throughout the bulk liquid phase. Flotation of cells is therefore maximized. These hydrodynamic characteristics render STR and bubble-column reactors undesirable in terms of cell protection. Lower shear in airlift bioreactors may be due to that gas bubbles are concentrated in the riser, and liquid recirculation around the free surface reduce cellular residence in the vicinity of the disengaging bubbles.

In view of above discussion, bubble-free oxygenation is one alternative. Monsanto's spin-filter system and NBS's CelliGen reactor are noted examples of commercial success (Chang and Furusaki, 1991). Other approaches in bubble-free oxygenation include head space gassing, gassing through permeable membranes (Su et al., 1992), or sparging within a wire cage (Spier and Griffiths, 1984). These designs, however, are difficult to scale up. Besides, membrane clogging, increased vulnerability to contamination due to the introduction of extra components into the reactor can be problematic.

REFERENCES

- Abu-Reesh, I. and Kargi, F. 1989. Biological responses of hybridoma cells to defined hydrodynamic shear stress. *J. Biotechnol.* **9**: 167-178.
- Augenstein, D.C., Sinskey, A.J., and Wang, D.I.C. 1971. Effect of shear on the death of two strains of mammalian tissue cells. *Biotechnol. Bioeng.* **13**: 409-418.
- Aunins, J.G., Croughan, M.S., and Wang, D.I.C. 1986. Engineering developments in homogeneous culture of animal cells: oxygenation of reactors and scaleup. *Biotechnol. Bioeng. Symp.* **17**: 699-723.
- Backer, M.P., Metzger, L.S., Slaber, P.L., Nevitt, K.L., and Boder, G.B. 1988. Large-scale production of monoclonal antibodies in suspension culture. *Biotechnol. Bioeng.* **32**: 993-1000.
- Backer, M.P., Metzger, L.S., and Kao, E.I. 1987. Shear and mixing in large-scale suspension culture. 80th Annual Meeting of the AIChE, New York, November.
- Bliem, R., Konopitzky, K., and Katinger, H. 1991. Industrial animal cell reactor

- system: aspects of selection and evaluation. *Adv. Biochem. Eng.* **44**: 1-26.
- Brennan, A. 1987. A suspension culture perfusion system for production of monoclonal antibodies. *ProBioTech (Suppl. Bioproc. Chem.)* **22**: 7-8.
- Chang, H.N. and Furusaki, S. 1991. Membrane bioreactors: present and prospects. *Adv. Biochem. Eng.* **44**: 27-64.
- Cherry, R.S. and Kwon, K. 1990. Transient shear stresses on a suspension cell in turbulence. *Biotechnol. Bioeng.* **36**: 563-571.
- Cherry, R.S. and Papoutsakis, E.T. 1988. Physical mechanisms of cell damage in microcarrier cell culture bioreactors. *Biotechnol. Bioeng.* **32**: 1001-1014.
- Cherry, R.S. and Papoutsakis, E.T. 1986. Hydrodynamic effects on cells in agitated culture reactors. *Bioproc. Eng.* **1**: 29-41.
- Croughan, M.S. and Wang, D.I.C. 1991. Hydrodynamic effects on animal cells in microcarrier bioreactors. p. 213-249. In *Animal Cell Bioreactors*, C.S. Ho and D.I.C. Wang, Eds, Butterworth-Heinemann, Boston.
- Croughan, M.S. and Wang, D.I.C. 1990. Reversible removal and hydrodynamic phenomena in CHO microcarrier cultures. *Biotechnol. Bioeng.* **36**: 316-319.
- Croughan, M.S. and Wang, D.I.C. 1989. Growth and death in overagitated microcarrier cell cultures. *Biotechnol. Bioeng.* **33**: 731-744.
- Croughan, M.S., Sayre, E., and Wang, D.I.C. 1989. Viscous reduction of turbulent damage in animal cell culture. *Biotechnol. Bioeng.* **33**: 862-872.
- Croughan, M.S., Hamel, J.F.P, Wang, D.I.C. 1988. Effects of microcarrier concentration in animal cell culture. *Biotechnol. Bioeng.* **32**: 975-982.
- Dodge, T.C. and Hu, W.S. 1986. Growth of hybridoma cells under different agitation conditions. *Biotechnol. Lett.* **8**: 683-686.
- Gardner, A.R., Gainer, J.L., and Kirwan, D.J. 1989. Effects of stirring and sparging on cultured hybridoma cells. *Biotechnol. Bioeng.* **35**: 940-947.
- Griffiths, B. 1991. Products from animal cells. P. 207-232. In *Mammalian Cell Biotechnology*, Butler, M., Ed., IRL Press, Oxford.
- Handa-Corrigan, A. 1990. Oxygenating animal cell cultures: the remaining problems. p. 124-132. In *Animal Cell Biotechnology*, Vol 4, R.E. Spier and J.B. Griffiths, Eds., Academic Press, London.
- Handa-Corrigan, A., Emery, A.N., and Spier, R.E. 1989. Effect of gas-liquid interfaces on the growth of suspended mammalian cells: Mechanisms of cell damage by bubbles. *Enzyme Microb. Technol.* **11**: 230-235.
- Handa-Corrigan, A., Emery, A.N., and Spier, R.E. 1987. On the evaluation of gas-liquid interfacial effects on hybridoma viability in bubble column bioreactors.

- Develop. Biol. Stand. **6**: 241-253.
- Hu, W.S. and Dodge, T.C. 1985. Cultivation of mammalian cells in bioreactors. *Biotechnol. Prog.* **1**: 209-215.
- Hu, W.S. 1983. Ph.D. thesis, Department of applied biological science, MIT, Cambridge, MA, USA.
- Jobses, I., Martens, D., and Tramper, J. 1991. Lethal events during gas sparging in animal cell culture. *Biotechnol. Bioeng.* **37**: 484-490.
- Kamen, A.A., Tom, R.L., Caron, A.W., Chavarie, C., Massie, B., and Archambault, J. 1991. Culture of insect cells in a helical ribbon impeller bioreactor. *Biotechnol. Bioeng.* **38**: 619-628.
- Kretzmer, G. and Schugerl, K. 1991. Response of mammalian cells to shear stress. *Appl. Microbiol. Biotechnol.* **34**: 613-616.
- Kunas, K.T. and Papoutsakis, E.T. 1990a. Damage mechanisms of suspended animal cells in agitated bioreactors with and without bubble entrainment. *Biotechnol. Bioeng.* **36**: 476-483.
- Kunas, K.T. and Papoutsakis, E.T. 1990b. The protective effect of serum against hydrodynamic damage of hybridoma cells in agitated and surface-aerated bioreactors. *J. Biotechnol.* **15**: 57-70.
- Lee, G.M., Huard, T.K., Kaminski, M.S., and Palsson, B.O. 1988. Effect of mechanical agitation on hybridoma cell growth. *Biotechnol. Lett.* **10**: 625-628.
- Leist, C.H., Meyer, H., and Fiechter, A. 1990. Potential and problem of animal cells in suspension culture. *J. Biotechnol.* **15**: 1-46.
- Low, K. and Harbour, C. 1985. Growth kinetics of hybridoma cells: (1) The effects of varying fetal calf serum levels. *Develop. Biol. Stand.* **60**: 17-24.
- Murhammer, D.W. and Goochee, C.F. 1990a. Sparged animal cell bioreactors: Mechanism of cell damage and pluronic F-68 protection. *Biotechnol. Prog.* **6**: 391-397.
- Murhammer, D.W. and Goochee, C.F. 1990b. Structural features of nonionic polyglycol polymer molecules responsible for the protective effect in sparged animal cell bioreactors. *Biotechnol. Prog.* **6**: 142-148.
- Murhammer, D.W. and Goochee, C.F. 1988. Scaleup of insect cell cultures: Protective effect of pluronic F-68. *Bio/Technol.* **6**: 1411-1418.
- Oh, S.K.W., Nienow, A.W., Al-Rubeai, M., and Emery, A.N. 1989. The effects of agitation intensity with and without continuous sparging on the growth and antibody production of hybridoma cells. *J. Biotechnol.* **12**: 45-62.
- Ozturk, S.S. and Palsson, B.O. 1991. Examination of serum and bovine serum

- albumin as shear protective agents in agitated cultures of hybridoma cells. *J. Biotechnol.* **18**: 13-28.
- Passini, C.A. and Goochee, C.F. 1989. Response of a mouse hybridoma cell line to heat shock, agitation, and sparging. *Biotechnol. Prog.* **5**: 175-187.
- Shi, Y., Ryu, D.D.Y., Park, S.H. 1992. Performance of mammalian cell culture bioreactor with a new impeller design. *Biotechnol. Bioeng.* **40**: 260-270.
- Sinskey, A.J., Fleischacker, M., Tyo, M.A., Giard, D.J., Wang, D.I.C. 1981. Production of cell-derived products: virus and interferon. *Ann. NY Acad. Sci.* **369**: 47-59.
- Smith, C.G., Greenfield, P.F., and Randerson, D.H. 1989. Effect of micromixing and gas incorporation on suspension culture of hybridomas. 8th Australian Biotechnology Conference, South Wales, Australia. February.
- Smith, C.G., Greenfield, P.F., and Randerson, D.H. 1987. A technique for determining the shear sensitivity of mammalian cells in suspension culture. *Biotechnol. Techniques* **1**: 39-44.
- Spier, R.E. and Griffiths, B. 1984. An examination of the data and concepts germane to the oxygenation of cultured animal cells. *Dev. Bio. Stand.* **55**: 81-92.
- Stathopoulos, N.A. and Hellums, J.D. 1985. Shear stress effects on human embryonic kidney cells in vitro. *Biotechnol. Bioeng.* **27**: 1021-1026.
- Su, W.W., Caram, H.S., Humphrey, A.E. 1992. Optimal design of the tubular microporous membrane aerator for shear-sensitive cultures. *Biotechnol. Prog.* **8**: 19-24.
- Tramper, J. and Vlak, J.M. 1988. Bioreactor design for growth of shear-sensitive mammalian and insect cells. p. 199-228. In *Upstream Processes: Equipment and Techniques*, A. Mizrahi, Eds., Alan R. Liss Inc., New York.
- Tramper, J., Joustra, D., and Vlak, J.M. 1987. Bioreactors design for growth of shear-sensitive insect cells. p. 125-136. In *Plant and Animal Cells: Process Possibilities*, C. Webb and F. Mavituna, Eds., Ellis Horwood, Chichester, England.
- Tramper, J., Williams, J.B., and Joustra, D. 1986. Shear sensitivity of insect cells in suspension. *Enzyme Microb. Technol.* **8**: 33-36.
- van Wezel, A.L. 1967. Growth of cell strains and primary cells on micro-carriers in homogeneous culture. *Nature* **216**: 64-65.

Chapter 3*

Physical Modeling of Animal Cell Damage by Hydrodynamic Forces in Suspension Cultures

3.1 INTRODUCTION

In suspension cultivation of animal cells, agitation and aeration provide mixing and oxygen but can cause damage to the cells which are vulnerable to hydrodynamic forces due to their relatively large size and lack of a protective cell wall. Studies in viscometers and shear devices of the capillary-tube type exposed cells to well-defined fluid fields, and critical shear stresses were obtained for various cell types. Animal cells in bioreactor cultures, however, are usually exposed to long-term, transient shear forces from liquid turbulence, which results from agitation and/or aeration. Small scale bioreactors, therefore, have been frequently used in cell damage studies (Kunas and Papoutsakis, 1990). Much of the literature regarding fluid-mechanical damage of animal cells in bioreactors has been recently reviewed by Papoutsakis (1991).

Cell damage mechanisms in surface-aerated stirred bioreactors were investigated by Kunas and Papoutsakis (1990) and Smith et al. (1989). When the reactor was operated without a head space, therefore without vortex formation and bubble entrainment, cells could be damaged by shear forces in the turbulent bulk liquid only at agitation rates as high as 700 rpm. However, when air bubbles were entrained into the liquid through the unstable gas-liquid interface, low agitation rates such as 220 rpm gave a dramatic reduction in apparent growth rates. They concluded that cell damage was due to vortex formation at the free surface accompanied by bubble entrainment and breakup in the surface-aerated bioreactor.

When sparging is used to provide oxygen and to keep cells in homogeneous suspension, recent studies have shown that contacting bubbles with cell suspensions is detrimental to mammalian cells (Handa-Corrigan et al., 1989;

* A version of this chapter has been published. John Wiley & Sons 1992. *Biotechnology and Bioengineering*, 40: 1277-1281.

Handa-Corrigan et al., 1987) and insect cells (Tramper et al., 1986). For example, the death rate of insect cells was found to be proportional to the air flow rate when a bubble column filled with a suspension of 10^6 cells·mL⁻¹ was sparged at different air flow rates (Tramper et al., 1986).

Handa-Corrigan et al. (1987, 1989) found that cell damage was due to bubble disengagement at the gas-liquid interface and identified three distinct mechanisms for cell damage; oscillatory disturbances caused by rapidly bursting bubbles in culture medium with antifoam, physical shearing in the draining liquid films (lamellae) around the bubble, and the actual loss of cells in the foam layer in the medium without antifoam. They also claimed that pluronic F-68 formed a stable foam layer which the cells did not penetrate, and therefore protected cells from physical damage.

Due to the complex relationships between culture medium, cell metabolism and bioreactor hydrodynamics, not only are the mechanisms of cell damage and protection in dispute, but shear sensitivity of cultured hybridoma cells depends on cell line, mode of growth, and culture age. Furthermore, cellular metabolism can be modified by shear stresses. A physical model for cells offers an alternative method for studying the role of hydrodynamic forces. By eliminating metabolic and cell membrane effects, a physical model allows direct study of the forces causing cell damage.

Poncelet and Neufeld (1989) have previously used a simple physical model to investigate the shear damage of biological cells in a turbine reactor. Nylon microcapsules containing an aqueous phase were prepared using an emulsion technique. Damage to the polymer membrane released an indicator which was then measured in solution. We used the same model to study the fluid-mechanical mechanisms of animal cell damage in both stirred tank reactors and sparged reactors. Suspensions of microcapsules were used to investigate the roles of bubble entrainment, sparging, and additives in physical damage under bioreactor conditions. Measurement of the size distribution of microcapsules before and after breakage gave the critical diameter for survival and an indirect measure of fluid forces.

3.2 MATERIALS AND METHODS

3.2.1 Preparation of Microcapsules

Chang's method (Chang, 1987) was followed for preparation of microcapsules, with some minor modifications. Dextran (Sigma, D-4626, MW 19,600) was used as an indicator for the microcapsule breakage study. An aqueous phase, containing the monomer 1,6-hexanediamine (Sigma, H-2381) and 10% dextran (w/v), was emulsified in an organic solvent (1:4 chloroform, Mallinckrodt AR, and cyclohexane, Anachemia) with the help of 1% (v/v) Span-85 (Sigma, S-7135). When the second monomer, terephthaloyl chloride (Aldrich, 12,087-1), was added into this emulsion, interfacial polymerization took place to give a nylon membrane enclosing the aqueous dextran phase. Polyethyleneimine (Sigma, P-3143), used as a cross-linking agent for the nylon polymerization, was found to be indispensable for the successful production of microcapsules. Microcapsules were collected by centrifugation and washed three times by 1% (v/v) Tween-20 (Fisher, BP 337-500) solution to give a sedimented volume of 25 mL per batch. Around 15 batches of microcapsules were pooled and then divided into aliquots for breakage studies. In each breakage experiment, 25 mL (sedimented volume) of microcapsules was diluted with RO water to make up a working volume of 1-L suspension.

Figure 3-1 is a scanned picture of microcapsules prepared by the emulsion technique. They had a cumulative volumetric distribution described in Figure 3-2. The individual microcapsules ranged from 20 μm to 300 μm in diameter with a number-average of 77 μm .

Microcapsules were washed by membrane filtration. The Tween residue level was monitored by measuring the surface tension of the filtrate using a standard curve from a series of prepared solutions (Figure 3-3). The Tween concentration in the suspension was always below the critical micelle concentration.

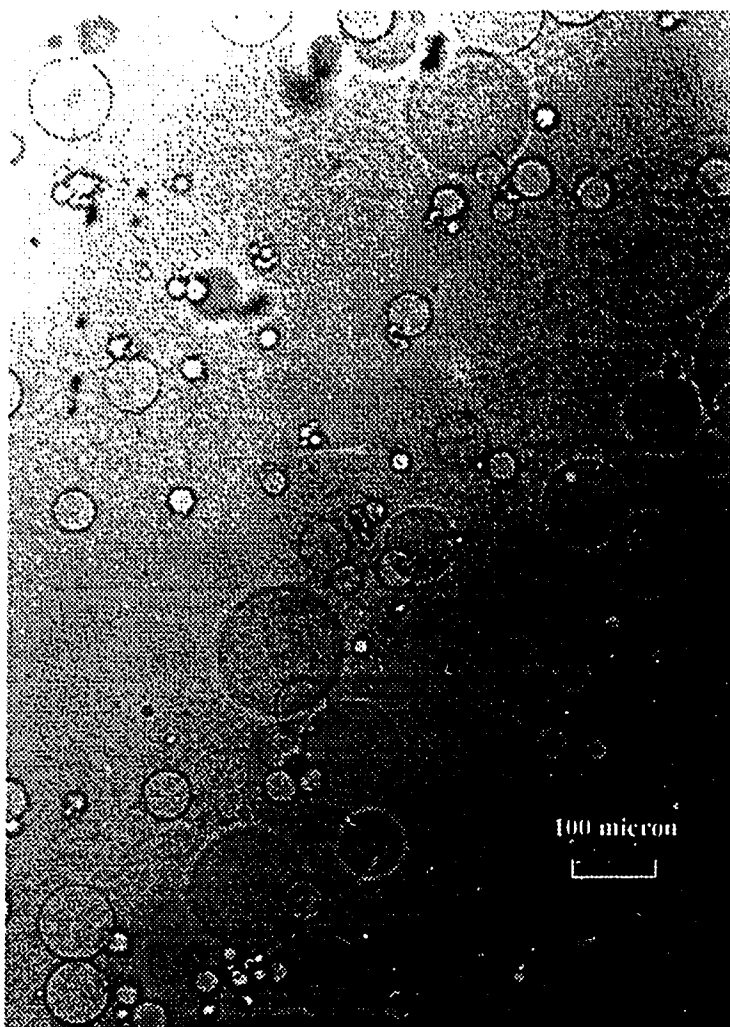


Figure 3-1. A scanned image of the microcapsules prepared by the emulsion technique.

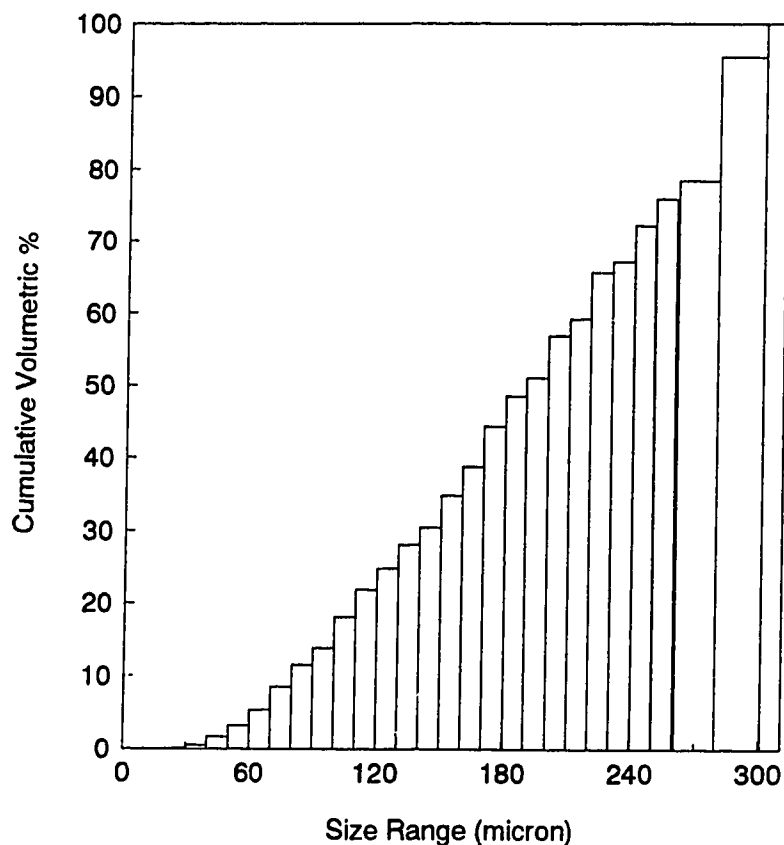


Figure 3-2. Cumulative volumetric distribution of the initial microcapsules.

3.2.2 Dextran Assay

A colorimetric method based on the phenol-sulfuric acid reaction was used for the dextran assay (Dubois et al., 1956). The orange-yellow color was stable and measured for absorbance at 488 nm. The standard curve showed a linear relation between absorbance readings and dextran concentrations for absorbance < 0.8.

3.2.3 Microcapsule Breakage Experiments

Microcapsule breakage was investigated in standard stirred-tank fermenters and in bubble columns. A 2-L New Brunswick Multigen fermenter was used to study microcapsule breakage under stirred conditions. A working volume of 1 L and an impeller rotation speed of 500 rpm were applied in all stirring experiments. A

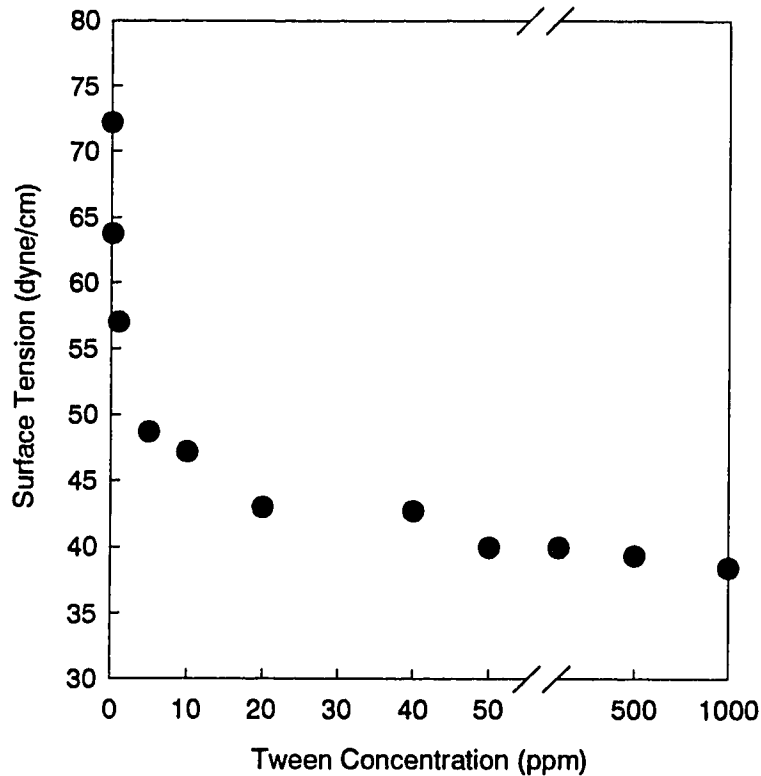


Figure 3-3. Surface tension measured for a series of standard Tween solution.

cylindrical plexiglass bubble column with a dimension of 91 mm diameter \times 360 mm height providing a working volume of 1 L was used in the sparging experiments. A cylindrical sintered glass sparger (14 \times 25 mm) placed at the bottom of the column gave an aeration rate of 1 L \cdot min⁻¹.

Antifoam emulsion C (Sigma, A-8011) and Pluronic F-68 (Sigma, P-1300) were used in the bubble column to study their effects on microcapsule breakage.

Experiments in the fermenter and bubble column were of 90 minutes in duration. Microcapsules and bubbles were photographed, and their size was determined using a digitizer (Sigma Scan, USA).

During the breakage experiments, samples of the microcapsule suspension were taken from a position 2 cm below the free surface and filtered by a membrane filter with a pore size of 0.7 μ m. The filtrate was then assayed for

dextran concentration. Absorbance readings were directly used in the following calculation for the volumetric breakage (%) at the time t:

$$V_{b,t} (\%) = \frac{< \text{absorbance} >_{t=t} - < \text{absorbance} >_{t=0}}{< \text{absorbance} >_{\text{total}} - < \text{absorbance} >_{t=0}} \quad (1)$$

where subscript "total" represents total disruption of the suspension using a homogenizer. Calculation (1) avoided any possible background interferences in the dextran determination.

3.3 RESULTS AND DISCUSSION

3.3.1 Microcapsule Breakage by Stirring

Microcapsule suspensions containing three different levels of Tween residue were stirred at 500 rpm for 90 min in the 2-L New Brunswick fermenter. The volumetric breakage data are presented in Figure 3-4.

All of the experiments followed apparent first-order kinetics, as follows:

$$V_{b,t} = V_{b,\infty} [(1 - \exp(-k \cdot t))] \quad (2)$$

where $V_{b,t}$ refers to volumetric breakage (%) at time t, $V_{b,\infty}$ was the maximum breakage when $t \rightarrow \infty$ and k was the breakage rate constant (min^{-1}). The $V_{b,\infty}$ and k values from the least-squares fits of the volumetric breakage data to Equation (2) are listed in Table 3-1.

Figure 3-4 shows that microcapsule breakage at 90 min decreased when the Tween-20 concentration in the microcapsule suspension was reduced. The decrease in breakage was not significant when Tween was decreased from 1000 ppm to 20 ppm, however, breakage was reduced from 60% to 38% when the concentration of Tween was reduced to 10 ppm.

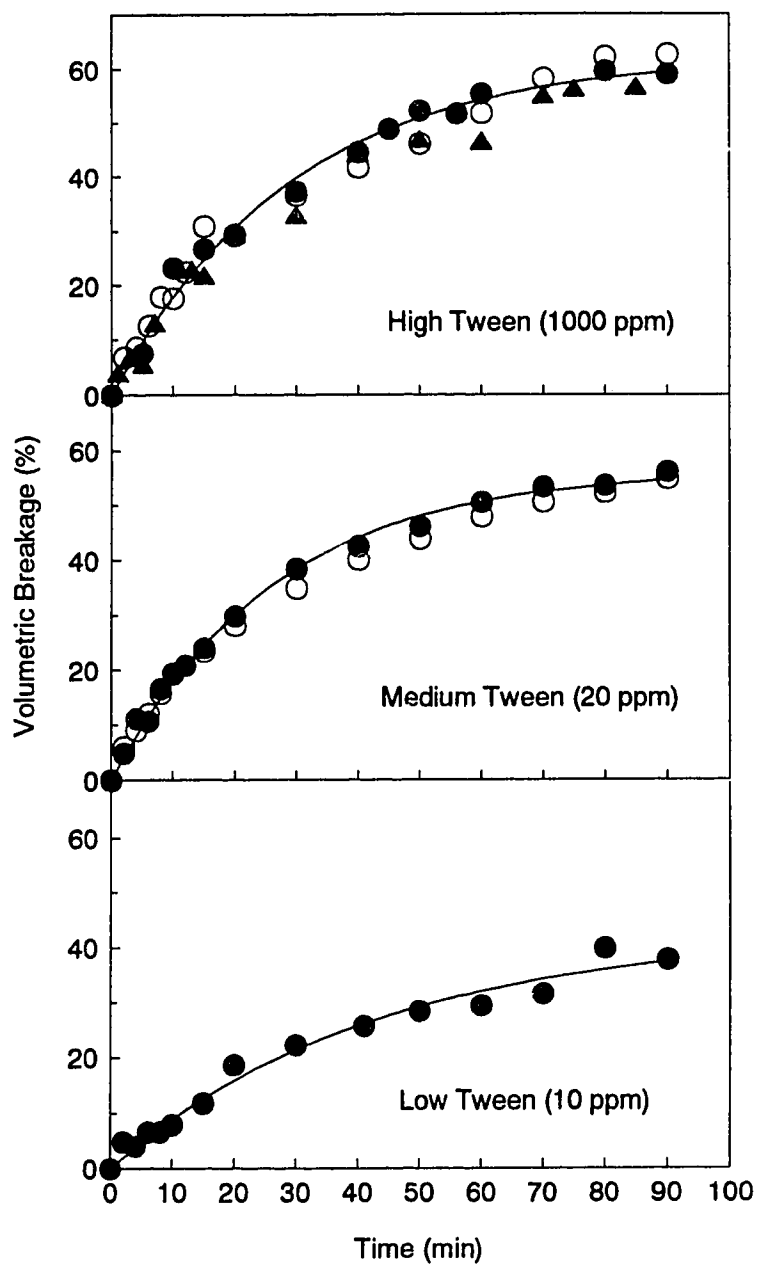


Figure 3-4. Volumetric breakage of microcapsules at 500 rpm in 2-L fermenter. Symbols show replicate experiments at high and medium Tween concentrations. Curves are least-squares fits to Eq. (2).

Table 3-1. Kinetic constants for breakage of microcapsules in an agitated fermenter. 1 L of microcapsule suspension containing different Tween concentrations were stirred at 500 rpm in the 2-L New Brunswick fermenter.

Tween concentration (ppm)	$V_{b,\infty}$ (%)	k (min ⁻¹)
1000	62.4	0.034
20	56.4	0.038
10	42.8	0.023

Fine bubbles (< 1 mm) were entrained into the liquid very quickly after the agitation was started in the microcapsule suspension with high Tween concentration (1000 ppm). The gas holdup was estimated to be 1-3% (v/v) at the end of 90 min agitation. Tests with Tween in water solutions in the fermenter confirmed that the presence of a small amount of Tween caused bubble entrainment. Bubble entrainment has been observed to damage hybridoma cells in a stirred bioreactor (Kunas and Papoutsakis, 1990; Smith et al., 1989).

When the Tween content was reduced to a low level (10 ppm), bubble entrainment was greatly reduced to the point where it was negligible during the first 15 min. The smaller values of $V_{b,\infty}$ (42.8%, compared to 62.4% and 56.4% at higher Tween levels) and k (0.023 min⁻¹ compared to 0.034 min⁻¹ and 0.038 min⁻¹) were the result of less bubble entrainment into the bulk liquid. Microcapsule breakage in the stirred fermenter was increased, therefore, when bubbles were entrained into the microcapsule suspension from the head space of the stirred fermenter, in agreement with the results of Kunas et al. (1990) with animal cells.

Breakage of microcapsules was almost complete after 90 min of stirring, when the rate of breakage declined almost to zero (Figure 3-4). The $V_{b,\infty}$ values were always less than 100%, therefore, microcapsules below a critical size (d_c) survived. When $V_{b,\infty} \approx 60\%$, we would expect $d_c \approx 165 \mu\text{m}$ according to the initial size distribution in Figure 3-2. This result was confirmed by measuring the cumulative size distribution of surviving microcapsules (Figure 3-5).

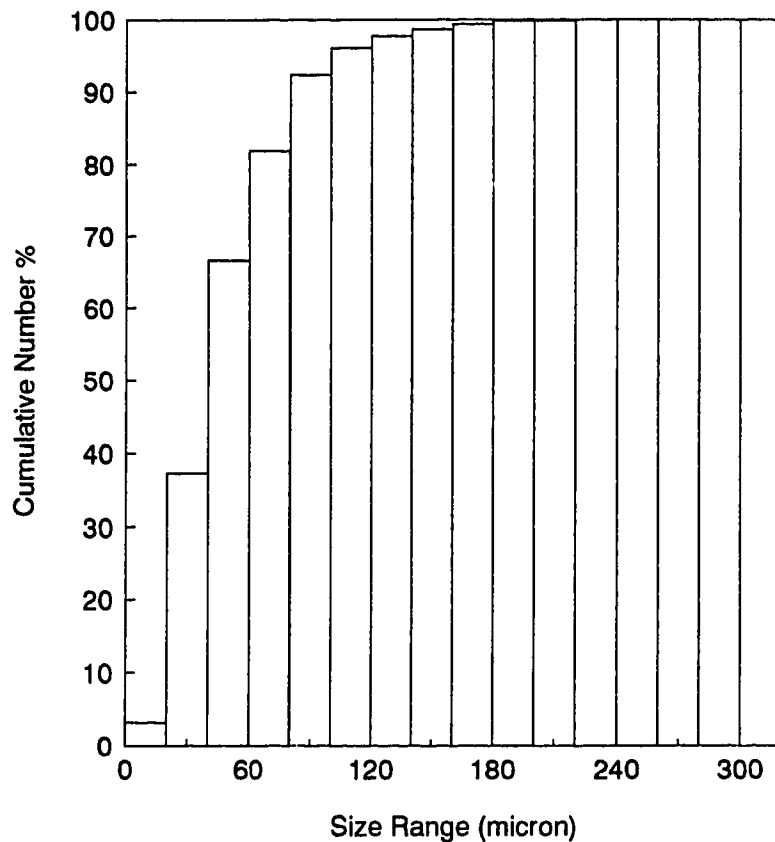


Figure 3-5. Cumulative number distribution of the microcapsules surviving 500 rpm stirring for 90 min in the 2-L fermenter. The 1-L microcapsule suspension used for the breakage study had a Tween concentration of 1000 ppm.

The breakage rate constant k was reduced when Tween was washed away, giving a decrease in bubble entrainment. The kinetic constant k reflects how frequently microcapsules larger than d_c were exposed to the maximum shear forces. When no gas is entrained in the liquid, we can assume that the high shear zone would be in the vicinity of impeller. k is then directly related to how often the microcapsules pass through this region. When bubbles are entrained into the bulk liquid, however, the hydrodynamics become much more complicated. The other mechanism is breakage by the bubble forces at the free gas-liquid interface, such as bubble incorporation into and escaping from the liquid as suggested by Kunas

and Papoutsakis (1990) and Handa-Corrigan et al. (1987, 1989). In this case, k depends on how often microcapsules contact the free surface and on the bubble forces there.

3.3.2 Microcapsule Breakage by Sparging

Bubble entrainment and release are difficult to study in a stirred-tank, therefore, a bubble column was used to study the roles of sparging, foaming, and bubble bursting in microcapsule breakage. A 1-L microcapsule suspension was aerated at 1 L/min for 90 min. Volumetric breakages are plotted in Figure 3-6. No microcapsule breakage was observed in the suspension with Tween concentration of 30 ppm except during the first two minutes. When antifoam was used to suppress foam formation, microcapsule breakage increased to 30% by volume at 90 min of sparging. Addition of Pluronic F-68, which has been frequently used as a protective agent in animal cell culture, did not appear to protect microcapsules from damage. When microcapsules were washed by membrane filtration to remove Tween, and therefore to avoid foaming, microcapsule breakage was the highest (50% at 90 min). The cumulative size distribution of the surviving microcapsules is plotted in Figure 3-7. Microcapsules larger than $190\ \mu\text{m}$ did not survive the 90 min of sparging. Microcapsule breakage followed apparent first-order kinetics; the $V_{b,\infty}$ and k values from the least-squares fits to Equation (2) are listed in Table 2. As the Tween concentration varied, the bubble size and foaming characteristics changed correspondingly (Table 2).

When the microcapsule suspension had a Tween concentration of 30 ppm, a stable foam layer was quickly formed. This foam layer reached 12 cm above the gas-liquid interface after 10 min. Microcapsules were entrained into the foam layer and deposited onto the column wall. At the end of experiment, the cumulative microcapsule entrainment in the foam accounted for 27% (v/v) of the total microcapsules used in the breakage study. Microscopic examination of foam samples showed that microcapsules survived intact in the foam; a stable foam layer appeared to have protected microcapsules from damage. If animal cells are entrained into a foam layer, however, they may not be able to survive due to nutritional limitations in the foam, and physical damage from bubble breakup and film draining.

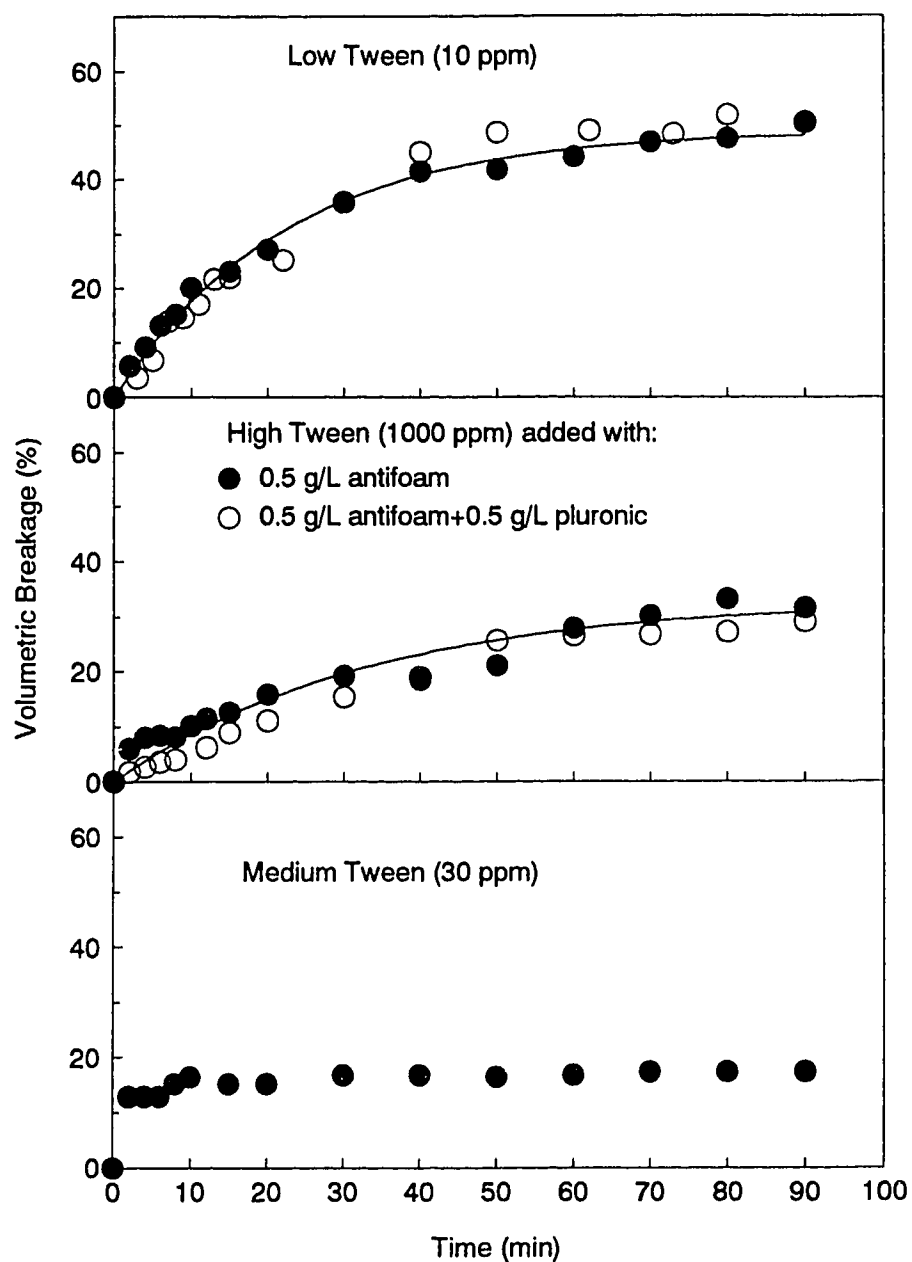


Figure 3-6. Volumetric breakage of microcapsules at $1 \text{ L} \cdot \text{min}^{-1}$ sparging in the bubble column. Symbols show replicate experiments, or otherwise noted on the plots. Curves are least-squares fits to Equation (2).

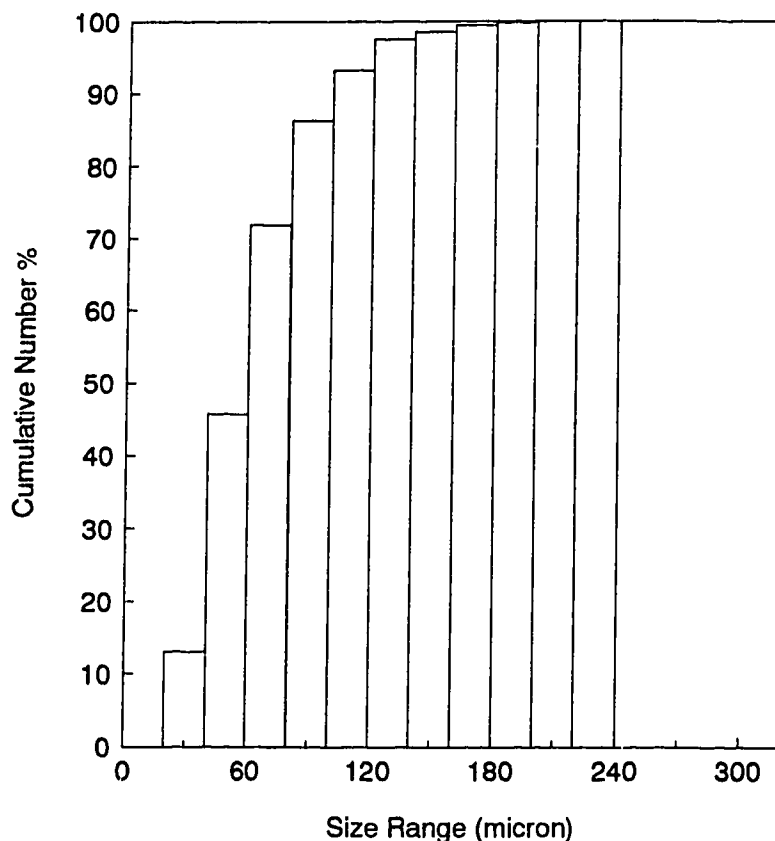


Figure 3-7. Cumulative number distribution of microcapsules surviving 1 L/min sparging for 90 min in the bubble column. The 1-L microcapsule suspension used for the breakage study had a Tween concentration of 10 ppm.

Addition of 0.5 g antifoam emulsion C into the 1-L microcapsule suspension suppressed foam formation. Bubbles disengaged from the gas-liquid interface and splashes of liquid could be seen on the column wall. The further addition of 0.5 g/L of pluronic gave similar breakage results (Figure 3-6). Murhammer et al. (1990) proposed that Pluronics protected cells from damage by interacting with the cell membrane. Similar interactions could not occur between Pluronic and the nylon membrane of the microcapsules.

In the third type of sparging experiment, microcapsules were vigorously washed and the Tween concentration was reduced to 10 ppm. There was no stable foam layer, and microcapsules were observed on large bubble films at the gas-

liquid interface and entrained by the unstable porous foam, then deposited on the column wall. When large bubbles escaped the interface, they burst to throw microcapsules as high as 10 cm above the interface to deposit onto the column wall. Microscopy of wall samples showed that only very small microcapsules ($< 30 \mu\text{m}$) survived this process. Long narrow streams of microcapsules were also seen on the column wall. The microcapsules deposited on the column wall at the end of the 90 min breakage experiment accounted for 25% (v/v) of the total microcapsules used.

Table 3-2. Foam characteristics and kinetics of microcapsule breakage in a bubble column. 1 L of microcapsule suspension containing different Tween concentrations was sparged at $1 \text{ L}\cdot\text{min}^{-1}$ with air.

Tween Concentration	d_b (mm)	foam	$V_{b,\infty}$ (%)	k (min^{-1})
Medium Tween (30 ppm)	1.2	stable	n.a.	n.a.
High Tween (1000 ppm) added with antifoam, with/without pluronic	1.0	no	33.0	0.030
Low Tween (10 ppm)	2.0	porous unstable negligible	48.8	0.045

Figure 3-6 indicates that microcapsules were protected from damage in the presence of a stable foam layer, therefore, microcapsules were only damaged at the gas-liquid interface. The sparger and bubble rising (bulk liquid) zones were not responsible for microcapsule breakage because these zones were similar in all three types of experiments.

Several reports have suggested that the air-liquid interface was the region where hybridoma cells were damaged by bubble bursting (Handa-Corrigan et al. 1987; 1989; Jobses et al. 1991). Handa-Corrigan et al. (1987, 1989) used 0.5 to 2 L bubble columns to study the damaging effects of the gas-liquid interface on hybridoma cells by varying air flow rates and column heights. With the help of the microscopic technique, they concluded that cell damage was due to bubble bursting and film drainage at the gas-liquid interface. Our experiments have demonstrated how microcapsules were damaged when a stable foam layer was absent, such as the case where antifoam was used or where surfactant was removed. These experimental observations and results agree with those from hybridoma cell studies in terms of the detrimental effects of unstable foam and bursting bubbles (Handa-Corrigan, 1989), and they also agree well with observations from microscopic study of cell-bubble interactions resulting from cell attachment on bubble films and entrainment into the foam layer (Bavarian, et al., 1991).

In the study of the mechanism of pluronic protection of cells from damage, Handa-Corrigan et al. (1989) proposed that pluronics, as surfactants, could form a stable foam layer which the cells did not penetrate and, therefore, protect them from the damaging effects of bursting bubbles and film drainage. Our experiments showed that a stable foam due to the presence of Tween surfactant protected the microcapsules from damage; but penetration of microcapsules into the foam layer was unavoidable. Microscopic observations by Bavarian et al. (1991) demonstrated entrainment of insect cells into the foam layer. Based on our microcapsule model studies, and reported results (Handa-Corrigan, 1987, 1989; Kunas and Papoutsakis, 1990) on damage mechanisms of animal cells, we conclude that foaming characteristics are important and there is a need to distinguish a stable foam from an unstable foam. Only a stable foam layer can prevent cell damage by bursting bubbles.

The present study suggests that microcapsule breakage in the absence of a protective foam layer is governed by two factors: flotation kinetics which would determine the frequency of microcapsule-interface interaction, and the forces associated with the gas-liquid interface such as bubble bursting and film draining.

The values of k and $V_{b,\infty}$ will depend on the frequency of exposure to shear damage at the interface and on the shear forces generated by bubble bursting. Flotation of microcapsules by air bubbles would increase exposure to the bubble disengagement zone. The high concentrations of microcapsules in the foam and on the column wall indicated the importance of flotation in carrying the particles to the interface. The k values in Table 2 indicate a slower breakage when more surfactant was present. This result could be partly due to the bubble surface losing its mobility when it picks up surfactant molecules, and therefore the collection efficiency of microcapsules would decrease (Weber et al., 1983). The present study showed significant enrichment of microcapsules in the foam layer. These results suggest that suppression of cell flotation could be an efficient method of protecting against damage due to gas bubbles. Observations by Bavarian et al. (1991) on cell-bubble interactions in the presence of Pluronic support this flotation mechanism. When Pluronic was added, cells were not observed on the bubble films. Hence, Pluronic prevented collection of cells by the rising bubbles by modifying the cell membrane or the bubble interface. In the present study, Pluronic F-68 did not affect microcapsule breakage, probably due to its lack of interaction with the nylon membrane.

The ultimate breakage, $V_{b,\infty} = 50\%$, corresponded to a survival diameter of $d_c \approx 190 \mu\text{m}$ which was consistent with Figure 3-7. Based on Laplace's Equation, Jay et al. (1968) found that the nylon microcapsules had an internal pressure that correlated well with the microcapsule diameter as:

$$P = \frac{4 \cdot T}{d} \quad (3)$$

where the tensile strength of the microcapsule membrane, T , was estimated as $1.84 \text{ N}\cdot\text{m}^{-1}$ for Nylon-6,10 microcapsules containing hemolysate. Assuming a similar membrane tensile strength for the microcapsules in the present study, then an external pressure equivalent to the shear force required to break microcapsules having the critical diameter $190 \mu\text{m}$ would be $3.9 \times 10^4 \text{ N}\cdot\text{m}^{-2}$.

3.4 CONCLUSION

1. Breakage of microcapsules in agitated suspension was increased by entrainment of gas bubbles.
2. Breakage of microcapsules in a bubble column was controlled by flotation, which concentrated the microcapsules near the liquid surface, and by bubble bursting at the liquid surface. The forces caused by bubble bursting were equivalent to an external pressure of *ca.* $4 \times 10^4 \text{ N} \cdot \text{m}^{-2}$ on the microcapsules.
3. Microcapsules suspended in stable foam were protected from breakage.

REFERENCES

- Bavarian, F., Fan, L.S., and Chalmers, J.J. 1991. Microscopic visualization of insect cell-bubble interactions. I: Rising bubbles, air-medium interface, and the form layer. *Biotechnol. Prog.* **7**: 140-150.
- Chang, T.M.S. 1987. Recycling of NAD(P) by multienzyme systems immobilized by microencapsulation in artificial cells. *Methods in Enzymology* **136**: 67-70.
- Dubois, M., Gilles, K.A., Hamilton, J.K., Rebers, P.A., and Smith, F. 1956. Colorimetric method for determination of sugars and related substances. *Anal. Chem.* **28**: 350-356.
- Handa-Corrigan, A., Emery, A.N., and Spier, R.E. 1989. Effect of gas-liquid interfaces on the growth of suspended mammalian cells: Mechanisms of cell damage by bubbles. *Enzyme Microb. Technol.* **11**: 230-235.
- Handa, A., Emery, A.N., and Spier, R.E. 1987. On the evaluation of gas-liquid interfacial effects on hybridoma viability in bubble column bioreactors. *Dev. Biol. Stand.* **6**: 241-253.
- Jay, A.W.L. and Edwards, M.A. 1968. Mechanical properties of semipermeable microcapsules. *Can. J. Physiol. Pharmacol.* **46**: 731-737.
- Jobses, I., Martens, D., and Tramper, J. 1991. Lethal events during gas sparging in animal cell culture. *Biotechnol. Bioeng.* **37**: 484-490.
- Kunas, K.T. and Papoutsakis, E.T. 1990. Damage mechanisms of suspended animal cells in agitated bioreactors with and without bubble entrainment. *Biotechnol. Bioeng.* **36**: 476-483.

- Murhammer, D.W. and Goochee, C.F. 1990. Structural features of nonionic polyglycol polymer molecules responsible for the protective effect in sparged animal cell bioreactors. *Biotechnol. Prog.* **6**: 142-148.
- Papoutsakis, E.T. 1991. Fluid-mechanical damage of animal cells in bioreactors. *Trends Biotechnol.* **9**: 427-437.
- Poncelet, D. and Neufeld, R.J. 1989. Shear breakage of nylon membrane microcapsules in a turbine reactor. *Biotechnol. Bioeng.* **33**: 95-103.
- Smith, C.G., Greenfield, P.F., and Randerson, D.H. 1989. Effect of micromixing and gas incorporation on suspension culture of hybridomas. 8th Australian Biotechnology Conference, South Wales, Australia. February.
- Tramper, J., Williams, J.B., and Joustra, D. 1986. Shear sensitivity of insect cells in suspension. *Enzyme Microb. Technol.* **8**: 33-36.
- Weber, M.E., Blanchard, D.C., and Syzdek, L.D. 1983. The mechanism of scavenging of waterborne bacteria by a rising bubble. *Limnol. Oceanogr.* **28**: 101-105.

Chapter 4*

Cultivation of Hybridoma Cells in an Inclined Bioreactor

4.1 INTRODUCTION

Compared to microbial cells, animal cells are more susceptible to damage by fluid-mechanical forces due to their large size and lack of a cell wall. This shear sensitivity poses a special challenge in bioreactor design and operation; to avoid exposure of cells to excessive shear while providing adequate mixing and oxygen for cell growth and product formation. Significant cell damage in bioreactors can be associated with interactions between bubbles and cells, therefore, several strategies have been proposed to use bubble-free aeration or to separate cells from bubbles.

Surface aeration is frequently used to supply oxygen to lab-scale agitated bioreactors, but the culture becomes oxygen limited when the bioreactor is scaled-up. If the impeller agitation speed is increased to achieve better mixing and oxygen supply, bubbles can be entrained into the liquid from the head space, and cause cell damage (Kunas and Papoutsakis, 1990).

Silicone tubing has been used to aerate bioreactors, by diffusion of oxygen through the tube walls (Aunins et al., 1986; Su et al., 1992). A significant length of tubing is required when the bioreactor is scaled up, the bioreactor internals are more complex and the tubing may leak. Other membrane methods use external oxygenators, through which liquid medium is recycled to replenish the dissolved oxygen. One example is hollow fiber bioreactors where cell-free medium is oxygenated in a gas exchange cartridge (Hirschel and Gruenberg, 1987). Scaling up of hollow fiber bioreactors is hindered, however, by the diffusion barrier across the fiber membrane which causes nutrient limitations and waste build-up, as well as formation of gradients within the cartridge (Hirschel and Gruenberg, 1987; Piret

* A version of this chapter has been submitted for publication. John Wiley & Sons. Biotechnology and Bioengineering. Submitted on Jan.6, 1994. A US patent application (serial no. 08/095,681) was filed on July 22, 1993.

and Cooney, 1990). It is also difficult to enumerate the cell population directly, which is an impediment to on-line monitoring and control.

Mechanical separation of cells from bubbles is another strategy used in the cultivation of shear sensitive cells. Mammalian cells were immobilized in ceramic matrix (Applegate and Stephanopoulos, 1992) and in gel beads (Bugarski et al., 1989; Lee et al., 1993) to avoid contact with damaging bubbles, but these methods are more complicated than conventional suspension cultures. Whiteside et al. (1985) and Brennan (1987) used a cage of wire gauze to contain gas bubbles and foams. Other designs use a bag of semipermeable film to suspend the cells in the culture medium (Watanabe et al., 1991). The common features of these designs are greater complexity of construction and operation than conventional bioreactors, and limitations on scale-up.

In conventional bioreactors for suspension cultures, such as stirred-tank bioreactors and air-lift bioreactors, cell damage was associated with the behavior of bubbles at the free gas-liquid interface, i.e. bubble bursting and film draining (Handa-Corrigan et al., 1987; Kunas and Papoutsakis, 1990). Bubbling of air is attractive in large scale bioreactors, but the number of cells in the vicinity of bursting bubbles should be minimized. Flotation of cells by rising bubbles must, therefore, be avoided by limiting contact between cells and rising bubbles. Gravity can be used to achieve this separation if a bioreactor is constructed from two inclined, vertical plates (Figure 4-1). Due to the inclination of the two parallel plates, bubbles travel along the upper plate by a very limited path and disengage from a small portion of the gas-liquid interface (Table 4-1). The rising bubbles also circulate the bulk liquid as illustrated in Figure 4-1. Fewer cells are able to reach the bubble-bursting zone due to gravity settling towards the lower plate and the recirculation of the liquid near the interface. Such hydrodynamic characteristics guarantee much reduced cell-bubble contact and therefore flotation, while bulk mixing and aeration due to well developed liquid circulation are not sacrificed. In contrast, when the plates are vertical, the bioreactor behaves like a rectangular bubble column.

A prototype bioreactor was built using this novel bioreactor concept. A murine hybridoma cell line was cultivated in this bioreactor to study the response

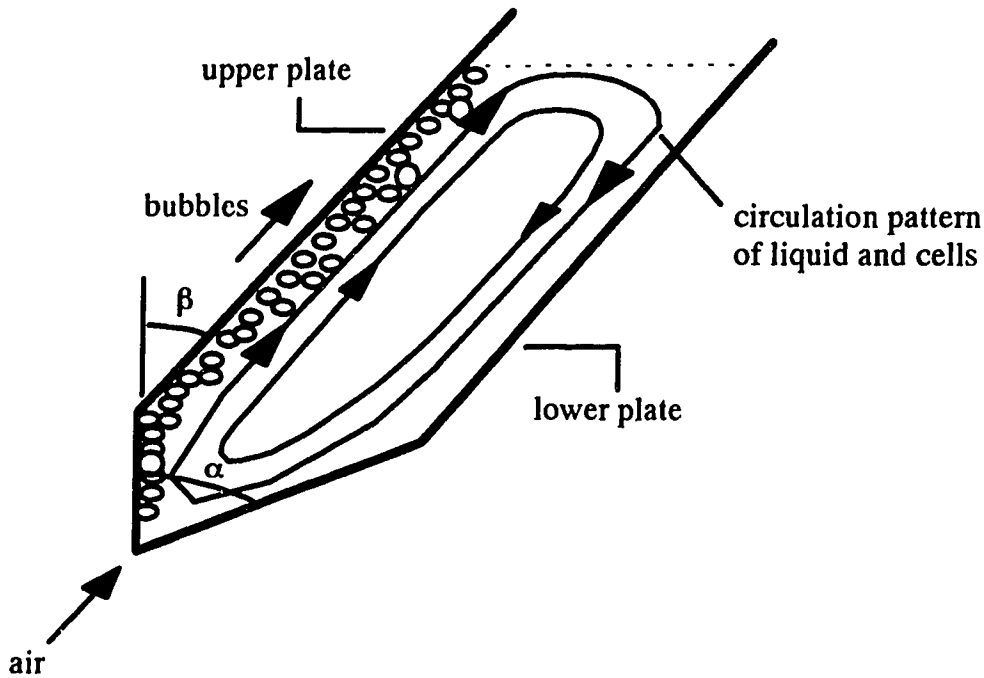


Figure 4-1. Schematic diagram of inclined-plate bioreactor showing liquid circulation.

of shear sensitive cells. Cell growth and product formation were measured during batch experiments at different inclination angles and aeration rates.

Table 4-1. A comparison of the free gas-liquid interfacial area in different bioreactor types having the same working volume.

Bioreactor Type	Aspect Ratio	Free Surface per Volume	% of Surface for Bubble Bursting	Bursting Area per Volume
Stirred-tank	3	1*	100	1*
Bubble Column	6	0.6	100	0.6
Airlift	6	0.6	80	0.5
Inclined-plate	10	0.5	5	0.025

* Note: The free surface to volume ratio is proportional to $(\text{aspect ratio})^{-2/3}$. Free Surface per Volume for the stirred-tank is assigned "1" in order to give a basis for comparison between different bioreactor types.

4.2 MATERIALS AND METHODS

4.2.1 Cell Line and Culture Medium

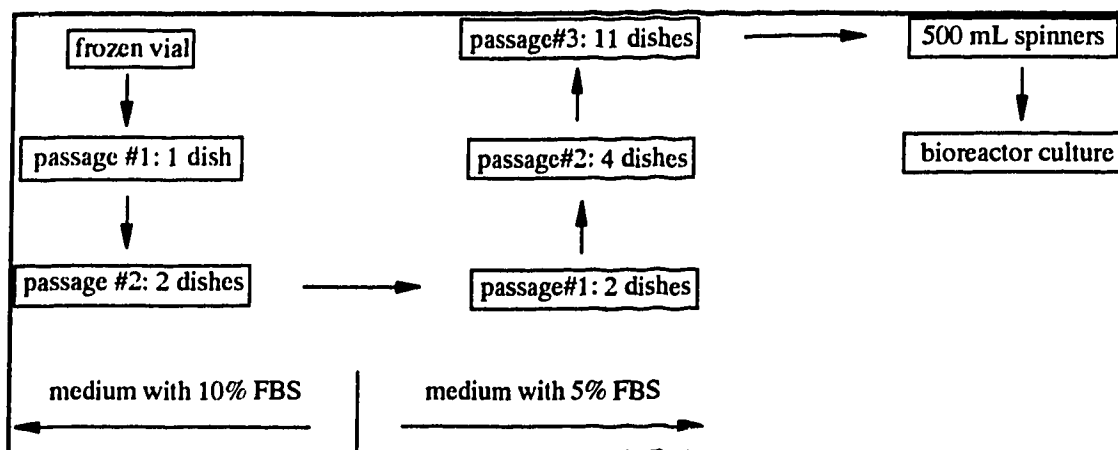
A murine hybridoma cell line, designated as 155H.7R.120, was kindly provided by Biomira Inc. (Edmonton, Alberta, Canada). It secreted an antibody (immunoglobulin G or IgG) that was reactive to human adenocarcinomas and cross-reactive to Human Serum Albumin (HSA).

Two vials of cells, stored in liquid nitrogen, were thawed into culture medium with 10% fetal bovine serum (FBS) and then subcultured for two weeks in the same medium. A master cell bank was then prepared for bioreactor experiments.

Culture medium was prepared from RPMI-1640 (Gibco, Grand Island, New York) supplemented with 1% glutamine (Gibco, Grand Island, New York) and 5% FBS (Gibco, Grand Island, New York). 400 ppm of Antifoam C (Sigma, St. Louis, Missouri) was added into the medium in advance when starting a bioreactor run.

4.2.2 Inoculum Preparation

A vial of cells from the working cell bank was thawed into culture medium with 10% FBS in a tissue culture dish. In medium supplemented with 10% FBS, viable cell concentration increased from an initial value of 1×10^5 cells/mL to ca. 8×10^5 cells/mL after two days in culture. At this point, cells were transferred to two fresh dishes for growth in the same medium. These two passages in culture medium with 10% FBS were followed by three passages in culture medium with 5% FBS. Viable cell count increased from an initial value of 1×10^5 cells/mL to ca. 6×10^5 cells/mL after two days in culture. Viability of dish cultures varied from dish to dish and from time to time, but it was typically 90% or higher in medium with 10% FBS, and 80% or higher in medium with 5% FBS. Two 500 mL spinners were used to prepare inoculum for bioreactor cultures. Similar growth was observed in spinners at this stage. The following diagram illustrates the process of inoculum preparation for bioreactor experiments:



This method of inoculum preparation ensured that all bioreactor experiments were started from cells with same cultivation history.

4.2.3 Bioreactor Cultures

An inclined-tube bioreactor was constructed from Pyrex glass to test the bioreactor concept (Figure 4-2). The reactor had a working volume of approximately 4 L. A minimum working volume of 1.8 L was required due to the position of the sampling port. The bioreactor tube had a diameter of 70 mm and was tapered at the bottom to form a cone angle of 50° (α in Figure 4-1). A sintered glass sparger with a pore size of 40 - 100 μm was centered at the base of the bioreactor tube.

To prevent cells from binding to any glass surface in contact, the bioreactor tube and all other glassware were treated with Prosil-28 following a procedure recommended by Corning. For all bioreactor experiments, the bioreactor tube was autoclaved at 121° for 45 min before use.

The water jacket of the bioreactor was maintained at 37°C using a circulating water bath. Aeration of 0.05 vvm (volume of air per volume of liquid per minute) was provided by gas cylinders containing 6.15% CO₂ with balance air. 2 L of culture medium with 5% FBS was pumped into the reactor and stabilized overnight before inoculation. Inoculum was prepared by growing cells for two days in spinners and then collected into 500 mL of fresh medium. The

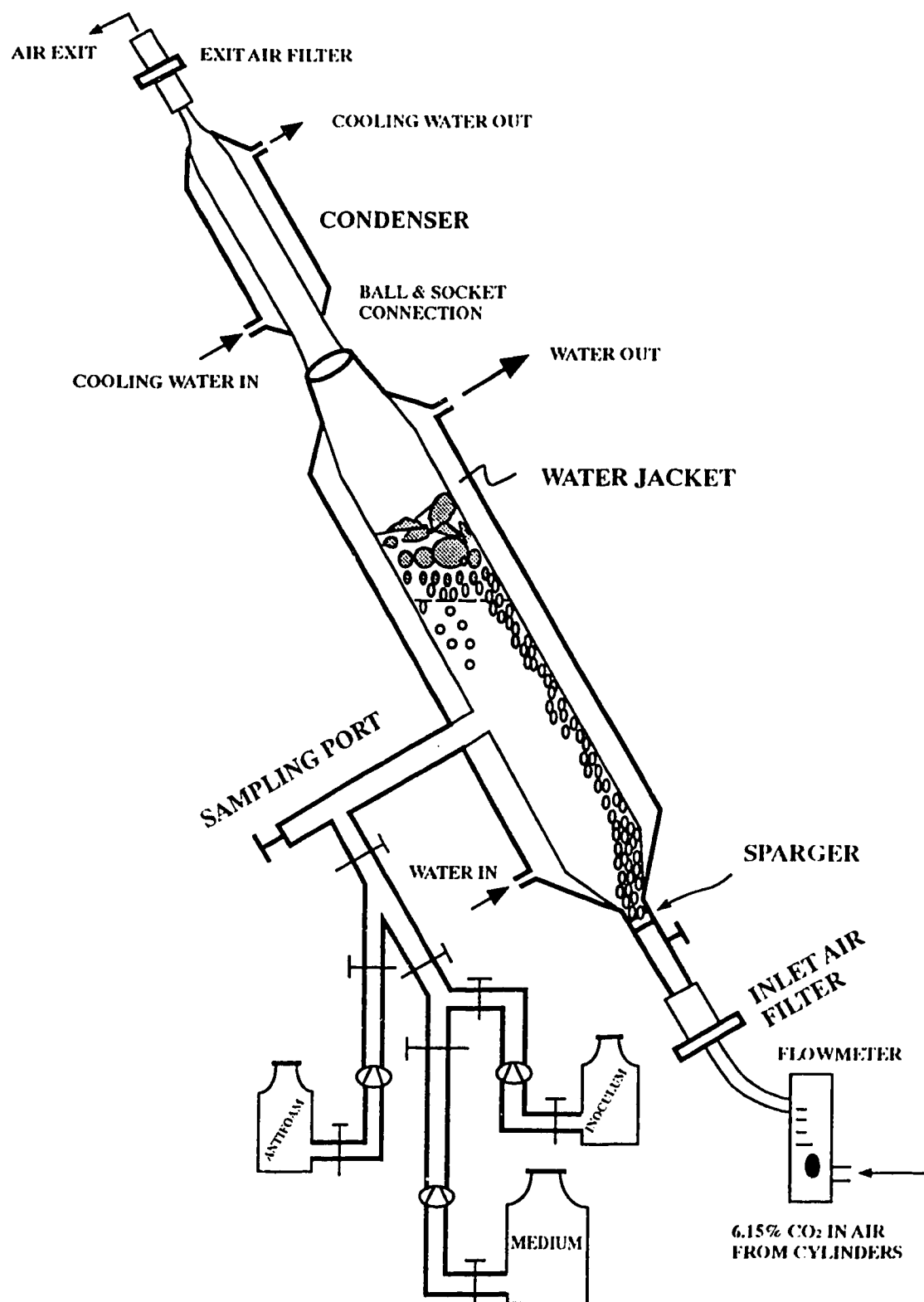


Figure 4-2. Schematic diagram of the experimental inclined-tube bioreactor.

culture volume was therefore 2.5 L in total, with an initial viable cell density of $1 - 1.5 \times 10^5$ cells/mL.

Some bioreactor runs had parallel controls in both dishes and spinners. When inoculating the bioreactor, several dishes and a 250 mL spinner were also inoculated with the same cells. Inclination of the bioreactor ranged from 0 to 45°. Experiments at different angles were carried out in a random sequence.

Samples were taken for every 12 h from the bioreactor. When the bioreactor was inclined, transient settling of cells along the lower bioreactor wall was visible, and the amount of this settling depended on the inclination angle. In order to take representative samples (volume-averaged samples), aeration was temporarily increased to 0.15 vvm for 2 min to mix the culture to ensure homogeneity. Cell count and pH were determined upon sampling. The supernatant was obtained by centrifuging the samples for 8 minutes at 700g, and then stored at 4°C for subsequent antibody, LDH, and glucose assays. Samples were stored at -20°C for amino acids, ammonia, and lactate assays.

4.2.4 Analytical Methods

Viable cell count and viability: The Trypan-blue exclusion method was used to obtain the viable cell count and viability. Viable and dead cells are counted from the four corner squares of a hemacytometer at the same time. If there were fewer than 100 cells in the four squares, then the total number of cells in the nine squares were counted.

IgG antibody: A sandwich type of ELISA assay was used to determine the antibody concentration of the cell supernatant. The assay procedure is summarized in Appendix A.1.

Lactate Dehydrogenase (LDH): LDH of the cell supernatants was determined by an enzymatic method using a TECHNICON DAX™ system. LDH catalyzes the conversion of L-lactate to pyruvate in the presence of NAD. The enzymatic activity of LDH is proportional to the rate of production of NADH. The reaction is monitored at 340 nm as a zero-order kinetic assay. LDH activity was lost after samples from the first few bioreactor experiments were stored at -80°C for two

weeks. Samples from later experiments, therefore, were stored at 4°C for less than two days before assay was carried out. It was found that LDH activity of the cell supernatants was stable at 4°C for at least two weeks.

Amino acids: The concentrations of primary amino acids were determined using a precolumn derivatization with o-phthaldialdehyde (OPA) followed by reversed-phase chromatography (Jones and Gilligan, 1983). The concentration of each amino acid was then obtained by measuring the area under the corresponding chromatographic peak and comparing with the standard.

Glucose: Glucose concentrations of the cell supernatants were determined by an enzymatic method using a TECHNICON DAX™ system.

Ammonia and L-lactate: An ammonia kit (cat. no. 1112723, Boehringer-Mannheim, Montreal, Canada) was used to determine the ammonia content of the supernatant samples. In the presence of glutamate dehydrogenase (GLDH) and reduced nicotinamide-adenine dinucleotide (NADH) ammonia reacted with 2-oxoglutarate to L-glutamate, whereby oxidation of NADH was measured by absorbance change at 340 nm. L-Lactate was determined by an assay kit (cat. no. 1112821) from Boehringer-Mannheim (Montreal, Canada). In the presence of L-lactate dehydrogenase (L-LDH) L-lactate was oxidized by nicotinamide-adenine dinucleotide (NAD) to pyruvate, whereby NADH was formed and measured by absorbance at 340 nm.

4.2.5 Flotation Experiments

Sample preparation: 1 vial of cells from the working cell bank was thawed into culture medium with 10% FBS (Gibco, Grand Island, New York) in a tissue culture dish. This dish was then expanded to 9 dishes after 2 passages in the same medium (4 days in culture). 20 mL of culture from different stages of growth was then collected for each flotation experiment.

Flotation experiments: Batch flotation experiments were carried out in a cylindrical tube (Pyrex™ glass, 1 cm in inner diameter, 20 mL in volume). A sintered glass type of sparger (pore size: 40 - 100 µm) was positioned at the base

of the tube. An aeration rate of 0.5 vvm was used to generate a foam, which was allowed to overflow from the top of the column.

Sampling and cell enumeration: 0.5 mL of sample was taken from a fixed point (1 cm below the liquid surface) at timed intervals (2 - 9 min apart) during the 45 min batch flotation experiment. Cell count (both viable and dead cells) was carried out using the Trypan-blue exclusion method to determine if cells were preferentially entrained and then lost into the foam phase.

4.3 RESULTS AND DISCUSSION

Table 4-2 indicates the matrix of six operating conditions for bioreactor experiments. The numbers were assigned to the bioreactor experiments only for the convenience of discussion, and do not indicate the actual sequence in which these bioreactor experiments were carried out. A typical aeration rate of 0.05 vvm was kept constant except the last experiment with 45° inclination. The inclination angle (β in Figure 4-1) was varied to study its effect on bioreactor performance (Table 4-2). The vertical experiment #1 was repeated to check the reproducibility of the bioreactor cultures. Parallel controls in dishes and spinners were carried out for two bioreactor experiments to ensure that cells inoculating different bioreactor experiments were indeed physiologically similar, and to provide low-shear or no-shear culture conditions for internal comparisons with the corresponding bioreactor culture.

Table 4-2. Organization of bioreactor experiments.

Experiment #	Aeration (vvm)	Inclination	Controls
1	0.05	vertical	yes
2	0.05	vertical	no
3	0.05	10°	no
4	0.05	30°	no
5	0.05	45°	yes
6	varied*	45°	no

* Aeration was 0.18 vvm for the first 30 h, and was then increased to 0.24 vvm.

4.3.1 Typical Bioreactor Culture and Control Experiments

Control experiments characterized the performance of the cell line in static culture (dishes) and in a low shear environment (spinners). Figure 4-3 summarizes the results from representative dish controls of Experiment #1. Cells entered the exponential growth phase upon inoculation, then viable cell count increased from an initial value of 1.8×10^5 cells/mL to a maximum of ca. 1×10^6 cells/mL in 45 h. At this point, the viability of the culture started dropping dramatically, but the viable cell population was sustained for the following 40 h during which period

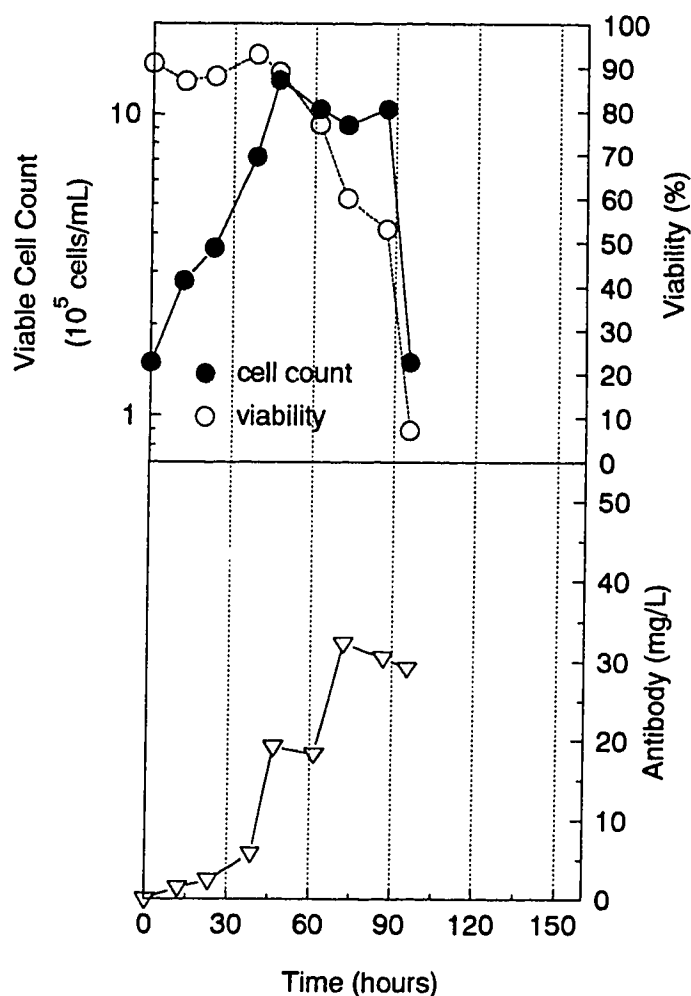


Figure 4-3. Cell counts and antibody titer versus time for control culture grown in Petrie dishes from the same inoculum as bioreactor experiment #1 (vertical).

antibody accumulated to a concentration of 30 mg/L (Figure 4-3). In the spinner control for the same bioreactor experiment (#1), the viable cell concentration reached a maximum of 7×10^5 cell/mL, but the final antibody concentration was similar to that from dish controls, i.e. 30 mg/L (Figure 4-4).

When the bioreactor was vertical, it was a bubble column (Experiment #1). Viable cell count increased from an initial value of 1×10^5 to 6×10^5 cells/mL in 60 h (Figure 4-5). Viability dropped from 83% to 70% within the first 24 h as a result of cells experiencing a new environment upon inoculating. Viability remained

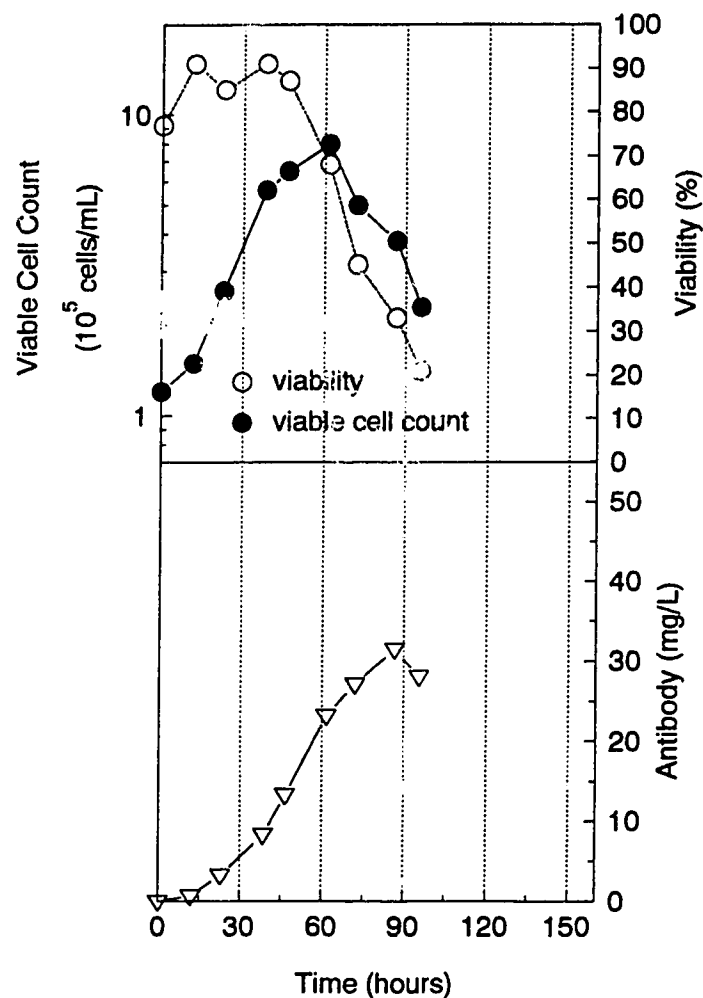


Figure 4-4. Cell counts and antibody titer versus time for control culture grown in spinner flasks from the same inoculum as bioreactor experiment #1 (vertical).

around 70% until 60 h when it dropped dramatically to 40% within 40 h. When viability was low (e.g. < 40%) at the end of the run, cell enumeration by the trypan-blue exclusion method was inaccurate due to the presence of large amounts of cell debris and dying cells (Figure 4-5). The stationary phase was such defined that it started when the viability started dropping significantly (e.g. > 10%) while the viable cell count had reached its maximum, and it ended when the viable cell count first started dropping significantly (e.g. > 2×10^5 cells/mL) within 12 h (samples were taken at an interval of 12 h for bioreactor experiments).

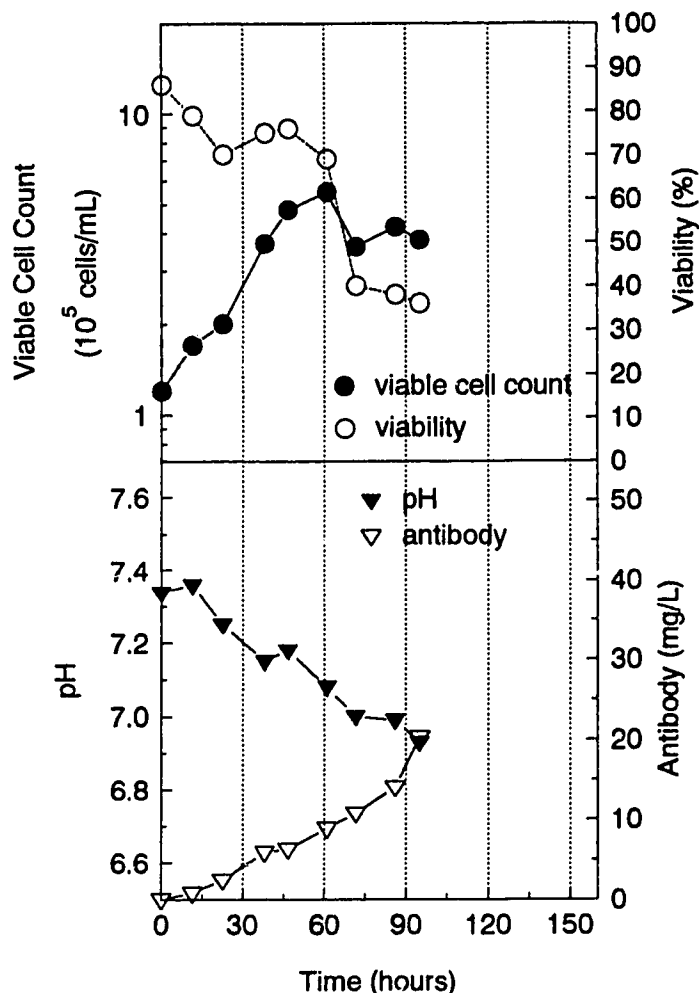


Figure 4-5. Cell growth and antibody formation as a function of time for bioreactor experiment #1 (vertical).

The vertical bioreactor experiment was repeated to check the reproducibility of the bioreactor cultures (Experiment #2). The growth and

antibody production (see Figure A-2 in Appendix A) were equivalent to the previous vertical experiment. Viable cell count reached a maximum of 6×10^5 cells/mL in 60 h. The antibody titer was 17 mg/L.

pH was not controlled but it was monitored for all bioreactor experiments. The pH of the culture decreased, due to the formation of lactate, from an initial value of 7.3 to 6.9 at the end of the vertical bioreactor experiment (Figure 4-5). This profile was typical of all of the bioreactor cultures. A pH range of 6.8 to 7.4 should be adequate for the cultivation of hybridoma cell lines (Doyle and Butler, 1990). Therefore, pH was not an important factor in these bioreactor experiments.

As described previously, 400 ppm of antifoam was always added to the medium at the beginning of each bioreactor experiment. Foaming was, however, inevitable due to the presence of FBS in the medium and the production of various proteins by the cultivated cells. Figure 4-6 shows foaming in the vertical bioreactor

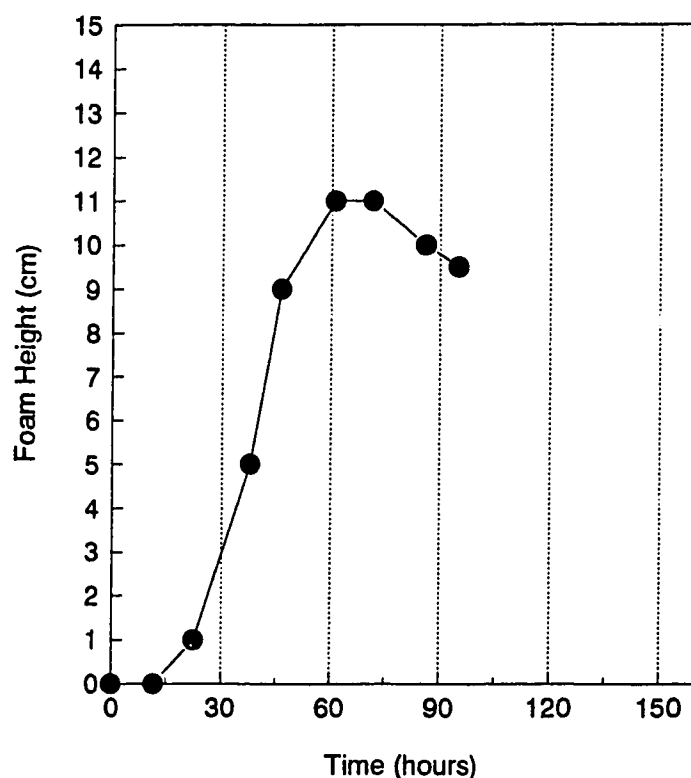


Figure 4-6. Foaming in bioreactor experiment #1 (vertical).

experiment #1 which was typical for these bioreactor experiments. Very little foam formed during the first 24 h. Foam height then reached 11 cm at the end of exponential growth phase. Foam receded towards the end of the culture. Because the time course of foaming followed the growth curve, proteins produced by the cells were likely the major contribution to foam formation.

LDH, an intracellular enzyme, normally resides in healthy animal cells, and is released into culture medium from dead or dying cells or when viable cells are physically broken apart. Measuring the LDH content of the medium has been frequently used as a tool in cell damage studies (Peterson et al., 1990; Wu et al., 1992). Figure 4-7 shows LDH accumulation in the medium for the vertical bioreactor experiment #1 along with its controls. More LDH was released from the bioreactor than from both the dish and spinner control in the first 60 h. Then the difference between the bioreactor and the controls became insignificant. Towards the end of the experiment, LDH level in the dish culture was much higher than

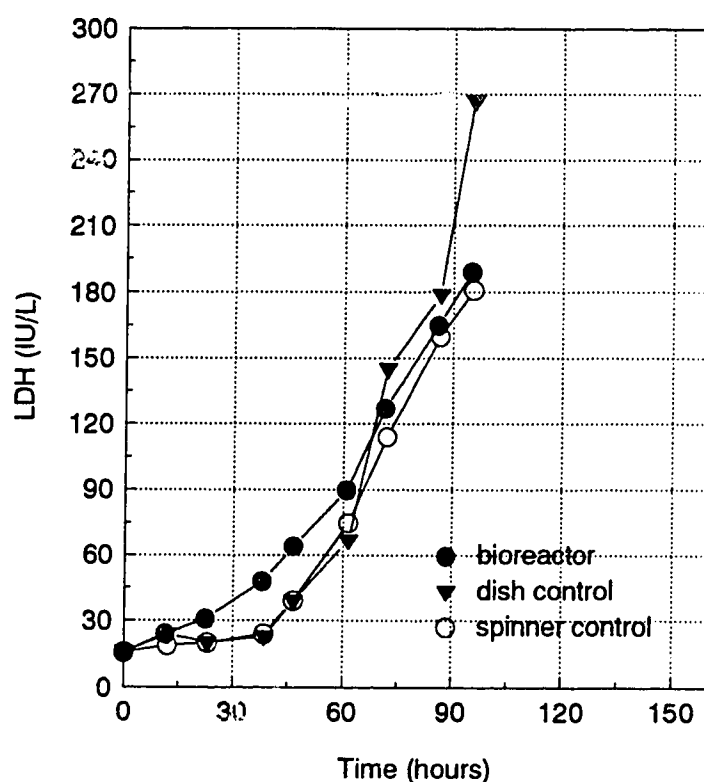


Figure 4-7. LDH release in bioreactor experiment #1 (vertical), compared with data from dish and spinner controls.

those in the bioreactor and in the spinner culture. Higher LDH release at the end corresponded to the much higher maximum cell number in the dish control (1×10^6 cell/mL in the dish compared to 6×10^5 cell/mL in the bioreactor). LDH measurement was effective for determining physical damage (cells torn apart) only when viability is high during the exponential growth phase in a batch culture. Later in the stationary phase or in the death phase, cell death due to depletion of some nutrient components or the buildup of wastes releases LDH out of the leaky cell membrane. Cell viability, therefore, was an important factor determining the amount of LDH released. A linear relation between LDH and viability was observed during the stationary phase and the death phase, suggesting that LDH from intact dead cells counted for an important part in the total LDH released (Figure 4-8). During the first 45 h, however, cells were exponentially growing both in the bioreactor and in the control cultures (Figure 4-3 to Figure 4-5). The higher LDH levels in the bioreactor from 20 h to 60 h were consistent with cell damage in the bioreactor.

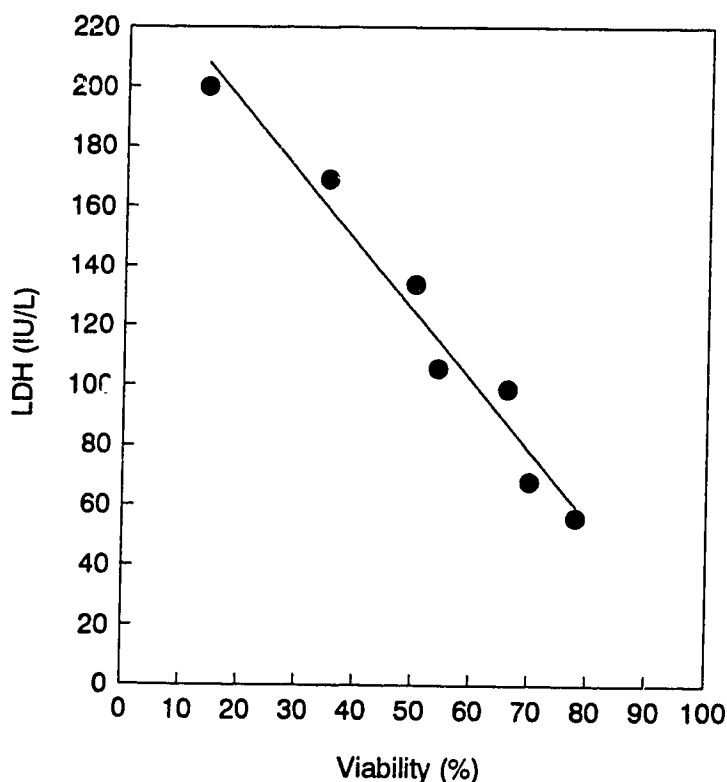


Figure 4-8. LDH release is linearly correlated with viability when cells enter the stationary phase.

4.3.2 Cell Growth and Antibody Production as a Function of Inclination

Figure 4-9 summarizes growth and antibody production at an inclination angle of 30° and an aeration rate of 0.05 vvm (Experiment #4). At 45 h a maximum viable cell count of 6×10^5 was reached, followed by a stationary phase of 45 h before the viable cell count dropped rapidly. Approximately 10 mg/L of antibody accumulated in the culture during the exponential growth phase. Another 30 mg/L of antibody was then produced during the period corresponding to the plateau of the stationary phase on the growth curve. This result was consistent with the common observation that antibody production of hybridoma cells is non-growth

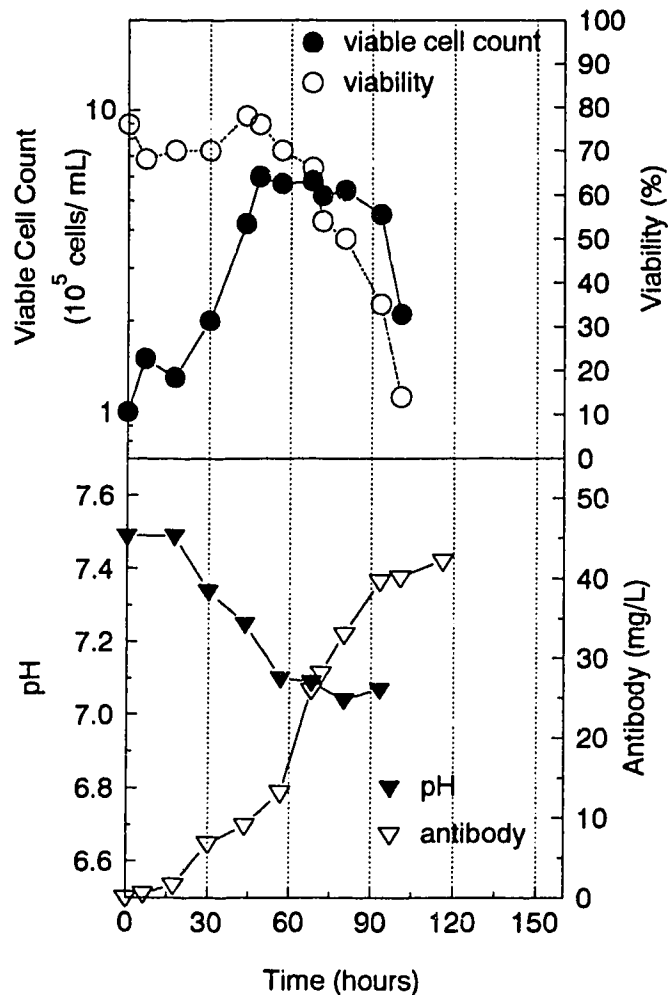


Figure 4-9. Growth and antibody production in bioreactor experiment #4 with 30° inclination.

associated (Birch et al., 1987). Other bioreactor cultures used inclination angles of 10° and 45° while the sparging rate was kept constant at 0.05 vvm (Experiment #3 and #5).

Figure 4-10 shows viable cell population and antibody accumulation for three different inclination angles, 10°, 30°, and 45° in comparison with the vertical. Except for the bioreactor experiment with 45° inclination, the exponential growth phase was similar for different angles of inclination, i.e. a maximum viable cell count of $5-7 \times 10^5$ cells/mL was reached at the end of exponential growth at 45 h. In all cases, antibody production was also similar during the first 45 h. Subsequent antibody formation was sensitive to inclination angle during the stationary phase. The maximum antibody titers were 17, 30, 42, and 12 mg/L for inclination angle of 0° (vertical), 10°, 30°, and 45° respectively. The doubling of antibody yield at 30° inclination corresponded to a much prolonged stationary phase compared to the vertical case. Table 4-3 summarizes the duration of stationary phase and the corresponding antibody production for four inclination angles. For the inclination angles tested, the best growth and antibody production were obtained at 30° inclination.

Smith and Greenfield (1992) investigated effects of fluid turbulence on metabolism of hybridoma cells in FBS-supplemented RPMI media. They found that agitation speeds up to 600 rpm, without entrainment of gas bubbles in a stirred-tank bioreactor, did not affect cell growth, metabolism, and antibody production. Limitations of essential amino acids were suggested to be the reason for the cessation of net growth at both 100 rpm and 600 rpm. In our bioreactor experiments, we analyzed concentrations of 21 primary amino acids in the culture supernatants, and found that none of them were completely depleted from the culture medium (Table A-1 in Appendix A). Smith and Greenfield (1992) also related reduced antibody titers at high agitation speeds to glucose limitations caused by accelerated glycolysis during the exponential growth phase in serum-free media. Glucose was therefore determined for samples from bioreactor culture 1 through 5; similar profiles in glucose consumption were observed in all cases. For all bioreactor experiments, a minimum of 2 mM of glucose still remained at the end of each experiment, in comparison with 10 mM of glucose in fresh culture media.

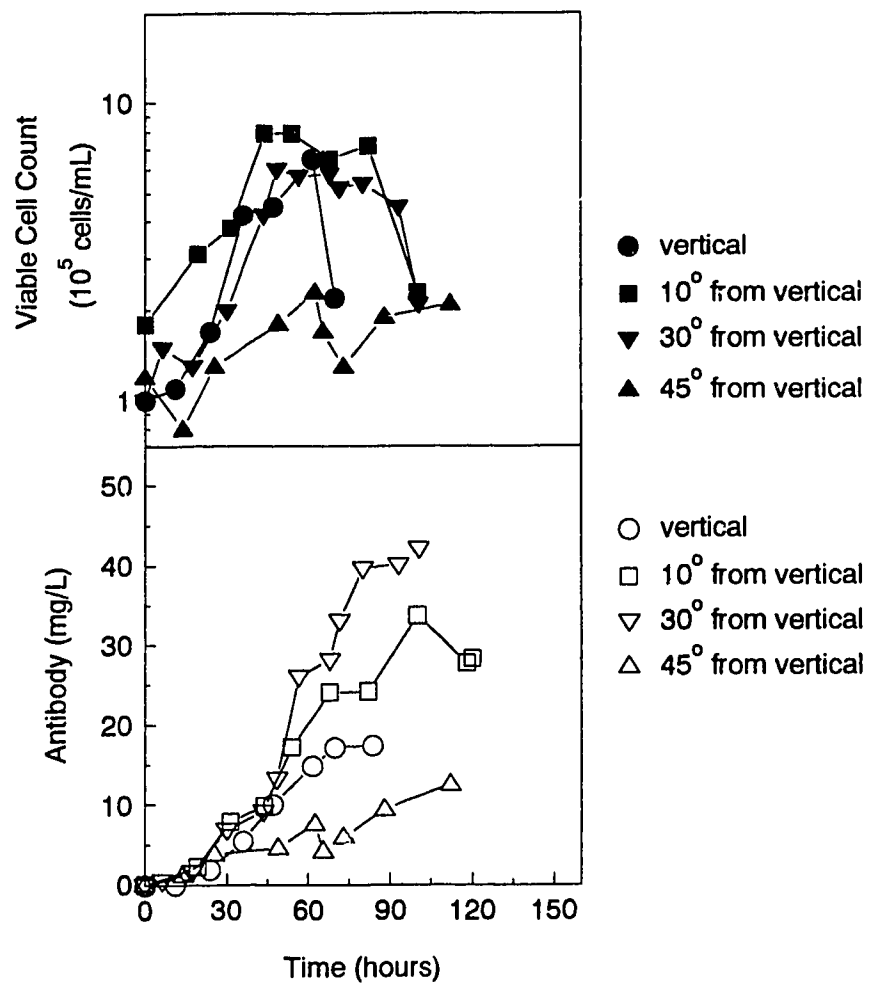


Figure 4-10. Comparison of growth and antibody production with time in the bioreactor at different angles of inclination.

Table 4-3. Duration of stationary phase and amount of antibody produced in bioreactor experiments.

Run #	1	2	3	4	5
Inclination	0°	0°	10°	30°	45°
Duration of Stationary Phase (hours)	0	0	35	45	N/A
Antibody Yield (mg/L)	18	17	30	42	12

Ammonia and lactate formation were determined for the vertical bioreactor experiment (#1). At the end of the culture, 3.4 mM of ammonia and 16 mM of lactate had accumulated in the media. These concentrations of ammonia and lactate were below the concentration range (4 mM for ammonia, and 28 mM for lactate) for inhibition of cell growth (Doyle and Butler, 1990; Reuveny et al., 1986).

In the bioreactor experiment with 45° inclination from vertical (#5), viability dropped from 80% to 60% in the first 15 h and cell count was very low throughout the experiment (Figure 4-10). At 60 h, 500 mL of spent medium was replaced by fresh medium, but growth remained poor.

4.3.3 LDH as an Indicator of Cell Damage

Figure 4-11 shows LDH release from bioreactor experiments with 0° (#1) and 30° inclination (#4) respectively. At the beginning of the bioreactor cultures, higher LDH levels in the run with 30° inclination corresponded to lower viability of the culture upon inoculation (75% vs. 85% of the vertical experiment). But during the first 45 h when cells were growing exponentially, LDH release from these two experiments were equivalent. More LDH was then released in the vertical experiment than in the experiment with 30° inclination starting at 45 h. The small difference between the two experiments was likely an indication of more cell damage in the vertical bioreactor.

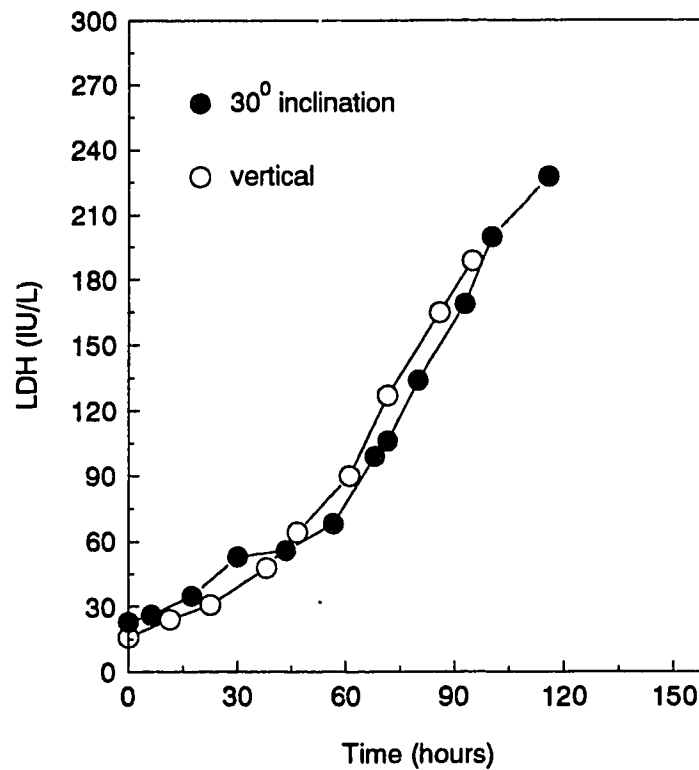


Figure 4-11. Comparison the time course of LDH release in the bioreactor between experiment #1 (vertical) and experiment #4 with 30° inclination.

4.3.4 Cell Sedimentation

Sedimentation of cells along the lower surface of the inclined-tube bioreactor was a strong function of the inclination angle at constant aeration rate (0.05 vvm in this series of bioreactor experiments). When the bioreactor tube was vertical, there was no sedimentation. A 10° inclination from the vertical gave some sedimentation, but the sedimentation layer was thin and transient. Cells were visible as a moving, white stream along the bottom of the bioreactor. As the inclination angle increased to 30°, more cells settled to the lower surface but the sedimented cells were flushed off the column surface by turbulent eddies and returned to the bulk liquid in an intermittent fashion. When the bioreactor tube was inclined 45° from vertical, however, cell settling was severe enough that sedimented cells in the immediate vicinity of the column surface became stagnant.

Cell sedimentation at 45° inclination was decreased when aeration rate was increased (Experiment #6). The step increase of air flow from 0.18 vvm to 0.24 vvm was insufficient to eliminate severe sedimentation, especially towards the lower end of the bioreactor vessel. These unusually high aeration rates caused more serious foaming. Growth was improved slightly (Figure 4-12) over the previous run of 45° inclination with 0.05 vvm of aeration. The maximum viable cell count was low, but it remained unchanged until approximately 120 h into the run. Correspondingly, antibody concentration reached 30 mg/L at the end of the experiment. This antibody titer was comparable with those from dish and spinner cultures, and better than that of the vertical bioreactor.

4.3.5 Reasons for Increased Antibody Production in the Inclined Bioreactor

If cells were preferentially floated to the gas-liquid interface during the stationary phase, then cell damage would be severe in the vertical column. Inclining the bioreactor at 10° and 30° would reduce flotation and prolong the stationary phase. This hypothesis was tested by measuring the flotation of cells into a foam layer in batch experiments. Neither live nor dead cells from different stages of the growth in a dish culture were preferentially removed with the overflowing foam, and therefore cell counts remained constant in the 45 min flotation experiments (Figure 4-13). These results were also confirmed by cell counts from the collected liquid of the foam phase. Fluctuations in the dead cell count were due to errors in counting few cells. Later flotation studies with cells from bioreactor cultures gave similar results. These hybridoma cells, therefore, did not undergo flotation in the bioreactor. These results are consistent with those obtained by Cherry and Hulle (Cherry and Hulle, 1992) from foam fractionation experiments with Sf-9 insect cells. Their study showed that cells were not preferentially carried into the foam phase. These results, however, contradict those reported by Bavarian et al. (1991) from microscopic observations. They observed insect cell attachment on bubbles which was a fundamental characteristic of active flotation. The degree of flotation and the role it plays in damage of cells in bioreactors are still not well defined. Flotation of cultivated

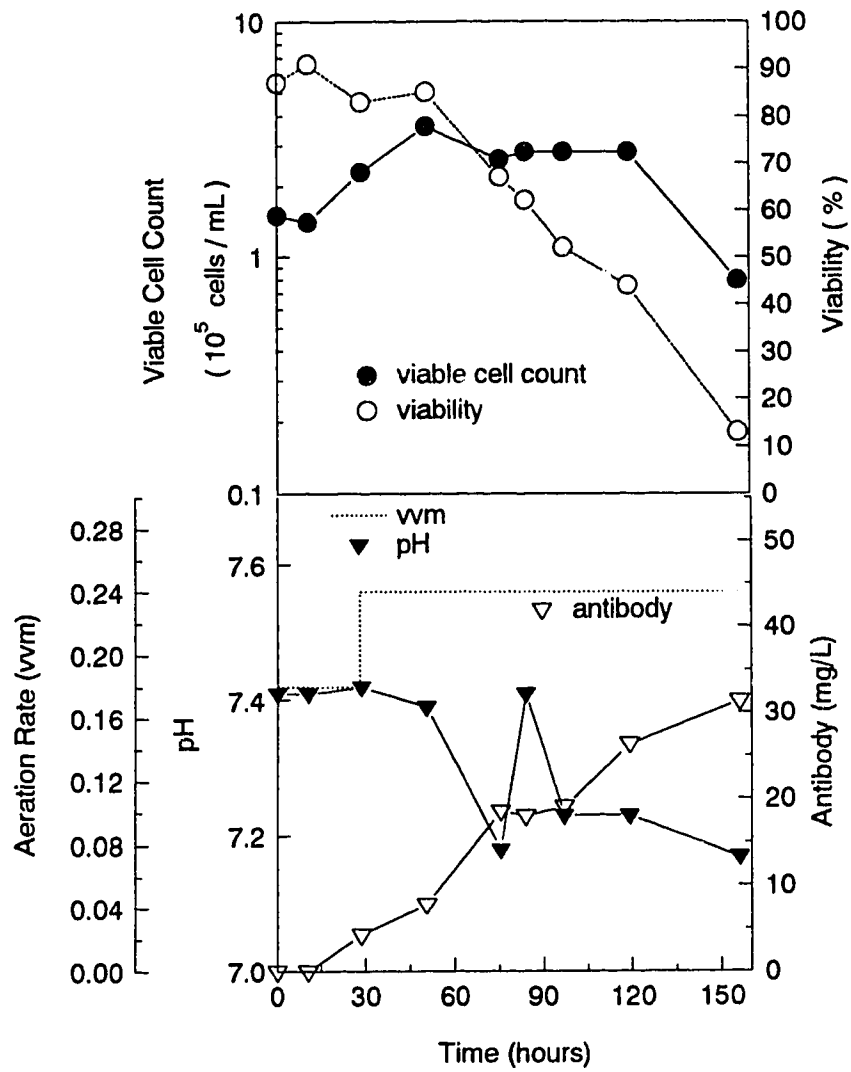


Figure 4-12. Growth and antibody production for bioreactor experiment #6 with 45°inclination and 0.18 to 0.24 vvm aeration rate.

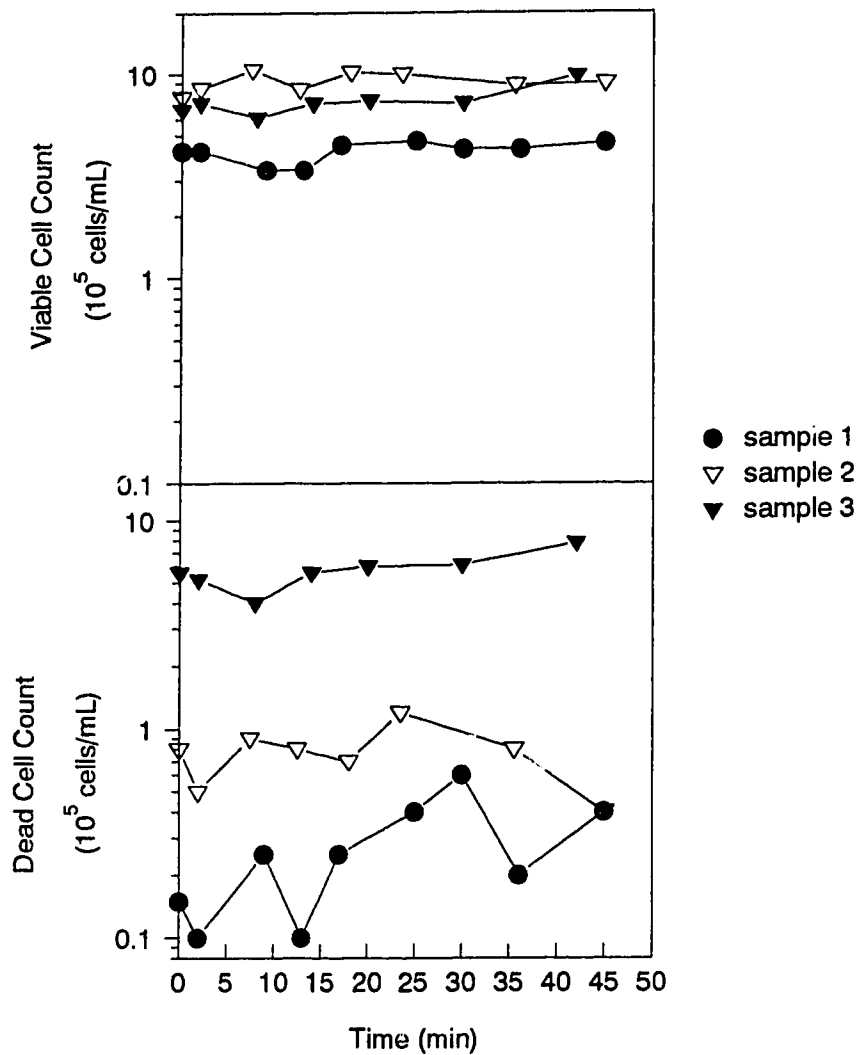


Figure 4-13. Viable and dead cell concentrations in the bubble column during a batch flotation experiment. Sample 1 was taken from mid-exponential growth phase at 35 h, sample 2 from stationary phase at 50 h, and sample 3 from death phase at 75 h.

animal cells would depend on medium properties, bubble size, and cell type or cell line.

Hybridoma cells from the stationary phase have been found to be more susceptible to shear forces compared to fast growing cells from the exponential growth phase (Peterson et al., 1988). The vertical bioreactor might have a more

turbulent hydrodynamic environment so that cells were undamaged during the exponential growth phase but were adversely affected during stationary phase. We do not, however, have experimental evidence for differences in hydrodynamic forces between the vertical and the inclined bioreactor.

4.4 CONCLUSIONS

1. At a constant sparging rate 0.05 vvm, the final antibody titers from bioreactor experiments at 10° and 30° inclination were higher than the vertical case. The maximal yield of 42 mg/L of antibody was higher than spinner or dish cultures which gave a yield of 30 mg/L.
2. Antibody was mainly released after the exponential growth phase. The doubling of antibody titer at an inclination angle of 30° corresponded to a prolonged stationary phase compared to the vertical case, in which the bioreactor was equivalent to a bubble column.
3. At 45° inclination, cell sedimentation along the lower surface of the bioreactor vessel gave a build-up of cells, especially towards the lower end of the bioreactor, and this stagnant sedimentation was likely the reason for poor growth and antibody formation. When the bioreactor was inclined at smaller angles, cell sedimentation was transient.

REFERENCES

- Applegate M.A., Stephanopoulos G. 1992. Development of a single-pass ceramic matrix bioreactor for large-scale mammalian cell culture. *Biotechnol. Bioeng.* **40**: 1056-1068.
- Aunins, J.G., Croughan, M.S., Wang, D.I.C., Goldstein, J.M. 1986. Engineering developments in homogeneous culture of animal cells: oxygenation of reactors and scaleup. *Biotechnol. Bioeng.* **17**: 699-723.
- Bavarian, F., Fan, L.S., Chalmers, J.J. 1991. Microscopic visualization of insect cell-bubble interactions. 1: Rising bubbles, air-medium interface, and the foam layer. *Biotechnol. Prog.* **7**: 140-150.

- Birch, J.R., Lambert, K., Thompson, P.W., Kenney, A.C., and Wood, L.A. 1987. Antibody production with airlift fermentors. p. 1-20. In *Large Scale Cell Culture Technology*, B.K. Lydersen, Ed. Hanser Publishers, Munich.
- Brennan, A. 1987. A suspension culture perfusion system for production of monoclonal antibodies. *ProBioTech (Suppl. Process Biochem.)* **22**: 7-8.
- Bugarski, B., et al. 1989. Performance of an external loop air-lift bioreactor for the production of monoclonal antibodies by immobilized hybridoma cells. *Appl. Microbiol. Biotechnol.* **30**: 264-269.
- Cherry, R.S. and Hulle, C.T. 1992. Cell death in the thin films of bursting bubbles. *Biotechnol. Prog.* **8**: 11-18.
- Doyle, C., Butler, M. 1990. The effect of pH on the toxicity of ammonia to a murine hybridoma. *J. Biotechnol.* **15**: 91-100.
- Handa-Corrigan, A., Emery, A.N., Spier, R.E. 1987. On the evaluation of gas-liquid interfacial effects on hybridoma viability in bubble column bioreactors. *Develop. Biol. Standard.* **66**: 241-253.
- Hirschel, M.D., Gruenberg, M.L. 1987. An automated hollow fiber system for the large scale manufacture of mammalian cell secreted product. p. 113-144. In *Large Scale Cell Culture Technology*, B.K. Lydersen, Ed. Hanser Publishers, Munich.
- Jones, B.N., Gilligan, J.P. 1983. O-phthaldialdehyde precolumn derivatization and reverse phase high performance liquid chromatography of polypeptide hydrolysates and physiological fluids. *J. Chromatog.* **266**: 471-482.
- Kunas, K.T., Papoutsakis, E.T. 1990. Damage mechanisms of suspended animal cells in agitated bioreactors with and without bubble entrainment. *Biotechnol. Bioeng.* **36**: 476-483.
- Lee, G.M., Chuck, A.S., Palsson, B.O. 1993. Cell culture conditions determine the enhancement of specific monoclonal antibody productivity of calcium alginate-entrapped S3H5/γ2bA2 hybridoma cells. *Biotechnol. Bioeng.* **41**: 330-340.
- Peterson, J.F., McIntire, L.V., Papoutsakis, E.T. 1990. Shear sensitivity of hybridoma cells in batch, fed-batch, and continuous cultures. *Biotechnol. Prog.* **6**: 114-120.
- Peterson, J.F., McIntire, L.V., Papoutsakis, E.T. 1988. Shear sensitivity of cultured hybridoma cells (CRL-8018) depends on mode of growth, culture age and metabolite concentration. *J. Biotechnol.* **7**: 229-246.

- Piret, J.M., Cooney, C.L. 1990. Immobilized mammalian cell cultivation in hollow fiber bioreactors. *Biotechnol. Adv.* **8**: 763-783.
- Reuveny, S., Velez, D., Macmillan, J.D., and Miller, L. 1986. Factors affecting cell growth and monoclonal antibody production in stirred reactors. *J. Immunol. Methods* **86**: 53-59.
- Smith, C.G., Greenfield, P.F. 1992. Mechanical agitation of hybridoma suspension cultures: metabolic effects of serum, pluronic F68, and albumin supplements. *Biotechnol. Bioeng.* **40**: 1045-1055.
- Su, W.W., Caram, H.S., Humphrey, A.E. 1992. Optimal design of the tubular microporous membrane aerator for shear-sensitive cell cultures. *Biotechnol. Prog.* **8**: 19-24.
- Watanabe, K. et al. 1991. Apparatus for floating animal cells in a double-bag container. U.S. Pat. No. 5,057,429.
- Whiteside, J.P., Farmer, S., Spier, R.E. 1985. The use of caged aeration for the growth of animal cells on microcarriers. *Develop. Biol. Standard.* **60**: 28? 290.
- Wu, J., Daugulis, A.J., Faulkner, P., Goosen, M.F.A. 1992. Correlation of LDH activity with loss of insect cell viability: an assessment of the LDH assay. *Biotechnol. Techniques* **6**: 335-340.

Chapter 5

Loss of Shear Sensitivity in Hybridoma Cells

5.1 INTRODUCTION

Agitation and/or aeration are frequently used as means of providing mixing and oxygen to animal cell bioreactors, but the resultant hydrodynamic forces can be detrimental to the cells in cultivation (Papoutsakis, 1991; Cherry, 1993). Bioreactor productivity is hindered as a result of reduced cell growth due to fluid-mechanical damage of the cells. Addition of protective agents such as serum and pluronic is a common practice to alleviate or overcome the problem of shear damage, although the underlying mechanisms are still in dispute (Murhammer and Goochee, 1990; Michaels, et al., 1991). Other researchers have found that shear sensitivity depended on the bioreactor operation mode (Petersen et al., 1990), growth rate (Martens et al., 1993), age of the culture in the case of batch operation (Petersen et al., 1988). Petersen et al. (1990) found that actively growing cells were less sensitive to shear, and that shear sensitivity did not depend on the growth rate, but a more recent report by Martens et al. (1993) indicated that shear sensitivity increased with increasing growth rate in an airlift bioreactor, and they attributed the discrepancy with the previous report (Petersen et al., 1990) to the different methods used in their shear sensitivity studies. Petersen et al. (1988) also showed that, in a batch culture, cells from the lag and stationary phase were more sensitive to shear than cells from the exponential growth phase.

Shear sensitivity, however, also depends on the cultivation history. Petersen et al. (1988) used hybridoma cells from the same T-flask to inoculate a T-flask and a 200 rpm spinner flask in parallel. The cultures were then sampled and sheared in a viscometer, and they found that the cells from the spinner were considerably less sensitive to shear than those from the T-flask. They therefore concluded that cells were more tolerant to shear due to prior exposure (Petersen et al., 1988). This type of acclimatization was further demonstrated by Boucheron et al. (1993) who found that a period of four-week acclimatization of a hybridoma cell line in roller bottles enabled cells to grow to 1.7×10^6 cell/mL in a subsequent spinner culture, but the

same cells were not able to grow over 7×10^5 cell/mL without the acclimatization period. They also indicated that cells grown over a prolonged period of time in static cultures lost their acclimatization characteristics and were therefore no longer able to grow under agitation in spinners. The mechanism of this behavior is unknown.

We described a novel bioreactor design in the previous chapter (see Chapter 4), i.e. an Inclined-plate Bioreactor. As a prototype of this design, an inclined-tube bioreactor was built from glass and used to grow a murine hybridoma cell line. We found that, given constant sparging rate, cell growth and antibody production were a strong function of the inclination angle. In those bioreactor experiments, exactly the same protocol for inoculum preparation was strictly followed for each experiment. But as we have discussed at the beginning of the introduction, cultivation history affected shear sensitivity of cells. Therefore, the history of bioreactor inoculum preparation could influence bioreactor performance.

This study is, therefore, to investigate the effect of cell line acclimatization on shear sensitivity, and its implication on operation and performance of the bioreactor based on the new design concept, especially in terms of cell growth and product formation.

5.2 MATERIALS AND METHODS

Cell line, culture medium, bioreactor setup, and analytical methods have been previously described (see Chapter 4). The procedure for inoculum preparation was, however, different in this study. A vial of cells, from a working cell bank which had been prepared for a previous study (see Chapter 4), was thawed into culture medium supplemented with 15% fetal bovine serum (FBS, Gibco, Grand Island, New York) in a tissue culture dish. Cells then recovered from freezing after two more passages in medium with 10% FBS; viable cell count increased from 1×10^5 to 7.8×10^5 cells/mL within 48 h with a viability of 90%. Cells were then transferred into medium with 5% FBS and maintained in dishes. Cells were transferred to dishes containing fresh medium every two days, with a starting viable cell count of 1×10^5 cells/mL. After every 6-7 transfers, a portion of the cells were grown in spinner flasks to prepare inoculum for the bioreactor.

Table 5-1 shows the matrix of four operating conditions for bioreactor experiments. The numbers were assigned to indicate the actual sequence in which these bioreactor experiments were carried out. A constant sparging rate of 0.05 vvm was used for all bioreactor experiments, but three different angles of inclination included vertical, 20°, and 45° from vertical. Control experiments in dishes and spinner flasks were carried out to investigate changes in cell line performance under static or low-shear culture conditions, and provided internal comparisons with the corresponding bioreactor culture.

Table 5-1. Organization of bioreactor experiments.

Experiment #	Aeration (vvm)	Inclination	Dish Control	Spinner Control
1	0.05	vertical	no	no
2	0.05	20°	yes	yes
3	0.05	45°	yes	yes
4	0.05	vertical	yes	yes

5.3 RESULTS AND DISCUSSION

Typical bioreactor culture and control experiments for unacclimatized cells have been previously presented (see Chapter 4). These results serve as a basis for comparison of cell line performance at different angles of inclination, and at different stage of cell line acclimatization.

5.3.1 Cell Line Acclimatization in Control Experiments

Figure 5-1 summarizes cell growth and antibody production in tissue culture dishes as control experiments. Unacclimatized cells, which were thawed from stock freezing vials and maintained or expanded for bioreactor inoculum preparation in tissue culture dishes within two weeks, are included to serve as a basis for comparison. Different symbols in the plots indicate that cells had been

maintained in tissue culture dishes for different periods of time, or different passage numbers before the respective control experiments were carried out.

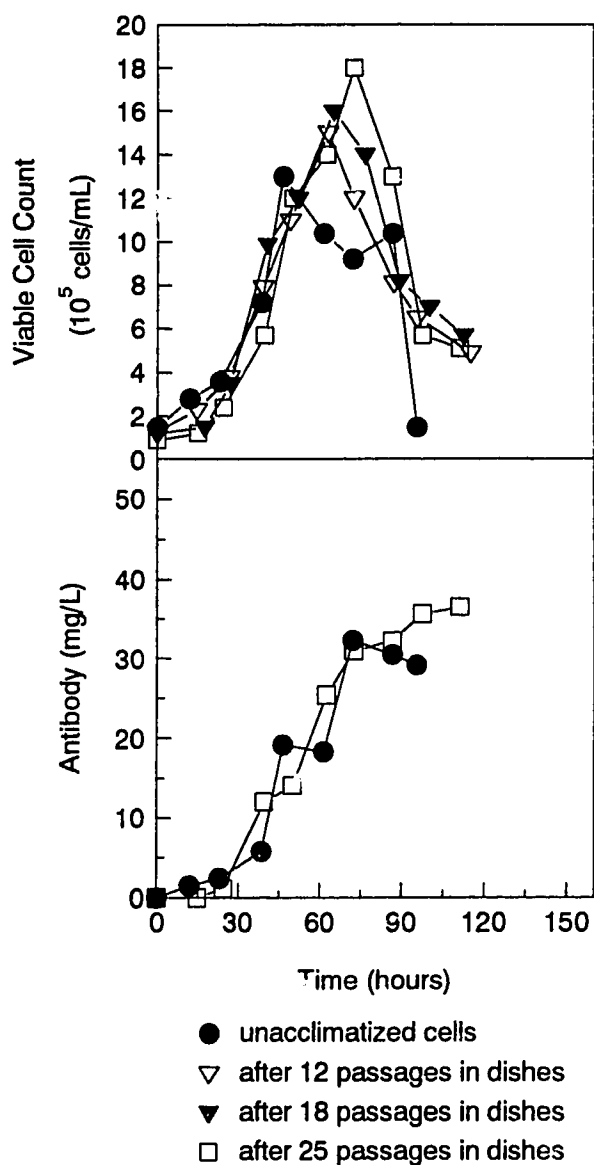


Figure 5-1. Viable cell count and antibody formation as a function of time in tissue culture dishes. Different symbols indicate that cells had been subcultured for different periods of time in tissue culture dishes prior to inoculating the dishes as control experiments for their respective bioreactor culture.

Cells entered an exponential growth upon transfer in all cases, and the exponential growth for all cells were similar. Unacclimatized cells reached a maximal viable population of 1.3×10^6 cells/mL at 45 h. For cells after 25 passages in dishes, however, the exponential growth extended to 75 h, and an increased maximum of 1.8×10^6 cells/mL in viable cell count was achieved. Cells maintained in dishes for a prolonged period of time, therefore, demonstrated better growth.

Figure 5-1 also gives the comparison in antibody formation for unacclimatized cells and those cells which had been maintained in dishes for 25 passages (approximately a period of 52 d). Antibody formation, however, was similar up to 75 h for both cases, in contrast to the growth enhancement due to cell line acclimatization. The final antibody titer for the acclimatized cells was slightly higher than that for the unacclimatized cells (36 mg/L compared to 30 mg/L), but the difference was not significant.

Parallel control experiments for bioreactor cultures were also carried out in spinner flasks (250 mL). Figure 5-2 gives the cell growth and antibody production for unacclimatized cells and cells which had been acclimatized to the culture medium. Growth in spinner flasks was generally not as good as those found in tissue culture dishes. For the first 45 h, all cells showed similar exponential growth and antibody formation. Then acclimatized cells grew much better than unacclimatized cells, in terms of both the extent of growth and the maximal viable cell count. For the unacclimatized cells, viable cell count reached a maximum of 8×10^5 cells/mL, and then quickly dropped upon entering the death phase. In comparison, the acclimatized cells had a viable cell population for a total duration of approximately 45 h. Correspondingly, antibody titer reached 46 mg/L compared to 30 mg/L for the unacclimatized cells.

Figure 5-3 shows the effect of passage number on the antibody producing capacities in dishes and spinner flasks. The final antibody titer remained unchanged at ca. 30 mg/L in both dishes and spinners after cells were transferred in dishes for 12 passages. As cells had been maintained for an even longer period of time, however, final antibody titers in both dishes and spinners were increased. For example, enhancement of antibody titer was approximately 50% in spinner cultures for 25 passages.

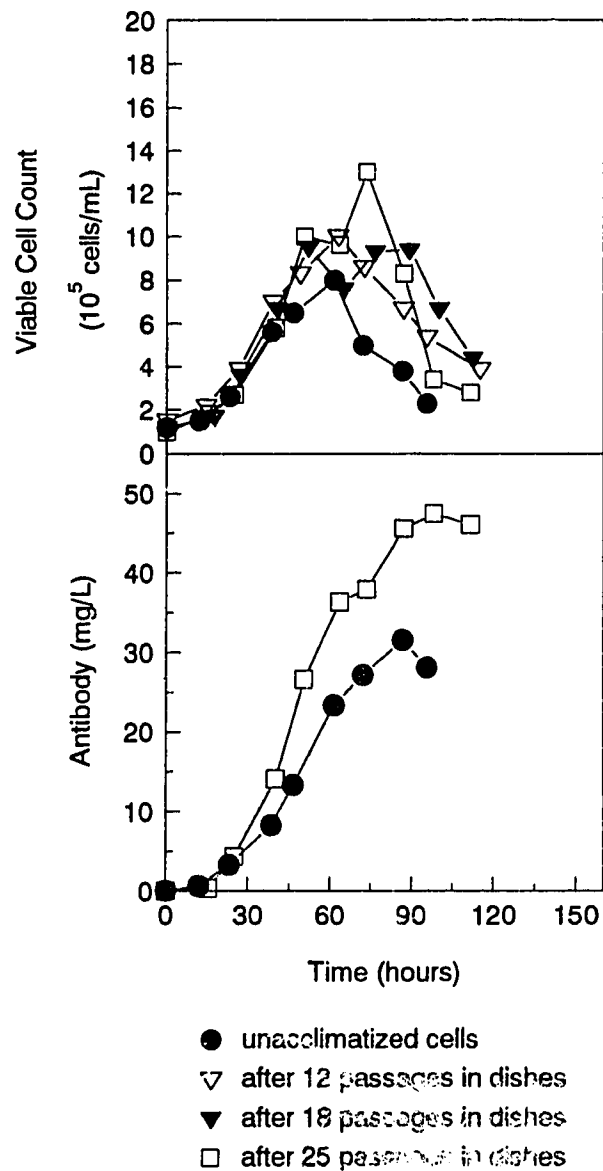


Figure 5-2. Viable cell count and antibody formation as a function of time in spinner flasks. Different symbols indicate that cells had been subcultured for different periods of time in tissue culture dishes prior to inoculating the spinners as control experiments for their respective bioreactor culture.

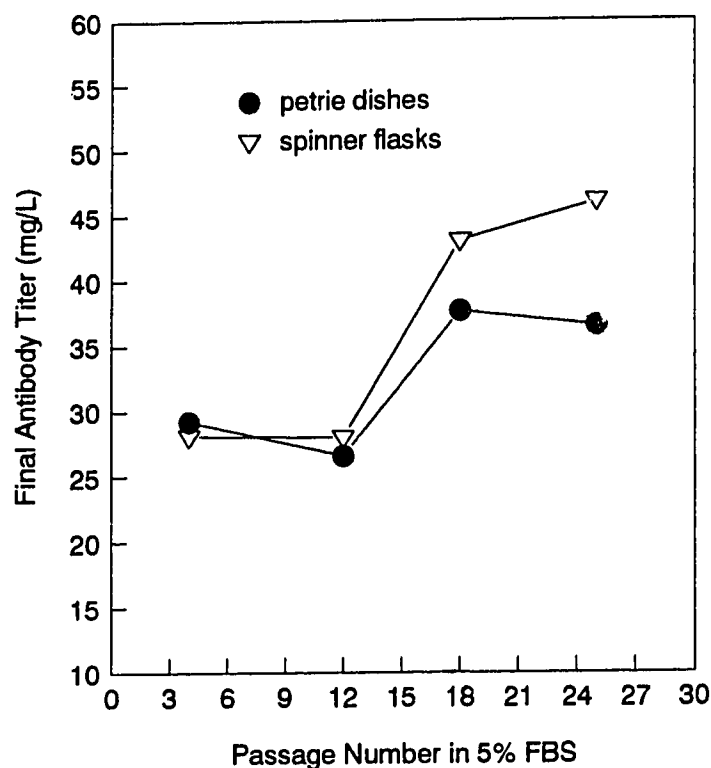


Figure 5-3. Effect of passage number of subculture on the final antibody titer in tissue culture dishes and in spinner flasks as control experiments for bioreactor cultures.

5.3.2 Cell Line Acclimatization in Bioreactor Experiments

Figure 5-4 shows the cell growth and antibody production in the vertical tube bioreactor. When the bioreactor inoculum was prepared following 7 passages in tissue culture dishes (Experiment #1), both growth and antibody formation were identical to those from the bioreactor culture with unacclimatized cells. In bioreactor experiment #4, however, inoculum was prepared after 25 passages in dishes. A higher maximum in viable cell count ca. 1×10^6 cells/mL was obtained at 60 h, in comparison to ca. 6×10^5 cells/mL for unacclimatized cells. Final antibody titer was 37 mg/L, approximately twice as much as that from the bioreactor experiment with unacclimatized cells. 25 mg/L of antibody was produced within the first 60 h during the exponential growth phase, compared to 8 mg/L of antibody produced for the same period of time from the unacclimatized culture.

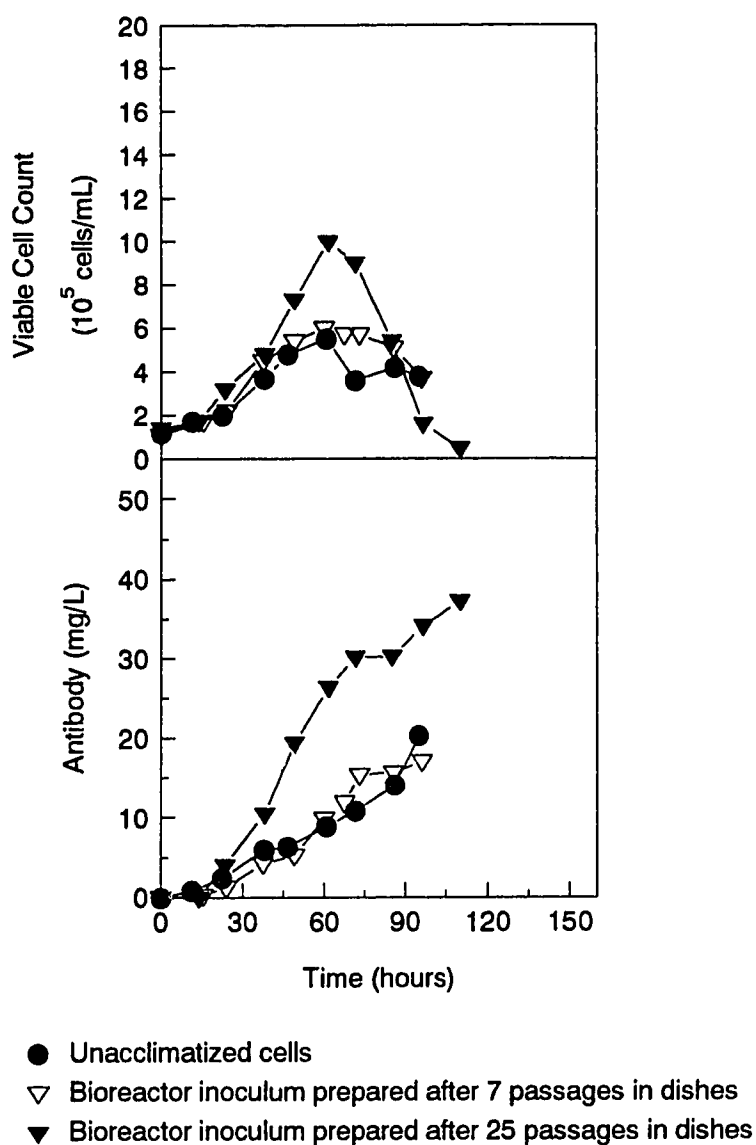


Figure 5-4. Viable cell count and antibody formation as a function of time from the vertical bioreactor. Different symbols show that cells had been subcultured in dishes for different periods of time prior to inoculum preparation for bioreactor cultures.

In order to investigate the effect of cell line acclimatization on the performance of the inclined bioreactor, culture experiments were carried out with

both unacclimatized cells and acclimatized cells for the inclination angle of 45°. Figure 5-5 compares both cell growth and antibody production. For cells without a prolonged period of acclimatization, viable cell population did not increase significantly after inoculation. In correspondence to this poor growth, final antibody titer was only 12 mg/L. In contrast, the same cell line, after subculturing in dishes for 18 passages, was able to grow to a maximal viable cell count of 1.1×10^6 cell/mL. The final antibody concentration reached 41 mg/L. Therefore, the acclimatized cells had similar performance in the spinner flasks and in the bioreactor inclined at 45° from vertical.

When the tube bioreactor was inclined at 45° from vertical, cell settling was observed along the lower tube wall. This settling appeared to be stagnant towards the bottom of the inclined bioreactor. We have previously attributed poor growth and low antibody titer to the stationary buildup of cells along the lower bioreactor wall at the inclination angle of 45° (see Chapter 4). After 18 passages in dishes, cells seemed to have become more tolerant to cell segregation in the bioreactor. The underlying mechanisms, however, still remained to be investigated. Both cell growth and antibody production were comparable to those from spinner flasks as controls.

5.3.3 Effect of Cell Line Acclimatization on Bioreactor Performance

In our previous study of the inclined bioreactor, we found that both growth and antibody production were a strong function of the inclination angle for a constant sparging rate of 0.05 vvm (see Chapter 4). Table 5-2 summarizes the maximum of viable cell count and final antibody titer as a function of inclination angle for both unacclimatized cells and acclimatized cells. For the unacclimatized cells, the maximal viable cell count was similar for vertical, 10°, and 30° from vertical, but growth was poor at 45° inclination. The maximal antibody titer was achieved at an inclination angle of 30°. We have previously related this high antibody yield to a prolonged stationary phase at 30° inclination which did not exist for vertical bioreactor. For the acclimatized cells, the maximal viable cell count was approximately 1×10^6 cells/mL which was independent on the inclination angle and significantly higher than the case when the cells were yet to be acclimatized (6×10^5 cells/mL for 0°). Antibody titer increased from 17 mg/L to ca. 40 mg/L,

which was consistent with the sequence in which these bioreactor experiments were carried out and was not a function of inclination angle.

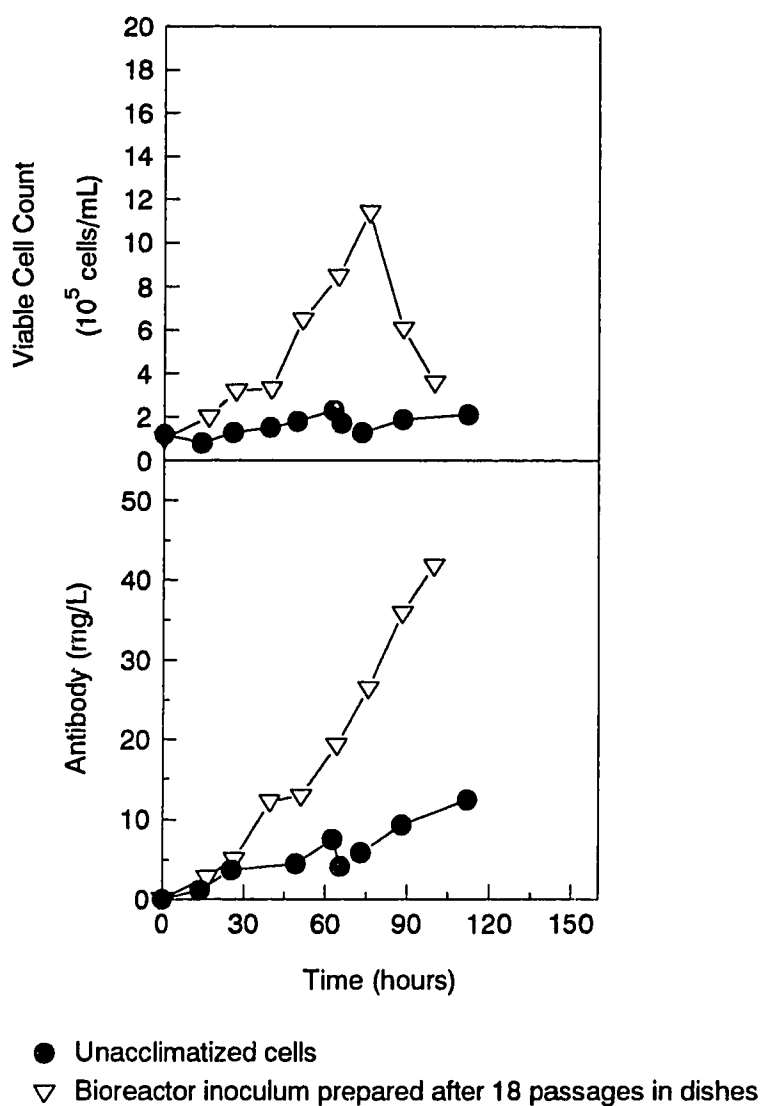


Figure 5-5. Viable cell count and antibody formation as a function of time from the bioreactor inclined at 45° from vertical. Different symbols show that cells had been subcultured in dishes for different periods of time prior to inoculum preparation for bioreactor cultures.

Table 5-2. Maximal viable cell count and antibody titer achieved for different inclination angles of the bioreactor: a comparison between unacclimatized and acclimatized cells.

Unacclimatized Cells			Acclimatized Cells		
Inclination angle	Max. (cell/mL)	Antibody (mg/L)	Inclination angle	Max. (cells/mL)	Antibody (mg/L)
0°	5.5×10^5	20.3	0°	6.0×10^5	17.0
10°	7.9×10^5	33.7	20°	9.5×10^5	23.2
30°	6.0×10^5	42.2	45°	1.1×10^6	41.8
45°	2.3×10^5	12.5		1.0×10^6	37.3

5.3.4 LDH Release

LDH release from cells into the culture medium has been frequently used as an indicator of the physiological state of the cells (Peterson et al., 1990; Wu et al., 1992). LDH concentration in the culture medium increases as cells are physically torn apart or dying cells excrete the intracellular enzyme into the medium. Assuming that LDH release was coupled to death, and there was no decay of LDH, then

$$\text{Death rate} = k_d X \quad (1)$$

and

$$\text{Rate of LDH release} = \frac{dC_{LDH}}{dt} = \alpha_{LDH} k_d X = k_{LDH} X \quad (2)$$

where C_{LDH} is the LDH concentration in the culture medium, X is the viable cell count, k_d is the apparent death rate, α_{LDH} is the LDH release per cell, and k_{LDH} is the specific LDH release rate. Integrating equation (2) gives

$$C_{LDH} = k_{LDH} \int X \cdot dt + C_{LDH}(t=0) \quad (3)$$

Plotting C_{LDH} against $\int X \cdot dt$ would yield a straight line, the slope of which is then k_{LDH} , the specific LDH release rate. Figure 5-6 gives a representative plot which shows two distinct linear relationships. The linear regression line with smaller slope corresponds to the exponential growth phase in which cells were actively growing and LDH was released from a small fraction of damaged or dying cells at a relatively slower rate (lower death rate k_d). The larger slope of the later section line reflects elevated LDH release as cells entered the stationary or death phase in which both viability and viable cell population were quickly dropping, and death rate increased.

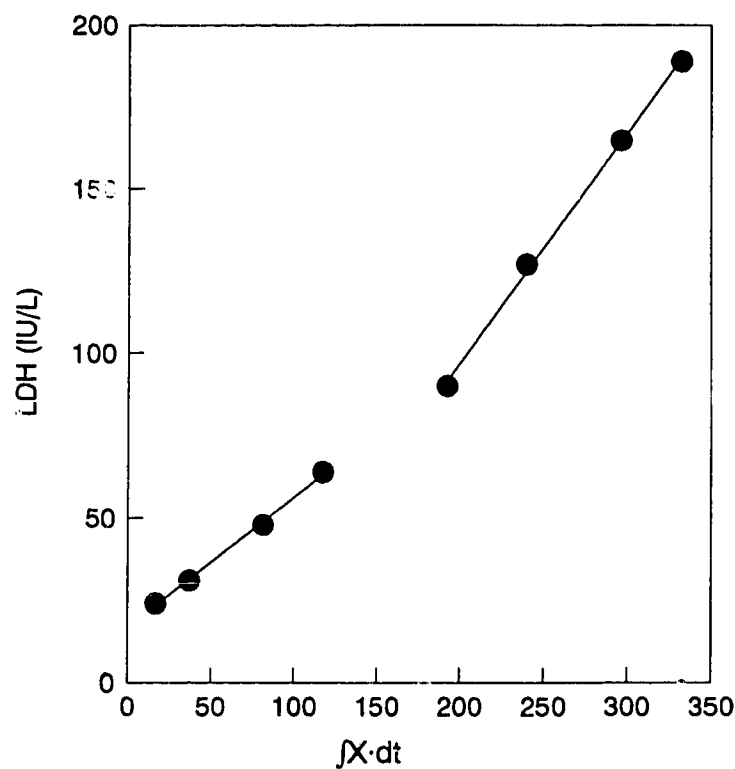


Figure 5-6. Plot of LDH vs. $\int X \cdot dt$ yields two distinct straight lines, slopes of which give the specific LDH release rates.

Table 5-3 shows LDH release in static culture (tissue culture dishes as controls) and in low-shear environment (spinner flasks as controls), comparing unacclimatized cells and acclimatized cells.

Table 5-3. LDH release in control experiments.

	Controls	K _{LDH} (IU/h/10 ⁹ cells)	
		Exp. Growth	Post Exp.Growth
Unacclimatized Cells	Dish	1.2	5.8
	Spinner	1.4	6.7
Acclimatized Cells (25 passages)	Dish	1.4	6.3
	Spinner	1.4	4.1

LDH release rate was much higher past the exponential growth phase. During the exponential growth phase, the specific LDH release rate was consistently low (1.4 IU/h/10⁹ cells). After prolonged subculture in dishes (25 passages), LDH release rate remained unchanged compared to the unacclimatized cells. This will serve a basis for comparison between different bioreactor experiments as higher LDH release rates in the bioreactor were likely due to cell damage by fluid-mechanical forces.

Table 5-4 lists the calculated specific LDH release rates for bioreactor experiments in a sequence in which they were actually carried out. There was no selective trend for the LDH release rates in the stationary and/or death phase. When the cells were exponentially growing, however, LDH accumulation in the culture medium was a good indicator of cell damage. We have previously cautioned that LDH determination as a measurement of cell damage was correct and effective only for the exponential growth phase before cell viability started to drop dramatically in a batch culture (see Chapter 4). This is further confirmed here by the calculations of the specific LDH release rates.

Table 5-4 shows that the specific LDH release rates of the acclimatized cells were consistently lower than that of the unacclimatized cells, regardless of the inclination angle of the bioreactor. When the bioreactor was vertical (0° inclination), the specific LDH release rate decreased as a result of prolonged

subculture in the dishes. Therefore, cells became physically more tolerant to hydrodynamic forces in the bioreactor due to cell line acclimatization by means of a series of transfer in tissue culture dishes prior to inoculum preparation.

Table 5-4. Specific LDH release rates for bioreactor experiments.

Experiment #	Inclination	K _{LDH} (IU/h/10 ⁹ cells)	
		Exp. Growth	Post Exp. Growth
Unacclimatized Cells	0°	4.0	7.0
1	0°	3.2	6.1
2	20°	1.9	5.8
3	45°	2.8	6.4
4	0°	2.5	8.6

5.3.5 Glucose Consumption

In some reported bioreactor studies, cell growth and product formation stopped as a direct result of glucose depletion from the culture medium (Boucheron et al., 1993; Smith and Greenfield, 1992). In our bioreactor experiments, therefore, glucose consumption was always monitored. In all cases, approximately 2 mM of glucose was still left at the end of each and every bioreactor culture, even though the consumption rates varied significantly for different bioreactor experiments. Figure 5-7 gives the time course of glucose consumption for two vertical bioreactor experiments, comparing the unacclimatized cells and the acclimatized cells. Increased glucose consumption by the acclimatized cells corresponded to better growth due to cell line acclimatization (same yield coefficient for the acclimatized cells and unacclimatized cells).

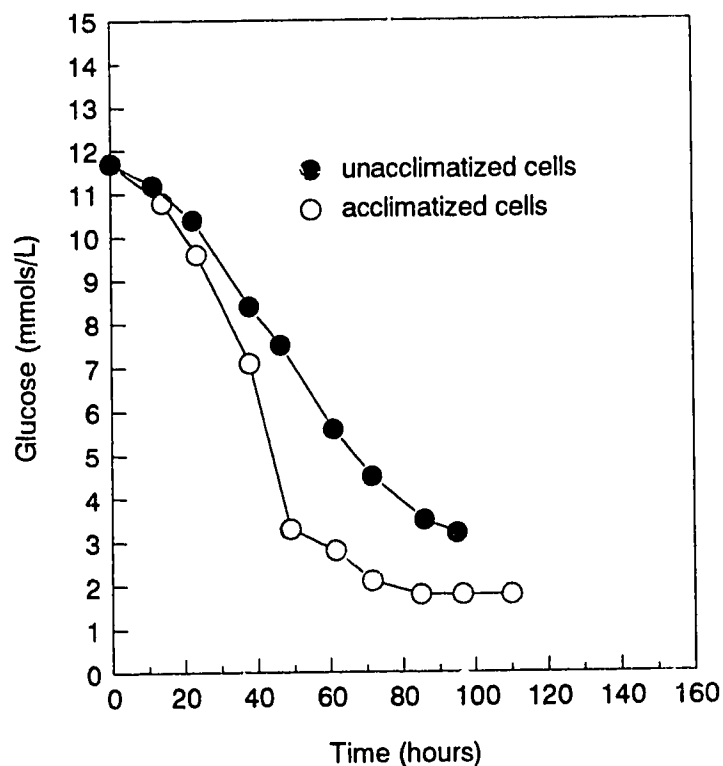


Figure 5-7. Time course of glucose consumption for two vertical bioreactor experiments, comparing the unacclimatized cells with the acclimatized cells.

Table 5-5 summarizes the specific glucose consumption rates for different bioreactor experiments. Glucose consumption rate was always higher in the exponential growth phase when cells were actively growing than in the stationary and/or death phase. However, there was no selective trend in the comparison of glucose consumption during the exponential growth phase for all bioreactor experiments. In the discussion of LDH as an indicator of cell damage, we suggested that cell line acclimatization as a result of prolonged maintenance in dishes rendered cells more tolerant to shear. In this series of bioreactor experiments, however, effects on glucose consumption due to cell line acclimatization were not significant.

Table 5-5. Specific glucose consumption rates for bioreactor experiments.

Experiment #	Inclination	K _{GLU} (mmol/h/10 ⁹ cells)	
		Exp. Growth	Post Exp. Growth
Unacclimatized Cells	0°	0.378	0.173
1	0°	0.382	0.088
2	20°	0.317	0.053
3	45°	0.446	0.031
4	0°	0.501	0.039

5.4 CONCLUSIONS

1. Prolonged subculture in tissue culture dishes prior to inoculum preparation resulted in acclimatization of the cell line as demonstrated by better cell growth and antibody production, both in control cultures and in bioreactor cultures.
2. Cells became acclimatized to medium as demonstrated by better yield, and became more resistant to shear stress in the bubble column (simultaneous effect).
3. Glucose consumption was not affected by the cell line acclimatization.

REFERENCES

- Boucheron, P., Andre, G., Brodeur, B.R., Larose, Y., and Chavarie, C. 1992. Response and adaptation of hybridoma cells to shear stress in agitated cultures. Personal communications.

- Cherry, R.S. 1993. Animal cells in turbulent fluids: details of the physical stimulus and the biological response. *Biotechnol. Adv.* **11**: 279-299.
- Handa-Corrigan, A., Emery, A.N., Spier, R.E. 1987. On the evaluation of gas-liquid interfacial effects on hybridoma viability in bubble column bioreactors. *Dev. Biol. Stand.* **66**: 241-253.
- Kunas, K.T., Papoutsakis, E.T. 1990. Damage mechanisms of suspended animal cells in agitated bioreactors with and without bubble entrainment. *Biotechnol. Bioeng.* **36**: 476-483.
- Martens, D.E., de Gooijer, C.D., van der Velden-de Groot, C.A.M., Beuvery, E.C., and Tramper, J. 1993. Effect of dilution rate on growth, productivity, cell cycle and size, and shear sensitivity of a hybridoma cell in a continuous culture. *Biotechnol. Bioeng.* **41**: 429-439.
- Michaels, J.D., Peterson, J.F., McIntire, L.V., and Papoutsakis, E.T. 1991. Protection mechanisms of freely suspended animal cells (CRL 8018) from fluid-mechanical injury: viscometric and bioreactor studies using serum, Pluronic F68 and polyethylene glycol. *Biotechnol. Bioeng.* **38**: 169-180.
- Murhammer, D.W., and Goochee, C.F. 1990. Structural features of nonionic polyglycol polymer molecules responsible for the protective effect in sparged animal cell bioreactors. *Biotechnol. Prog.* **6**: 142-148.
- Papoutsakis, E.T. 1991. Fluid-mechanical damage of animal cells in bioreactors. *Trends in Biotechnol.* **9**: 427-437.
- Peterson, J.F., McIntire, L.V., Papoutsakis, E.T. 1990. Shear sensitivity of hybridoma cells in batch, fed-batch, and continuous cultures. *Biotechnol. Prog.* **6**: 114-120.
- Peterson, J.F., McIntire, L.V., Papoutsakis, E.T. 1988. Shear sensitivity of cultured hybridoma cells (CRL-8018) depends on mode of growth, culture age and metabolite concentration. *J. Biotechnol.* **7**: 229-246.
- Smith, C.G., Greenfield, P.F. 1992. Mechanical agitation of hybridoma suspension cultures: metabolic effects of serum, Pluronic F68, and albumin supplements. *Biotechnol. Bioeng.* **40**: 1045-1055.
- Wu, J., Daugulis, A.J., Faulkner, P., Goosen, M.F.A. 1992. Correlation of LDH activity with loss of insect cell viability: an assessment of the LDH assay. *Biotechnol. Techniques* **6**: 335-340.

Chapter 6

Hydrodynamics and Mixing in an Inclined Bubble Column

6.1 INTRODUCTION

One major engineering problem in animal cell bioreactors is cell damage by a variety of hydrodynamic forces created by agitation and/or sparging (Papoutsakis, 1991). In conventional bioreactors, such as the stirred-tank bioreactor and the bubble column bioreactors, cell-bubble interactions at the gas-liquid interface have been found to be responsible for cell damage (Handa-Morgan, 1987; Kunas and Papoutsakis, 1990). In light of these mechanisms, a novel bioreactor concept, i.e. Inclined-plate Bioreactor, was proposed (see Chapter 4) in which gravity was used to achieve the separation of cells from bubbles within two inclined plates (see Figure 4-1). Due to the inclination of the two parallel plates, bubbles travel along the upper plate and circulate the liquid as illustrated in Figure 4-1. Such hydrodynamic characteristics greatly reduce cell-bubble contact, while bulk mixing and aeration due to well developed liquid circulation are not sacrificed. In contrast, when the plates are vertical, the bioreactor behaves like a rectangular bubble column.

As part of the design and scale-up, we needed to investigate the hydrodynamics and mixing in the Inclined-plate Bioreactor. Mixing studies in bubble columns found that slight departures from vertical alignment ($< 2^\circ$) could significantly increase the axial dispersion coefficient (Tinge and Drinkenburg, 1986; Rice and Littlefield, 1987). Valdes-Krieg et al. (1975) observed that vertical misalignment of 1° strongly affected surfactant removal in a foam fractionation column. Gas holdup was found to decrease with increasing inclination angle and a correlation was presented by Yamashita (1985) for inclination angles up to 30° .

In the Inclined-plate Bioreactor, the only driving force for liquid circulation and mixing is the rising air bubbles. Masliyah et al. (1993) have previously studied rising of a single bubble in a stagnant fluid in an inclined rectangular column. For low bubble Reynolds number and Weber number, the drag coefficient of the

bubbles was found to be uniquely correlated with the air bubble Reynolds number Re_b and Eotvos number Eo_m , which were modified to include the inclination angle. The correlation was given as:

$$C_{Db} = (16 / Re_b)(1 + 0.077 Re_b^{0.65})(1 + 1.31 Eo_m^{0.51}) \quad (1)$$

Corresponding bubble sizes were in the range of 1.7 - 2.9 mm. To compliment these results in view of bioreactor scale-up, both single bubble and swarms of bubbles of larger size also require investigation.

When a swarm of bubbles rises against the upper wall of an inclined rectangular bubble column, bulk liquid circulation will be developed (see Figure 4-1). Liquid velocity and its profile in the column are important for hydrodynamic characterization. As an important experimental tool, a number of flow visualization schemes, such as particle seeding, liquid tracers, tuft method, and Laser Doppler Anamometry (LDA) have been frequently used (Gad-el-Hak, 1988; Kresta, 1992; Freymuth, 1993). In other studies, a different flow visualization scheme, i.e. the hydrogen bubble technique was used to characterize the flow field (Davis and Fox, 1967; Rodkiewicz and Roussel, 1973; McAlister and Carr, 1979; Merzkirch, 1987). The basic principle is the electrolysis of water. If a very fine wire is used for the cathode and placed normal to the flow, a row of microhydrogen bubbles will be formed along the wire, carried away with the flow and deformed according to the local velocity profile. Successive rows of hydrogen bubbles produced by pulsing the voltage at a constant frequency appear as "time lines" on the photographs which are then digitized to calculate the local velocity and its profile.

Mixing studies in chemical reactors have frequently used non reactive tracers (Levenspiel, 1984). One of the most frequently used was the technique of injecting a salt solution and measuring the conductivity response at a distance from the injection point (Ohki and Inoue, 1970; Tinge and Drinkenburg, 1986; Wilkinson, et al., 1993). For characterization of mixing in chemical reactors, the one-dimensional axial dispersion model has been widely used (Baird and Rice, 1975; Tinge and Drinkenburg, 1986; Wilkinson et al., 1993; Ohki and Inoue, 1970). In most cases, however, the axial dispersion model is merely used as a

sophisticated form of curve-fitting. The theoretical basis for applying this model to the actual mixing problem has been frequently neglected, and the dispersion coefficients obtained from the curve-fitting results likely do not contain any physical information, and will find very little use for the understanding and scale-up of the involved mixing processes. Recently, scale-up of bioreactors were based on mixing models (Mayr et al., 1994; Nagy et al., 1994). A physical mixing model derived from the tanks-in-series concept was used to describe mixing in a stirred-tank bioreactor equipped with three Rushton turbines (Mayr et al., 1994). Four adjustable parameters contained in this model depended on the operational conditions of the bioreactor. The pitfall of this model was that it was only applicable to stirred-tank bioreactors with Rushton turbines. Different models have to be used for other types of bioreactors. In general, more sophisticated mixing models than the simple axial dispersion model are then required in order to reflect the true hydrodynamic characteristics in bioreactors. Scale-up based on these mixing models will be possible only when parameters contained in these models can necessarily relate to some measurable parameters in lab-scale bioreactors.

There is no literature available for the hydrodynamics and mixing in an inclined bubble column, except for the limited studies on bubble columns with departure from vertical by a few degrees (e.g. $< 2^\circ$). The objectives of this study, therefore, are several fold. To complement the previous study of single bubble rising in an inclined bubble column, we first studied a swarm of bubbles of larger size (2.5 - 4.0 mm) rising in the same bubble column. Profiles of liquid velocity were then measured using the hydrogen bubble technique. Finally, the salt injection method was used to characterize mixing in the inclined bubble column. The inclination angle in this study was varied in the range of 0 - 45° . Air sparging rates were chosen to be typical of those used for conventional bioreactors for animal cell cultures.

6.2. MATERIALS AND METHODS

6.2.1 Inclined Bubble Column

Figure 6-1 shows the experimental set-up for the inclined bubble column. The rectangular column was constructed of Plexiglass™ except for the upper surface

which was made of glass. When the column was inclined from vertical, air bubbles rose against the upper surface and the glass surface was good for visualization and photography of the rising bubbles. The column had a total length of 123 cm, and a square cross-section with a side length of 53 mm.

A sparger was constructed of a rectangular copper tube which had a dimension of 6×6×56 mm. 25 holes with a diameter of 0.33 mm were drilled along the tube. The sparger was placed 25 mm above the bottom of the bubble column, and was inserted into the bubble column from side. Air was provided via a mass flow meter (Unit Instrument) which had been previously calibrated. Sparging rates used in this study, in the range 0.001 to 0.06 vvm (volume of air per min per liquid volume), were typical for sparged bioreactors for animal cell cultures. Superficial gas velocity based on the entire cross section of the column can be calculated by

$$u_g = \frac{G \cdot V}{A} \cdot \frac{1}{60} = G \cdot H \cdot \frac{1}{60} \quad (2)$$

For $H = 120$ cm, $u_g = 2 \cdot G$ (cm/s).

Tap water at room temperature (21.5°C) was used as working fluid throughout this study. The column was always filled up to 120 cm except for those experiments in which the liquid height was varied to obtain a different aspect ratio.

6.2.2 Flow Visualization

The cathode was a tungsten wire with a diameter of 0.05 mm, placed 50 cm from the bottom of the column. The tungsten wire was mounted on a support which was a copper wire coated with enamel for insulation and marked with white finger nail oil for the purpose of calibration. The anode was a stainless steel wire (1 mm in diameter), and placed 63.5 cm up the column. Voltage pulses of 30 - 40 volts at a repetition rate of 3 cps (cycles per second) were generated by the DC power (HP Harrison 6200B) and pulse generator (Model 51, Interstate Electronics Co., Anaheim, California). Hydrogen bubbles produced from the cathode were 25 μ m in diameter, and had a maximum rise velocity of approximately 0.3 cm/s (Rodkiewicz and Roussel, 1973). Approximately 200 mg of sodium chloride (ACS

783, BDH Inc., Toronto) was added to the tap water to enhance the conductivity for better hydrogen bubble production.

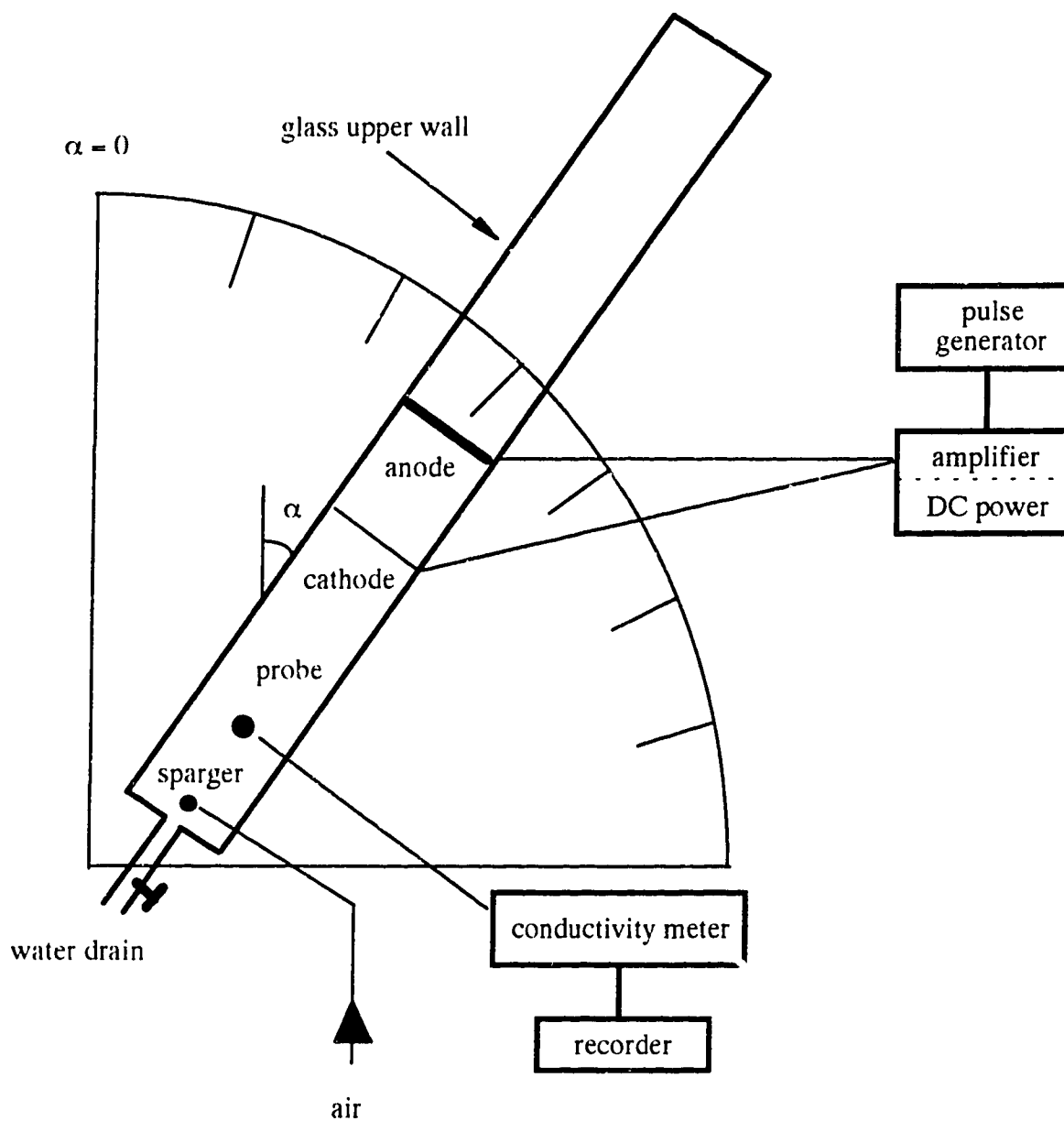


Figure 6-1. Experimental set-up of the inclined bubble column.

The photographs of hydrogen bubbles were taken with a Nikon camera using a shutter speed of 1/60 s and f5.6. 100 ASA black and white film was used. Illumination was supplied by an electronic flash placed to the side facing the glass upper wall.

6.2.3 Bubble Size and Rise Velocity

Air bubbles from the sparger were photographed by the same camera and the same settings as above except that f8 was used. The size of rising bubbles was not constant as the hydrostatic pressure changed along the column. Therefore, pictures of bubbles were always taken from the same spot (half way up the column). Pictures were digitized by Sigma Scan (Jandel Scientific, Corte Madera, California). All bubbles appeared to be ellipsoidal, and their volumes were calculated assuming a geometry of perfect ellipse. The volume-equivalent diameters were then calculated.

Bubble rise velocity was estimated by measuring the time of traveling through certain marked interval (90 cm) along the column using a stop watch. At least 8 measurements were carried out to obtain an average for the calculation of bubble rise velocity.

6.2.4 Computational Fluid Dynamics (CFD) Simulation

Computational fluid dynamics (CFD) simulation was carried out using the FLOW3D package (Release 3.2.1, CFDS, AEA Technology, Harwell, UK). A rectangular grid was generated by the Grid Generator. The command file (see Appendix B) was executed by FLOW3D as a batch file to produce the solution which was then processed by the Graphics Module to obtain the velocity profiles for the inclined bubble column.

The current release of FLOW3D allows an arbitrary number of phases to be specified for multiphase flow simulation. Using the multiphase feature for the inclined bubble column, however, required significant additional study which would exceed the scope of this thesis.

6.2.5 Mixing Study

Mixing studies were carried out using the salt injection method. Salt solution for injection was prepared by dissolving 6 g of sodium chloride (ACS 783, BDH Inc., Toronto) in 50 ml of tap water. 3 - 4 mL of this solution was injected into the top of the bubble column via a 5 mL plastic syringe. A conductivity probe (cat# L-19500-20, Cole-Parmer, Chicago) was positioned 10 cm from the bottom of the bubble column, and connected to a conductivity controller (cat# 19300-00, Cole-Parmer, Chicago). The DIP switch setting on the controller corresponded to a conductivity range of 0 - 999 $\mu\text{S}/\text{cm}$. The measured conductivity was fed to a chart recorder (HP Moseley 7100B Strip Chart Recorder, Model 7127A). The recorder was set to 1 V, and 1 inch per min for paper speed.

As the measured conductivity was proportional to the corresponding salt concentration, the conductivity response curve was directly used to derive the mixing time t_m which was defined as the time taken to reach the extent of mixing Y . As suggested by other reports (Krishna Murthy and Elliott, 1992), Y was chosen to be 95%, i.e.

$$Y = \frac{S(t) - S_0}{S_\infty - S_0} \quad (3)$$

where S_0 , $S(t)$, and S_∞ were the conductivity of initial, time t , and final equilibrium respectively. To ensure that S_∞ was indeed reached at the end of each experiment, air sparging was increased to enhance mixing in the bubble column and to confirm that the conductivity remained constant. Figure 6-2 is a scanned image of a representative conductivity response curve showing $t_{95\%}$ and $t_{5\%}$. $t_{95\%}$ is the mixing time defined as above. $t_{5\%}$, the time required for 5% change on the conductivity response curve, was used to estimate the downward liquid circulation velocity.

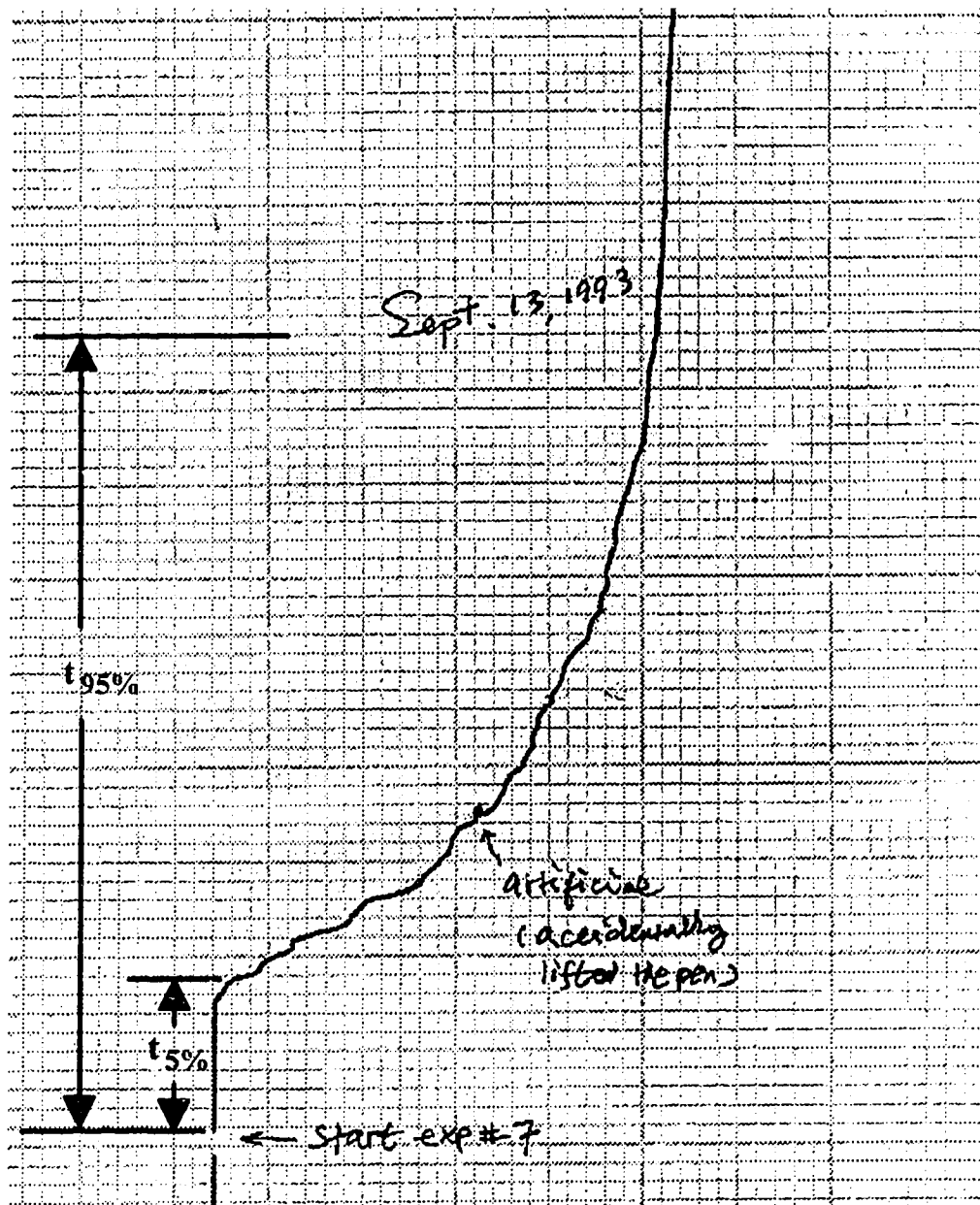
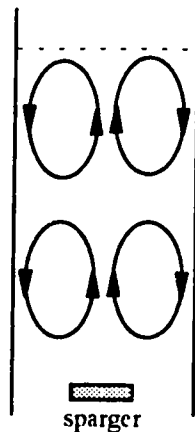


Figure 6-2. Conductivity response curve recorded by the chart recorder for the experiment with superficial gas velocity of 0.02 cm/s and inclination angle of 30°.

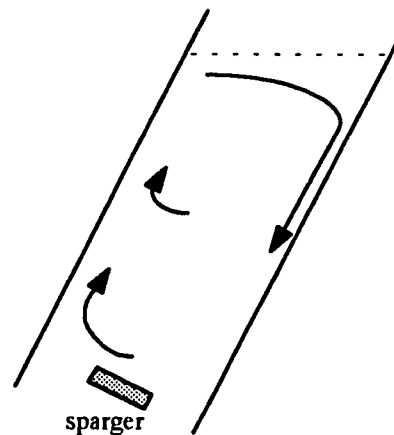
6.3 RESULTS AND DISCUSSION

6.3.1 Qualitative Observations

Preliminary studies using near neutrally buoyant particles such as polystyrene beads and plant cells indicated a different liquid circulation pattern in the inclined bubble column in contrast to a vertical bubble column (Figure 6-3). We also tried to use the dye injection technique to obtain some qualitative information about the flow field in the inclined bubble column. A circulation pattern similar to that shown in Figure 4-1 was observed. More quantitative data, however, were not obtained, because even at very slow sparging rate, such as 0.005 vvm (volume of air per min per liquid volume), turbulence existed in the bulk liquid phase and dispersed the injected dye stream so rapidly that any photography was difficult.



(a) Vertical bubble column
(Joshi and Sharma, 1979)



(b) Inclined bubble column

Figure 6-3. Liquid circulation patterns in vertical and inclined bubble columns.

6.3.2 Bubble Size and Rise Velocity

Figure 6-4 shows sizes of air bubbles as a function of inclination angle for four superficial gas velocities, i.e. 0.002, 0.01, 0.02, and 0.1 cm/s. For $u_{gs} = 0.002$, and 0.01 cm/s, only one stream of bubbles was produced from the sparger, that is, single bubbles traveled at a distinct interval along the column. Therefore the bubble size was uniform. At higher gas velocities, however, more than one stream of bubbles from the sparger gave a distribution in bubble size which was indicated by the 95% confidence interval. All bubbles were approximately in the range of 2.5 - 4.0 mm in equivalent diameter. Bubble size appeared to increase with the angle of inclination. This could be due to the distortion of bubbles as a result of traveling against an inclined surface, but this hypothesis has not been confirmed experimentally.

Bubble rise velocity was also plotted as a function of the inclination angle for different superficial gas velocities (Figure 6-5). At a very low sparging rate (0.002 cm/s), bubble rise velocity was approximately 23.5 cm/s, and was not affected by inclination. At higher aeration rates, however, bubble rise velocities increased with the angle of inclination for $\alpha < 10^\circ$, and remained nearly constant for $10^\circ < \alpha < 45^\circ$.

At the lowest sparging rate (0.002 cm/s), single bubbles were produced from the sparger. In the inclined bubble column, these bubbles had a size range of 3.2 - 3.6 mm, which was larger than those used by Masliyah et al. (1993). The larger bubbles were deformed in shape, and rose against the inclined column wall in a rolling fashion. Masliyah et al. (1993) found that the bubble rise velocity decreased as the column was inclined from vertical for smaller bubbles which traveled in a sliding fashion. The rolling behavior for the larger bubbles likely explained the lack of change of the rise velocity with the inclination angle. Figure 6-6 plots Equation (1) and the experimental data from this study. The following properties were used for water in the calculations: density = 1000 kg/m^3 , viscosity = $0.001 \text{ Pa}\cdot\text{s}$, and surface tension = 0.07 N/m . All dimensionless groups were previously defined by Masliyah et al. (1993). The larger bubbles had a much higher Reynolds number ($Re = 600 - 900$), compared to the upper limit for equation (1). The correlation derived for small bubbles by Masliyah et al. (1993) could not apply to the larger bubbles used in this study.

For the same superficial gas velocity, both bubble size and bubble rise velocity were not affected by the aspect ratio which was defined as the ratio of liquid height to column width (Figure B-1 and Figure B-2 in Appendix B).

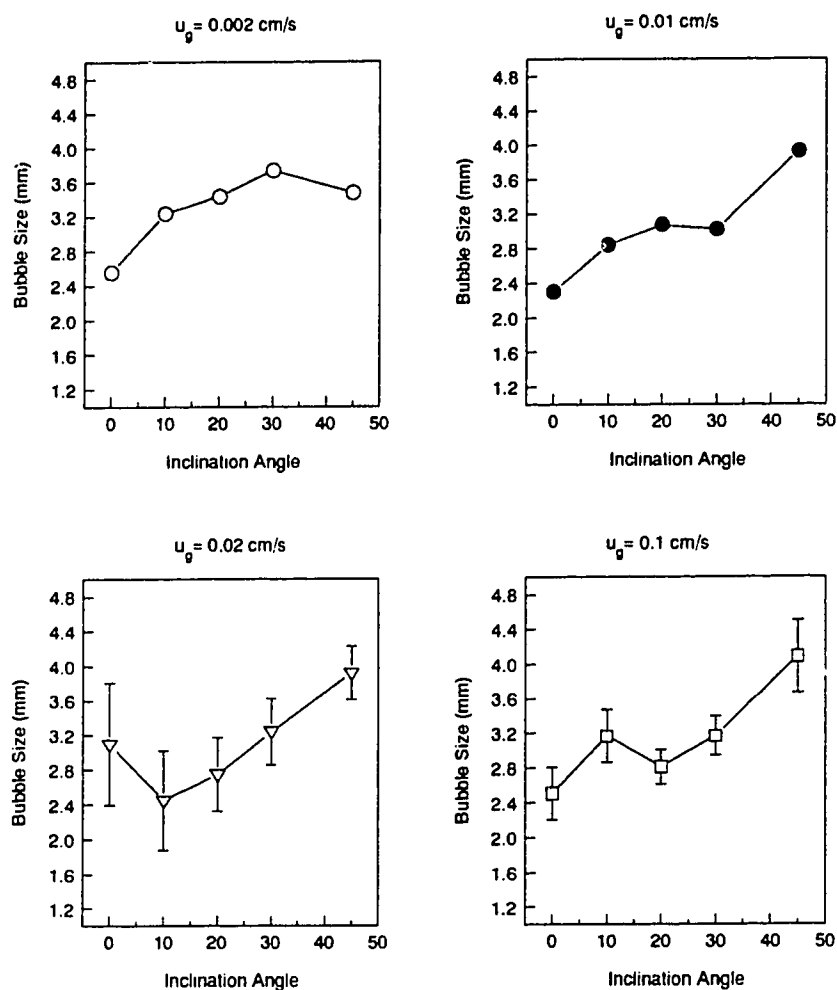


Figure 6-4. Bubble size as a function of inclination angle for four different superficial gas velocities. Error bars represent 95% confidence interval.

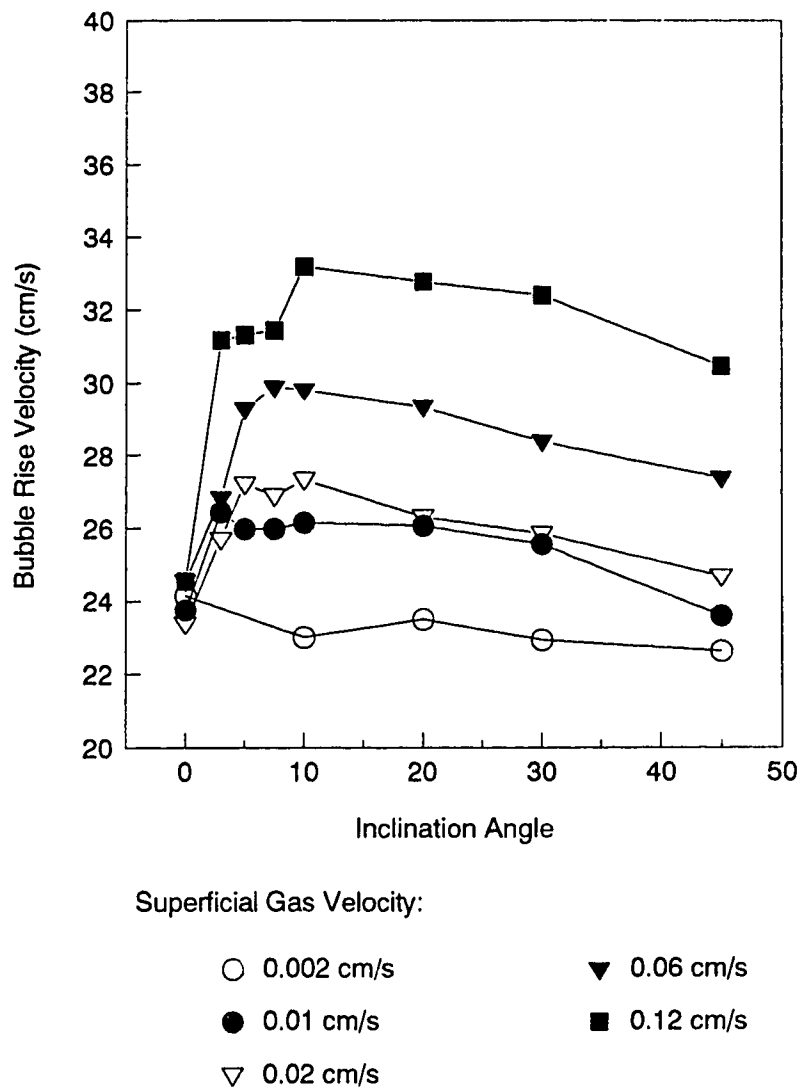


Figure 6-5. Bubble rise velocity as a function of inclination angle for five different superficial gas velocities.

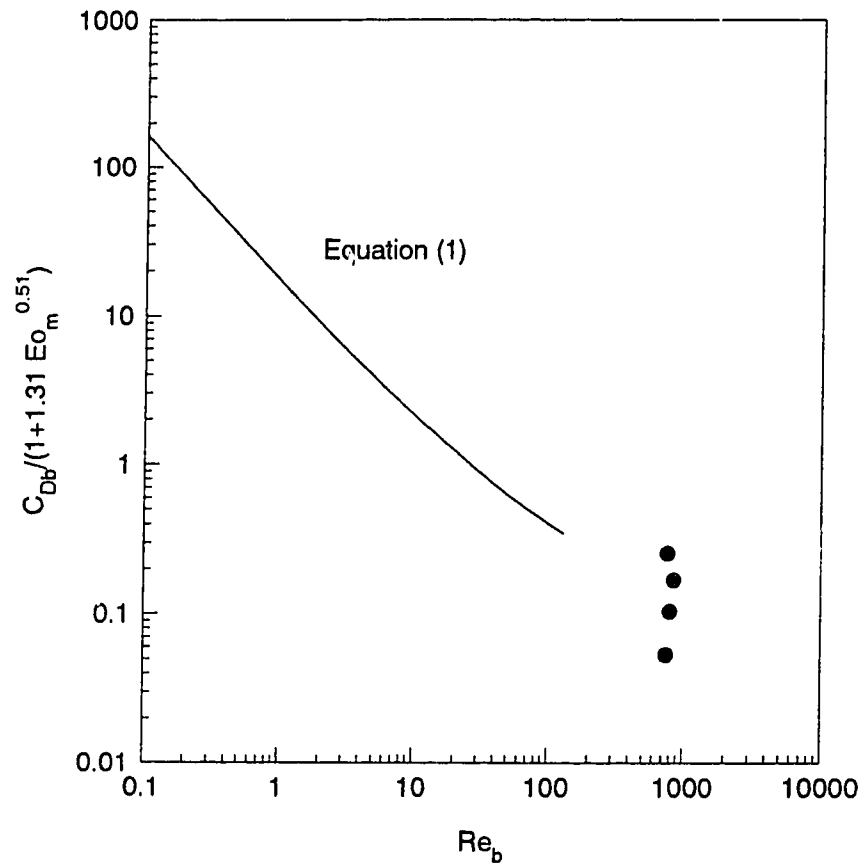


Figure 6-6. Air bubbles in this study were larger in size than those used by Masliyah et al. (1993), and Re was greater than 130 which was the upper limit for Equation (1). Symbols represent the experimental data obtained from the inclined bubble column for a superficial gas velocity of 0.002 cm/s.

6.3.3 Liquid Velocity Profile

Figure 6-7 gives liquid velocity profiles measured by the hydrogen bubble technique for the bubble column with an inclination angle of 30° and a superficial gas velocity of 0.02 cm/s. There was some variability in the velocity profiles obtained from different hydrogen bubble pictures, indicating the time-dependent characteristic of the local liquid velocity as a result of turbulence. Hydrogen bubble technique was designed for measuring velocities of uniform flows whose velocity profiles had been previously determined (Davis and Fox, 1967). For non-uniform turbulent flow, this technique was not effective for the quantitative determination of velocity profiles (Davis and Fox, 1967).

Upward circulating liquid in the vicinity of rising bubbles had a high turbulent velocity. Profiles of hydrogen bubbles in this zone were not recognizable. Therefore, we were mainly focusing on the downward liquid flow between the zero-velocity cross point and the lower wall of the bubble column.

At the lowest superficial gas velocity, i.e. 0.002 cm/s, bulk liquid circulation was practically negligible. Microhydrogen bubbles were rising in an almost stagnant liquid. The estimated rise velocity was 0.8 cm/s which was somewhat larger than the reported value of 0.3 cm/s (Rodkiewicz and Roussel, 1973). This rise velocity of microhydrogen bubbles was used to correct the liquid velocities derived from the hydrogen bubble pictures. All liquid velocities derived from the hydrogen bubble pictures were added with the rise velocity of hydrogen bubbles, i.e. 0.8 cm/s.

At high superficial gas velocities, such as 0.1 cm/s, the liquid phase was so turbulent that profiles from hydrogen bubble pictures were difficult to identify, and estimates could bear significant errors. Therefore, the downward circulation velocity is given as the maximum downward velocity (Table 6-1) and average downward velocity (Figure 6-8). The distance from the zero-velocity cross-point to the lower column wall from the hydrogen bubble pictures is also summarized in Table 6-1. For the vertical column, air bubbles were fairly evenly distributed across the bubble column, and in the vicinity of each rising bubble, there was a high local velocity. The liquid circulation was not well defined to produce the time lines of the microhydrogen bubbles. The maximum downward liquid velocity and

the position of cross points (Table 6-1) were, therefore, not available for the vertical column.

In the mixing study using conductivity measurement, we used 15% to estimate the downward liquid circulation velocity (Figure 6-9). These results were consistent with those obtained from the hydrogen bubble experiments (Figure 6-8). For the same inclination angle and superficial gas velocity, liquid velocity did not depend on the aspect ratio used in this study (Figure 6-10).

Both Figure 6-8 and Figure 6-9 show that the liquid circulation velocity increased as the bubble column was inclined to 3° from vertical. This increase was more significant for high superficial gas velocities (e.g. 0.10 cm/s) than for low superficial gas velocities (e.g. 0.002 cm/s). For example, the liquid circulation velocity was approximately 3.3 cm/s at the vertical position, and 5.7 cm/s at 3° inclination (Figure 6-9). Only a small inclination from vertical (i.e. 3°) was required for the onset of bulk liquid circulation in the inclined bubble column. As soon as the liquid circulation was established, the liquid circulation velocity did not change significantly as a function of the inclination angle for up to 45°. These results are consistent with the bubble rise velocity (Figure 6-5) which drives the liquid circulation. The enhanced liquid circulation in the inclined bubble column, especially at high gas velocities (e.g. 0.10 cm/s), was likely responsible for the increased apparent bubble rise velocities as the upward liquid flow in the bubble-rising zone would in return increase the bubble rise velocity.

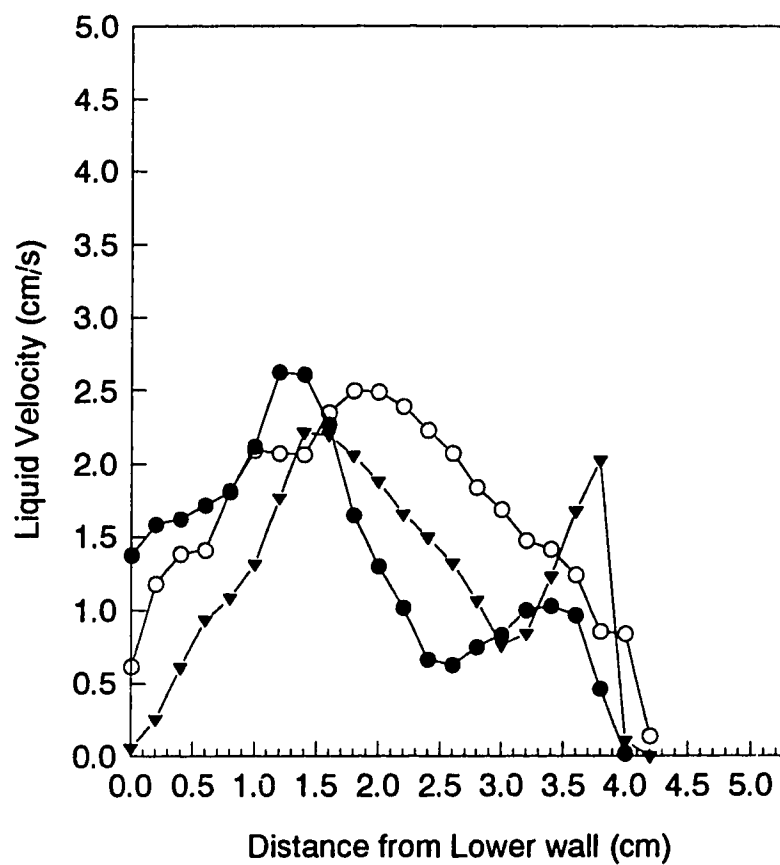


Figure 6-7. Velocity profiles were determined from the hydrogen bubble pictures from the experiment with a superficial gas velocity of 0.02 cm/s and an inclination angle of 30°. Different symbols represent profiles obtained from different pictures.

Table 6-1. Maximum downward liquid velocity and the distance of the zero-velocity cross point from the lower wall of the inclined bubble column.

Inclination Angle	Superficial Gas Velocity (cm/s)	Maximum Velocity (cm/s)	Cross-Point (cm)
45°	0.002	N/A	N/A
	0.01	2.0	4.1
	0.02	2.9	4.2
	0.1	6.5	4.2
30°	0.002	N/A	N/A
	0.01	2.1	4.6
	0.02	3.4	4.3
	0.1	N/A	N/A
20°	0.002	N/A	N/A
	0.01	2.1	4.0
	0.02	4.6	4.3
	0.1	6.8	4.7
10°	0.002	N/A	N/A
	0.01	3.1	4.3
	0.02	4.0	4.1
	0.1	7.0	N/A

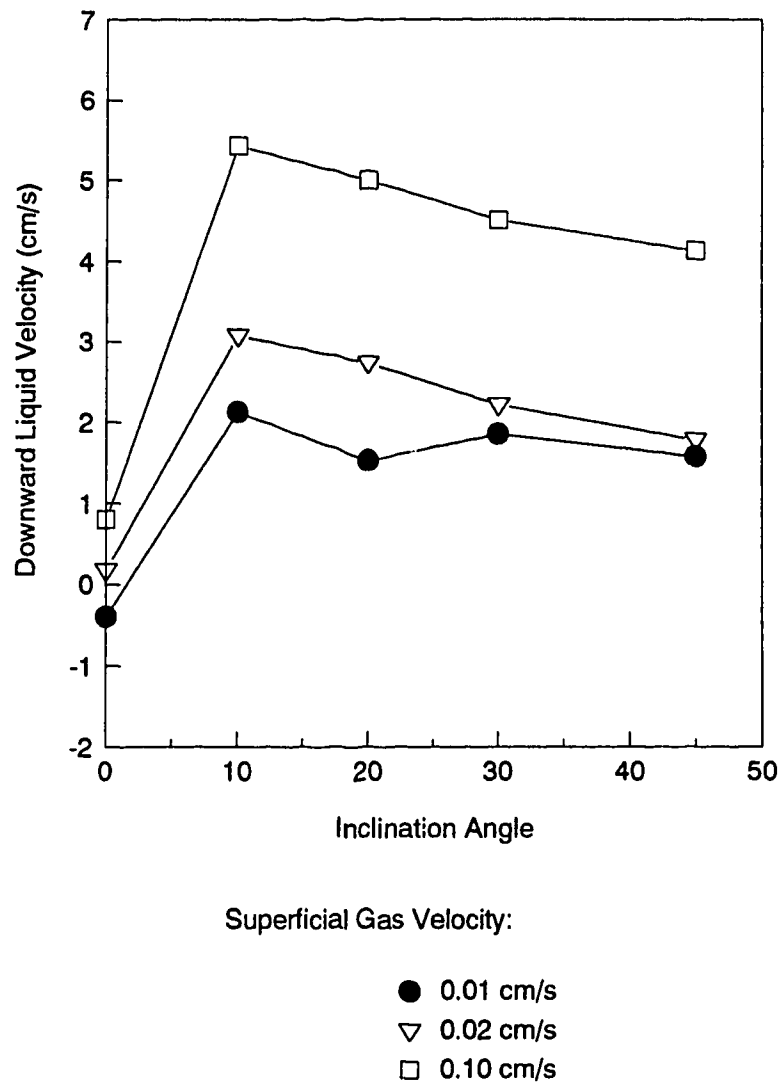
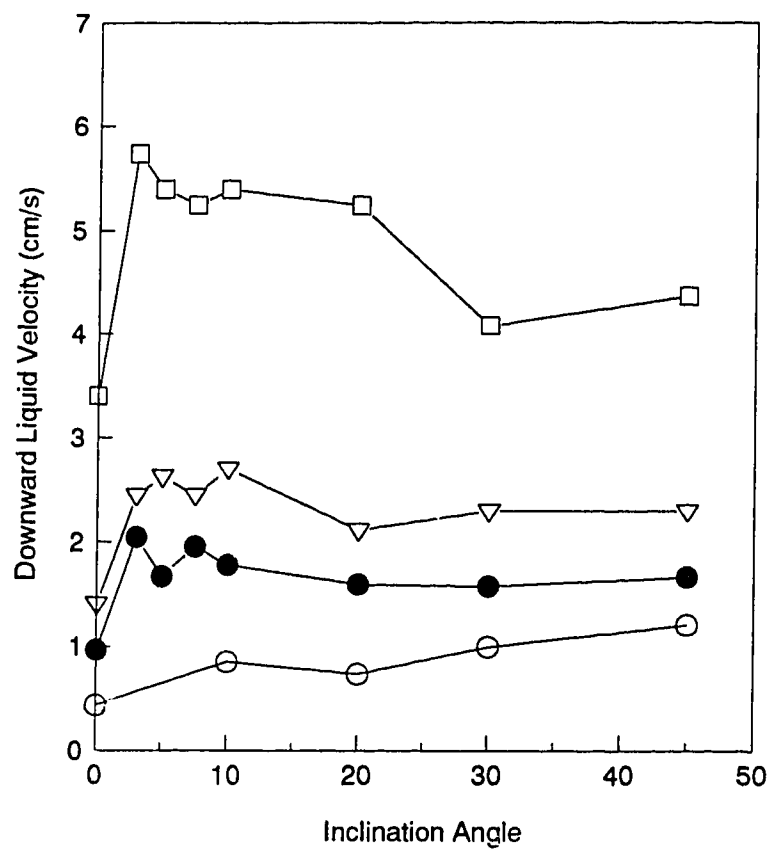


Figure 6-8. Average downward liquid velocity as a function of inclination angle for three different superficial gas velocities from hydrogen bubble experiments.



Superficial Gas Velocity:

○ 0.002 cm/s

● 0.01 cm/s

▽ 0.02 cm/s

□ 0.10 cm/s

Figure 6-9. Downward liquid velocity estimated from the conductivity response curve.

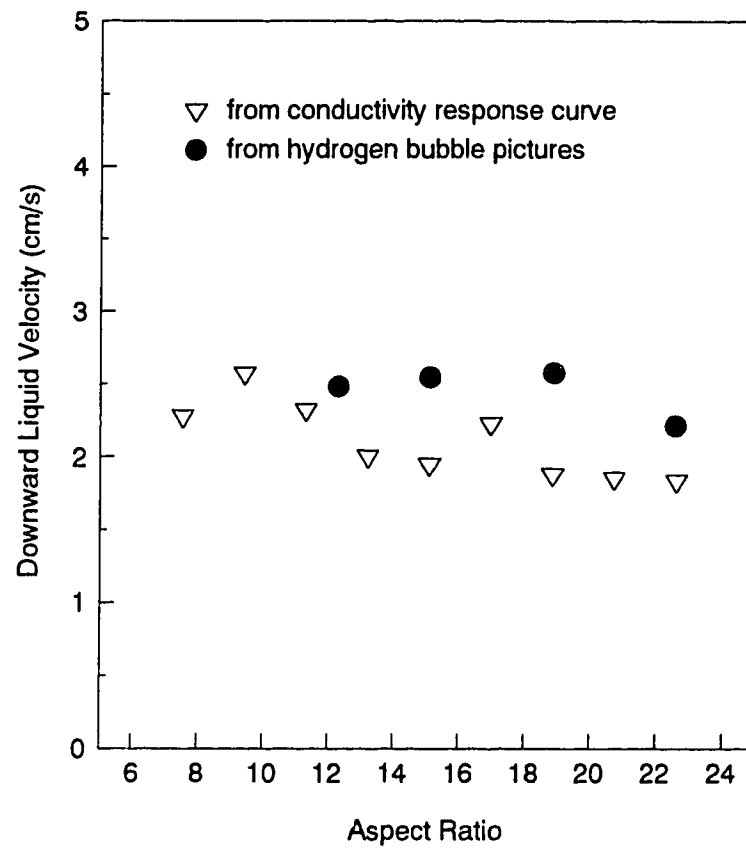


Figure 6-10. Downward liquid velocity as a function of aspect ratio.

6.3.4 CFD Simulation

As the liquid circulation in the inclined column was solely driven by the rising air bubbles, the hydrodynamic characterization of the bubble zone became critical for the simulation of the liquid circulation. To avoid using the multiphase feature in FLOW3D (see 6.2.4), an appropriate boundary condition had to be used to describe the rising bubbles for the simulation. Two different boundary conditions were examined as follows:

BC (1) - to describe the bubble column as a two parallel plate system consisting of a moving upper plate and a stationary lower plate. The bubble rising velocity for the corresponding inclination and sparging rate was used for the upward-moving velocity of the upper plate.

BC (2) - plug flow for liquid in the bubble zone; a layer of liquid whose thickness was equivalent to the average bubble size for the corresponding inclination and sparging rate moving upward at the same velocity as the rising bubbles.

The k- ϵ model was used to describe the turbulence in the liquid. Non-slip boundary condition was used for the lower wall and the bottom wall of the column. The boundary condition at the free liquid surface defined zero total mass flow through the column.

CFD simulations by FLOW3D were carried out for a superficial gas velocity of 0.02 cm/s, and an inclination angles of 30°. Under these conditions, the liquid velocity profile was obtained from the hydrogen bubble experiments, making a comparison between the simulation results and experimental data possible. The command file for the FLOW3D simulation using BC (1) was attached in Appendix B.

Figure 6-11 compares the simulation results using BC (1) with the liquid velocity profile determined by the hydrogen bubble technique. The simulation predicted a maximum downward liquid velocity of approximately 3 cm/s, which was similar to that measured by the hydrogen bubble technique. However, an asymmetric velocity profile was predicted by FLOW3D, in contrast to the

symmetric profile observed experimentally. The discrepancy likely reflects that the moving-plate-model used for the FLOW3D simulation was an oversimplification.

Figure 6-11 also shows the velocity profile predicted by FLOW3D using BC (2) which assumed plug flow for the liquid in the bubble zone. The asymmetric profile was similar to that obtained with BC (1). An over-estimated liquid velocity likely indicated that the velocity of the plug-flow did not actually reach the bubble rise velocity. Another major difference between the simulation results and the experimentally measured results was the position of the zero-velocity cross-point. The simulations predicted a cross-point located 3.3 cm (using BC (1)) and 3.7 cm (using BC (2)) from the lower wall, compared to approximately 4.0 cm from the lower wall which was obtained from the hydrogen bubble experiments.

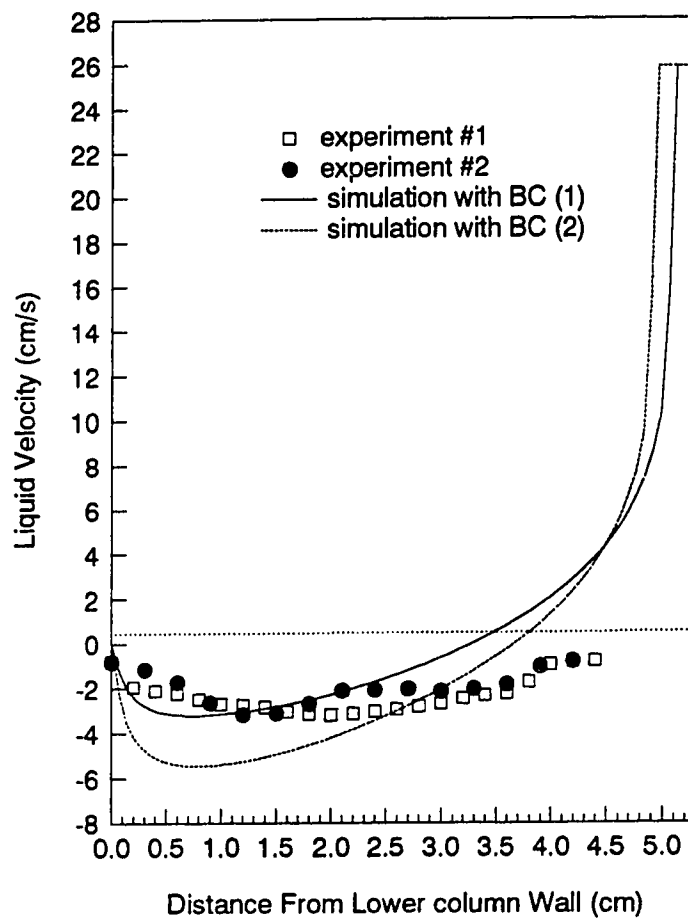


Figure 6-11. A comparison of the liquid velocity profiles between the simulation results and experimental data. The upward liquid velocity in the vicinity of rising bubbles were not available from the hydrogen bubble method.

6.3.5 Mixing Time

Figure 6-12 shows mixing time as a function of inclination angle for four superficial gas velocities. When the bubble column was inclined from vertical up to 5° , the mixing time was greatly reduced, especially at low superficial gas velocities. For example, for a superficial gas velocity of 0.01 cm/s, the mixing time was approximately 19 min for the vertical column; but a 3° inclination of the column reduced the mixing time to approximately 7 min. Mixing time did not change significantly when the bubble column was further inclined from vertical (e.g. $\alpha > 10^\circ$). These results are consistent with the bubble rise velocity (Figure 6-6) and the liquid velocity (Figure 6-8 and Figure 6-9). When the bubble column was inclined to approximately 5° from the vertical, the bubble rise velocity increased significantly, which then induced better liquid circulation indicated by higher liquid velocity, and the mixing time was reduced. Bubble velocity, liquid circulation, and mixing time were not affected by further inclining the bubble column.

Given the angle of inclination and sparging rate, the mixing time was found to linearly increase with the aspect ratio (Figure 6-10). In the same bubble column, larger t_m corresponded to larger liquid height. The linear dependence of mixing time on the liquid height indicated that the mixing time was proportional to the circulation time. From the average downward liquid velocity and position of zero-velocity cross-point, the circulation time for 30° inclination and superficial gas velocity of 0.02 cm/s was estimated to be 1.7 min. For the corresponding mixing time of 4.5 min, approximately three circulations were required for 95% mixing.

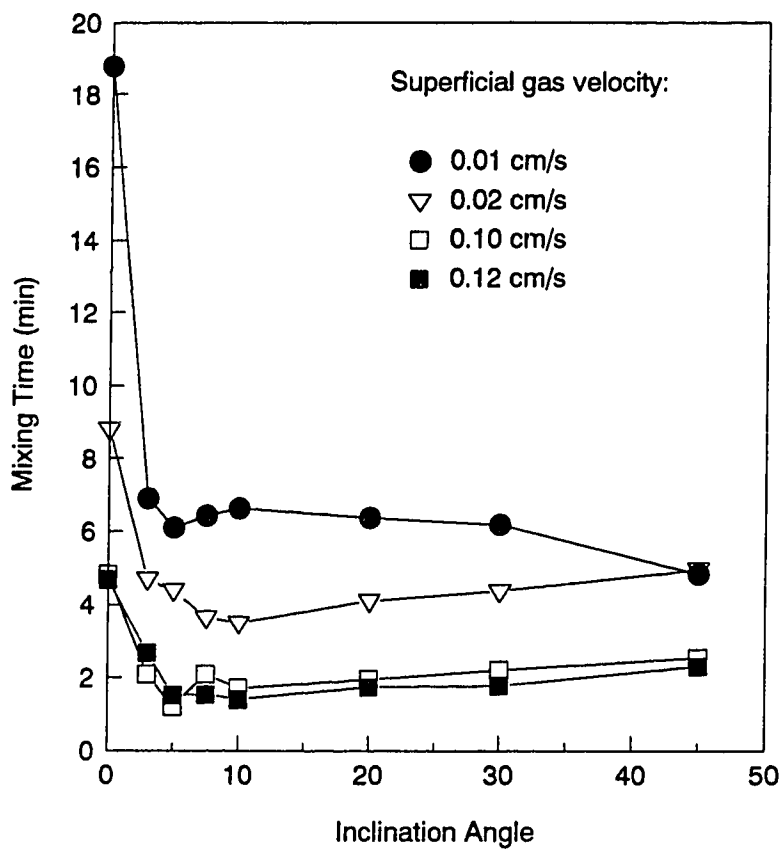


Figure 6-12. Mixing time as a function of inclination angle for different superficial gas velocities.

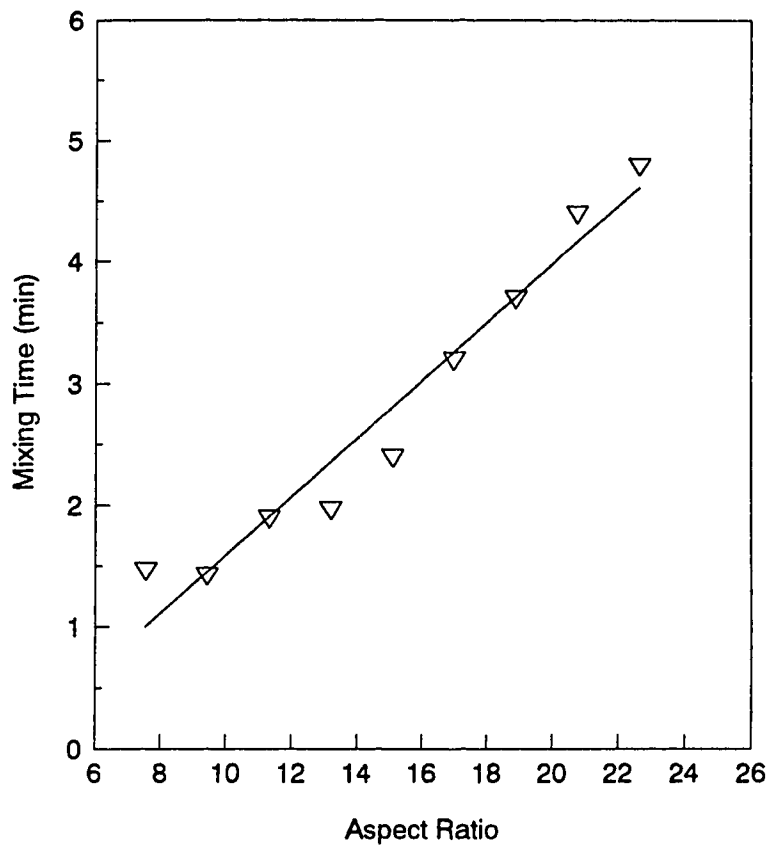
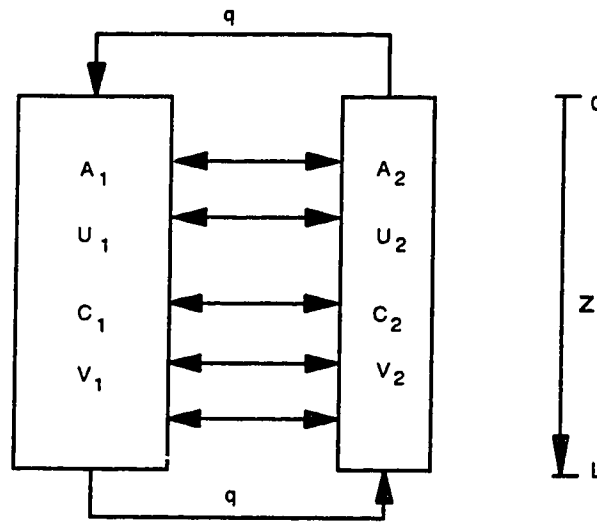


Figure 6-13. Mixing time as a function of aspect ratio.

6.3.6 Mixing Model

Based on the observed flow pattern in the inclined bubble column, we proposed to use an appropriate mixing model. The recycle-cross-flow model was first proposed by Hochman and McCord (1970) for the study of residence time distribution in a flow-through system with a high aspect ratio (L/D). For the inclined-tube bioreactor, this model represented the observed circulation patterns in the column. We modified this model to account for mixing in a batch system. Figure 6-14 illustrates the set-up of this model. q , the liquid flow rate within the system, is the actual liquid flow rate circulating in the column. The two legs represent the downward and upward flow zone for the liquid phase respectively. k is a cross-flow coefficient. To simplify the equations for the first step in the modeling, plug flow was assumed for both legs. Axial dispersion can be included for further sophistication of this model.



A = area U = velocity C = concentration V = volume L = length

Define: $K = k \cdot L / q$ $x = z / L$

Figure 6-14. Recycle-cross-flow model.

A differential mass balance on each of the two legs gives the following partial differential equations:

$$\tau_1 \frac{\partial C_1}{\partial t} + \frac{\partial C_1}{\partial x} + K(C_1 - C_2) = 0 \quad (4)$$

$$\tau_2 \frac{\partial C_2}{\partial t} - \frac{\partial C_2}{\partial x} - K(C_1 - C_2) = 0 \quad (5)$$

where $\tau_1 = V_1/q$, $\tau_2 = V_2/q$, C_1 and C_2 are normalized concentrations. These two partial differential equations had to be solved for the following initial conditions and boundary conditions:

$$C_1(0, x) = C_2(0, x) = 0 \quad (6)$$

$$C_1(t, 0) - C_2(t, 0) = \delta(t) \quad (7)$$

$$C_1(t, 1) - C_2(t, 1) = 0 \quad (8)$$

Notice that the Dirac Delta Function $\delta(t)$ represents the pulse injection of a salt solution in the conductivity response experiments. For the convenience of mathematical derivations, define

$$W_1 = C_1$$

and

$$W_2 = C_1 - C_2$$

Then Equations (4) and (5) become

$$\tau_1 \frac{\partial W_1}{\partial t} + \frac{\partial W_1}{\partial x} + KW_2 = 0 \quad (9)$$

$$\tau_2 \frac{\partial W_1}{\partial t} - \tau_2 \frac{\partial W_2}{\partial t} - \frac{\partial W_1}{\partial x} + \frac{\partial W_2}{\partial x} - KW_2 = 0 \quad (10)$$

Laplace transform on t yields

$$\tau_1[-W_1(0, x) + s\bar{W}_1] + \frac{d\bar{W}_1}{dx} + K\bar{W}_2 = 0 \quad (11)$$

$$\tau_2[-W_1(0, x) + s\bar{W}_1] - \tau_2[-W_2(0, x) + s\bar{W}_2] - \frac{d\bar{W}_1}{dx} + \frac{d\bar{W}_2}{dx} - K\bar{W}_2 = 0 \quad (12)$$

Inserting the initial conditions, $W_1(0, x) = W_2(0, x) = 0$, and adding up (11) and (12) give

$$\bar{W}_1 = \frac{1}{\tau_1 s + \tau_2 s} \left[-\frac{d\bar{W}_2}{dx} + \tau_2 s \bar{W}_2 \right] \quad (13)$$

Plugging (13) back into (11) yields the following second-order ordinary differential equation for \bar{W}_2 :

$$\frac{d^2 \bar{W}_2}{dx^2} + (\tau_1 s - \tau_2 s) \frac{d\bar{W}_2}{dx} - [\tau_1 \tau_2 s^2 + K(\tau_1 s + \tau_2 s)] \bar{W}_2 = 0 \quad (14)$$

Solving this ordinary differential equation produces

$$\bar{W}_2 = Ae^{m_1 x} + Be^{m_2 x} \quad (15)$$

where $m_1 = -\frac{\tau_1 - \tau_2}{2}s + \frac{\tau_1 + \tau_2}{2}\sqrt{s^2 + \frac{4K}{\tau_1 + \tau_2}}s$ (16)

$$m_2 = -\frac{\tau_1 - \tau_2}{2}s - \frac{\tau_1 + \tau_2}{2}\sqrt{s^2 + \frac{4K}{\tau_1 + \tau_2}}s \quad (17)$$

The transformed boundary conditions are as follows:

$$\bar{W}_2(s, 0) = 1$$

$$\bar{W}_2(s, 1) = 0$$

Inserting the above boundary conditions into (15) results in two equations for the unknown constant A and B:

$$Ae^{m_1} + Be^{m_2} = 0 \quad (18)$$

$$A + B = 1 \quad (19)$$

Solving for A and B, we have

$$A = -\frac{e^{m_2}}{e^{m_1} - e^{m_2}}$$

$$B = \frac{e^{m_1}}{e^{m_1} - e^{m_2}}$$

Therefore,

$$\overline{W}_2 = \frac{e^{m_1+m_2x} - e^{m_1x+m_2}}{e^{m_1} - e^{m_2}} \quad (20)$$

Inserting (20) into (13) and rearranging gives

$$\overline{W}_1 = \frac{1}{\tau_1 s + \tau_2 s} \left[\frac{m_1 e^{m_1x+m_2} - m_2 e^{m_1+m_2x}}{e^{m_1} - e^{m_2}} + \tau_2 s \frac{e^{m_1+m_2x} - e^{m_1x+m_2}}{e^{m_1} - e^{m_2}} \right] \quad (21)$$

$$\overline{W}_1(x=1) = \frac{1}{\tau_1 s + \tau_2 s} \frac{(m_1 - m_2)e^{m_1+m_2}}{e^{m_1} - e^{m_2}} = \frac{e^{-\frac{\tau_1 - \tau_2}{2}s}}{s} \frac{\sqrt{s^2 + \frac{4K}{\tau_1 + \tau_2}} s}{e^{\frac{\tau_1 + \tau_2}{2} \sqrt{s^2 + \frac{4K}{\tau_1 + \tau_2}}} - e^{-\frac{\tau_1 + \tau_2}{2} \sqrt{s^2 + \frac{4K}{\tau_1 + \tau_2}}}}$$

Rewritten as

$$\overline{W}_1(x=1) = \frac{1}{2} \frac{e^{-as}}{s} \frac{\sqrt{s^2 + bs}}{\sinh(c \cdot \sqrt{s^2 + bs})} \quad (22)$$

where
$$a = \frac{\tau_1 - \tau_2}{2} \quad b = \frac{4K}{\tau_1 + \tau_2} \quad c = \frac{\tau_1 + \tau_2}{2} \quad (23)$$

The inverse of (22) will give $W_1(t, x=1) = C_1(t, x=1)$ which is the response at $x = 1$ for an impulse injection at $x = 0$ at $t = 0$. An analytical solution of the inverse, however, is not available, and a numerical method is required. An alternative would be to integrate equations (4) and (5) directly.

τ_1 and τ_2 are calculated from the average downward liquid velocity U_1 and the cross section ratio A_1/A_2 , which were obtained by the hydrogen bubble technique.

$$\tau_1 = \frac{L}{U_1} \quad \text{and} \quad \tau_2 = \frac{L}{U_1} \frac{A_2}{A_1} \quad (24)$$

Therefore, for a given value of K , the constants a , b , and c are calculated according to (23) and (24). The numerical inverse could be computed to obtain $C_1(t, x=1)$, which is then used to curve-fit the experimental data to get the K value for the corresponding set-up of the inclined bubble column.

6.4 CONCLUSIONS

1. In the inclined bubble column, the bubble rise velocity increased with inclination angle up to 10° from vertical, then became nearly constant as a function of inclination angle up to 45° . The liquid velocity showed consistent behavior; velocity increased with 10° inclination and then remained constant.
2. Bubble size, rise velocity, and liquid circulation were not affected by aspect ratio for constant sparging rate and inclination angle.
3. Mixing time was significantly reduced in columns inclined by more than 5° , compared to the vertical column. Further inclination had little effect on mixing time, which was consistent with the bubble and liquid velocities. For constant

sparging rate and inclination angle, mixing time linearly increased with aspect ratio.

REFERENCES

- Baird, M.H.I., and Rice, R.G. 1975. Axial dispersion in large unbaffled columns. *Chem. Eng. J.* **9**: 171-174.
- Davis, W., and Fox, R.W. 1967. An evaluation of the hydrogen bubble technique for the quantitative determination of fluid velocities within clear tubes. *J. Basic Eng.* December. 771-781.
- Freyduth, P. 1993. Flow visualization in fluid mechanics. *Rew. Sci. Instrum.* **64**: 1-18.
- Gad-el-Hak, M. 1988. Visualization techniques for unsteady flows: an overview. *J. Fluids Eng.* **110**: 231-243.
- Handa-Corrigan, A., Emery, A.N., and Spier, R.E. 1987. On the evaluation of gas-liquid interfacial effects on hybridoma viability in bubble column bioreactors. *Develop. Biol. Stand.* **6**: 241-253.
- Hochman, J.M., and McCord, J.R. 1970. Residence time distributions in recycle systems with crossmixing. *Chem. Eng. Sci.* **25**: 97-107.
- Joshi, J.B., and Sharma, M.M. 1979. A circulation cell model for bubble columns. *Trans. International Chem. Eng.* **57**: 244-251.
- Kresta, S. 1991. Flow visualization. p. 19-49. PhD thesis. McMaster University.
- Kunas, K.T. and Papoutsakis, E.T. 1990. Damage mechanisms of suspended animal cells in agitated bioreactors with and without bubble entrainment. *Biotechnol. Bioeng.* **36**: 476-483.
- Levenspiel, O. 1984. Flow pattern and contacting. p. 61.1-61.17. In: *The chemical reactor omnibook⁺*. OSU Book Stores. Corvallis.
- Masliyah, J., Jauhari, R., and Gray, M. 1993. Drag coefficients for air bubbles rising along an inclined surface. Accepted by *Chem. Eng. Sci.*
- Mayr, B., Nagy, E., Horvat, P., and Moser, A. 1994. Scale-up on basis of structured mixing models: a new concept. *Biotechnol. Bioeng.* **43**: 195-206.
- McAlister, K.W., and Carr, L.W. 1979. Water tunnel visualizations of dynamic stall. *J. Fluids Eng.* **101**: 376-380.
- Merzkirch, W. 1987. Visualization of velocity profiles. p. 69-75. In: *Flow visualization*. 2nd ed. Academic Press. Orlando.

- Murthy, G.G.K., and Elliott, J.F. 1992. Definition and determination of mixing time in gas agitated liquid baths. *ISIJ Int.* **32**: 190-195.
- Nagy, E., Mayr, B., and Moser, A. 1994. Bioprocess scale-up using a structured mixing model. *Computers Chem. Eng.* **18**: S663-S667.
- Ohki, Y., and Inoue, H. 1970. Longitudinal mixing of the liquid phase in bubble columns. *Chem. Eng. Sci.* **25**: 1-16.
- Papoutsakis, E.T. 1991. Fluid-mechanical damage of animal cells in bioreactors. *Trends Biotechnol.* **9**: 427-437.
- Rice, R.G., and Littlefield, M.A. 1987. Dispersion coefficients for ideal bubbly flow in truly vertical bubble columns. *Chem. Eng. Sci.* **42**: 2045-2053.
- Rodkiewicz, C.M., and Roussel, C.L. 1973. Fluid mechanics in a large arterial bifurcation. *J. Fluids Eng.* March. 108-112.
- Tinge, J.T., and Drinkenburg, A.A.H. 1986. The influence of slight departures from vertical alignment on liquid dispersion and gas hold-up in a bubble column. *Chem. Eng. Sci.* **41**: 165-169.
- Valdes-Krieg, E., King, C.J., and Sephton, H.H. 1975. Effect of vertical alignment in the performance of bubble and foam fractionation columns. *AIChE J.* **21**: 400-402.
- Wilkinson, P.M., Haringa, H., Stokman, F.P.A., and Van Dierendonck, L.L. 1993. Liquid mixing in a bubble column under pressure. *Chem. Eng. Sci.* **48**: 1785-1791.
- Yamashita, F. 1985. Effect of liquid depth, column inclination and baffle plates on gas holdup in bubble columns. *J. Chem. Eng. Japan.* **18**: 349-353.

Chapter 7

Hydrodynamic Behavior of Microcarriers in an Inclined Bubble Column

7.1 INTRODUCTION

Microcarrier culture has been carried out in agitated bioreactors (Hirtenstein, Clark, and Gebb, 1982; Croughan and Wang, 1991), and stirred-tank bioreactors of up to 4,000 liters have been used for the production of human interferon (Griffiths, 1991). One limiting factor encountered with scale-up of agitated bioreactors for the cultivation of anchorage dependent cells on microcarriers is damage by hydrodynamic forces, which can remove cells from the microcarrier and cause cell death (Croughan and Wang, 1989, 1991).

Sparging with air represents a simple scheme for supplying oxygen and mixing. One report on using direct sparging for microcarrier bioreactors found that microcarriers were entrained into the foam layer in the absence of antifoam (Aunins et al., 1986). Foam could be eliminated using an antifoam agent, but it was shown that even very mild sparging was detrimental to FS-4 cells grown on microcarriers in the presence of antifoams. The mechanisms of such damaging effect of sparging on microcarrier cultures, yet to be investigated, are likely to be the same as those from suspension cultures (Croughan and Wang, 1991), that is, cell damage as results of bubble bursting and film draining. These observations and mechanisms are similar to those found with the microcapsule model previously used to mimic animal cells cultivated in agitated or sparged bioreactors (see Chapter 3). These microcapsules had a similar size range to microcarriers such as Cytodex 1 (130 - 220 μm), and therefore, bore physical similarity as a model.

We hypothesize that flotation plays an important role in sparged bioreactors by concentrating the microcarriers near the free gas-liquid interface, which is likely harmful to the cells grown on the microcarriers. This hypothesis led us to investigate the potential use of the inclined bioreactor concept (see Chapter 4) for

microcarrier cultures. Flotation of microcarriers can be minimized in an inclined bioreactor due to the segregation of microcarriers from rising bubbles. Microcarriers are also expected to settle towards the lower plate even more efficiently than suspended animal cells due to their order of magnitude larger size.

In order to explore the use of the novel bioreactor concept for microcarrier cultures, the hydrodynamic behavior of microcarriers in the inclined bioreactor was examined. We used a glass bubble column with adjustable inclination angles to examine the difference in flotation and foam entrainment of microcarriers between the vertical and inclined bubble column. When foam was suppressed by the addition of an antifoam agent, we studied the reduction of microcarrier concentration near the damaging gas-liquid interface in the inclined bubble column.

7.2 MATERIALS AND METHODS

7.2.1 Microcarriers and Medium

Cytodex 1 microcarriers (Sigma, St. Louis, Missouri) were used in the flotation experiment. Dulbecco's Modified Eagle's (DME) medium (Cat# D5648, Sigma) was supplemented with 5% Fetal Bovine Serum (FBS, Gibco, Grand Island, New York) and 400 ppm of Antifoam C (Sigma). This medium ensured that the bubble-microcarrier interactions were representative of actual fermentation conditions.

7.2.2 Preparation of Microcarrier Suspension

8.5024 g of dry microcarriers were added to Phosphate Buffered Saline (PBS, Cat# D5652, Sigma) in two 500 mL spinners and gently stirred for 3 h. Microcarriers were then allowed to settle, the PBS was discarded, and microcarriers were collected as total remaining volume of approximately 200 mL. This microcarrier suspension was then transferred to the bubble column which contained 1 L of DME medium.

7.2.3 Inclined Bubble Column

Figure 7-1 shows a diagram of the inclined bubble column along with detailed dimensions. It was constructed from Pyrex™ glass, and mounted on to a support so that the inclination angle could be easily adjusted. 7% CO₂ in air was used for sparging, and a constant sparging rate of 0.05 vvm (volume of air per minute per volume of liquid) was maintained throughout, which was typical of rates used for sparged bioreactors for animal cell culture. Inclination angles were 0° (vertical), 10°, 20°, 30°, and 40° from vertical.

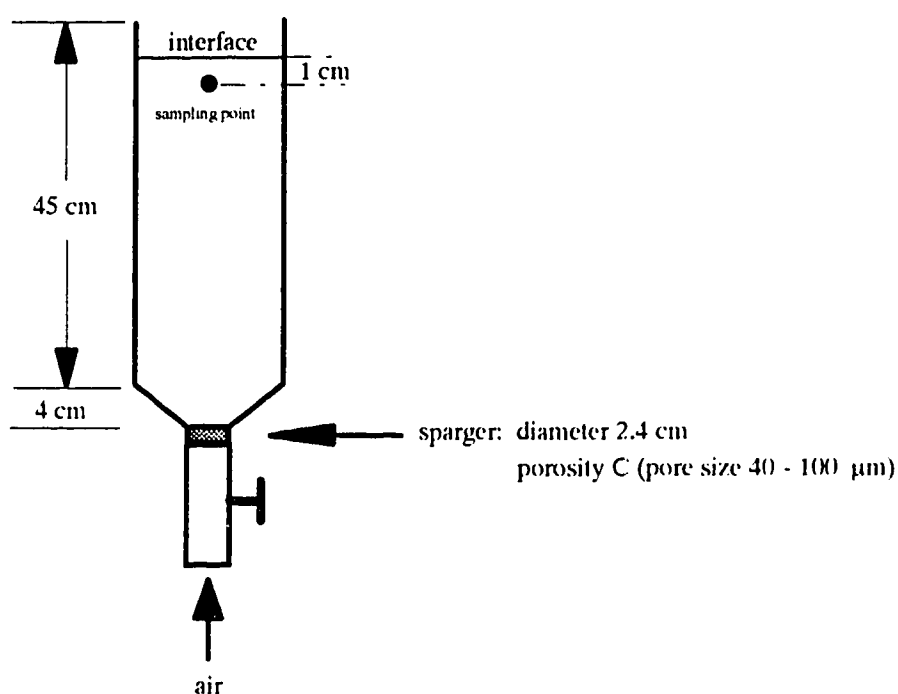


Figure 7-1. A schematic diagram of the experimental bubble column.

To prevent the microcarriers from attaching or binding to the glass surface, the bubble column, and all other glassware including pipettes for sampling purpose, were coated with the siliconizing agent dichlorodimethylsilane following a procedure recommended by Corning for siliconizing spinner flasks.

7.2.4 Sampling

20 mL of suspension sample was taken from a fixed point, 1 cm below the gas-liquid interface along the axis of the bubble column as soon as the steady state was established (approximately 10 min after a new inclination angle was set for the column). The sequence of experiments with different inclination angles was randomized. For each inclination angle, at least four samples were taken in total. Microcarrier beads were collected by filtering samples on #4 Waterman paper for weight determination.

7.3 RESULTS AND DISCUSSION

7.3.1 Sparging Without Antifoam

In our preliminary experiments, the microcarrier suspension in a vertical bubble column was sparged at 0.05 vvm in the absence of antifoam. Due to the presence of serum in the medium, severe foaming occurred as soon as the sparging started. A foam layer formed at the free gas-liquid interface quickly, and continued to grow as sparging carried on. Microcarrier entrainment into the foam phase was easily visible. Clumps of microcarriers were also found to adhere to the column wall above the gas-liquid interface. Entrained microcarriers left the bubble column as the foam overflowed from the top of the column. These observations were similar to those found with our previous experiments with microcapsules (see Chapter 3), and to those indicated by Aunins et al. (1986) with microcarrier cultures for FS-4 cells.

7.3.2 Sparging With Antifoam

As aeration of microcarriers in serum-supplemented medium was not practical to operate due to the severe foaming, and subsequent microcarrier loss in the foam phase, non-toxic antifoams should be used to suppress the foam formation (Aunins, et al., 1986). The free gas-liquid interface is still present, even without a foam phase, and poses potential problems to microcarrier cultures in light of collection of microcarriers by rising air bubbles, and fluid-mechanical damage of cells at the interface.

Figure 7-2 shows the microcarrier concentration at a fixed point (1 cm below the liquid surface) as a function of inclination angle for a constant sparging rate of 0.05 vvm. When the bubble column was vertical, the microcarrier concentration was approximately 9.2 g/L. When the column was inclined to 10° from vertical, the microcarrier concentration near the interface did not change significantly. As the column was further inclined to greater than 10° from the vertical, however, the microcarrier concentration linearly decreased with the increase of the inclination angle. This decrease in microcarrier concentration near the liquid surface corresponded with the qualitative observation of enhanced cell settling when the bubble column was inclined from the vertical.

Initially, the total dry microcarriers added to the bubble column weighed 8.5024 g. The equivalent average microcarrier concentration, based on a total liquid volume of 1.2 L was therefore approximately 7.1 g/L. Compared to this calculated volumetric average of 7.1 g/L, the microcarrier concentrations near the interface were approximately 30% higher for the vertical column, and 10% higher for the column inclined at 40° respectively. The enhanced microcarrier concentrations near the interface suggest the existence of flotation in the bubble column. However, we could not draw more quantitative conclusions due to the lack of microcarrier concentration measurements at other positions in the bubble column. The microcarrier concentration near the liquid surface likely depended on the following hydrodynamic characteristics in the inclined bubble column: flotation by air bubbles, liquid circulation, and microcarrier settling. For a constant sparging rate, flotation likely played a most important role at small angles of inclination, while settling dominated at large inclination angles. At intermediate inclinations, such as 10°, reduction in microcarrier concentration near the interface by settling was probably balanced out by the increased liquid circulation (see Chapter 6), resulting a comparable microcarrier concentration to the vertical column.

In the vertical bubble column, microcarrier segregation was negligible. As the column was inclined between 10° to 30° from vertical, transient settling of microcarriers towards the lower surface of the bubble column was observed. Microcarriers settled to the lower column surface, but were transiently stirred up and entrained into the liquid. Microcarrier settling became more severe as the

column was further inclined to 40° from vertical. Towards the bottom of the column, the settling appeared to be stagnant.

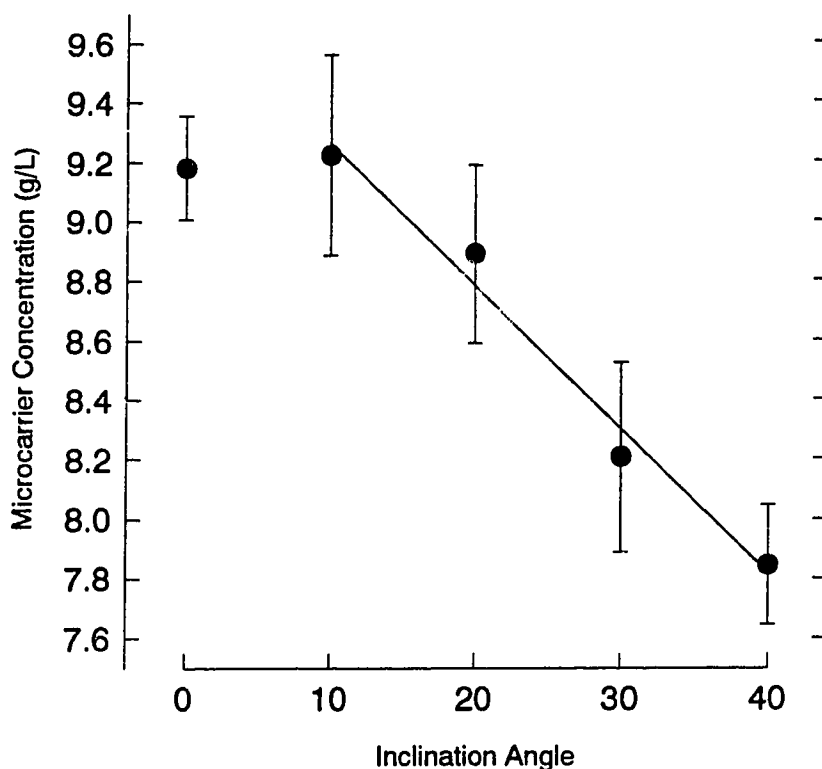


Figure 7-2. Microcarrier concentration near the liquid surface as a function of the inclination angle for a constant sparging rate of 0.05 vvm. The straight line is from a linear regression of the data from 10° to 40° inclination. Error bars represent 95% confidence interval.

7.4 CONCLUSIONS

1. In the absence of antifoam, a growing foam phase was formed at the liquid surface due to the serum supplement in the medium. Microcarriers were floated by air bubbles, and entrained into the foam phase.
2. Foam formation was suppressed by the addition of 400 ppm of antifoam. Compared to the vertical bubble column, the microcarrier concentration in the

vicinity of the liquid surface remained constant for an inclination angle of 10° , but linearly decreased with θ for inclination angles of up to 40° .

3. Microcarrier settling was not visible for the vertical bubble column. Transient settling was observed for 10° , 20° , and 30° inclinations. A stagnant zone was formed near the bottom of the bubble column for the inclination angle of 40° . These qualitative observations on settling explained the reduced microcarrier concentration near the liquid surface.

REFERENCES

- Aunins, J.G., Croughan, M.S., Wang, D.I.C., and Goldstein, J.M. 1986. Engineering developments in homogeneous culture of animal cells: oxygenation of reactors and scaleup. *Biotechnol. Bioeng. Symp.* **17**: 699-723.
- Croughan, M.S., and Wang, D.I.C. 1989. Growth and death in overagitated microcarrier cell cultures. *Biotechnol. Bioeng.* **33**: 731-744.
- Croughan, M.S., and Wang, D.I.C. 1991. Hydrodynamic effects on animal cells in microcarrier bioreactors. pp. 213-249. In: *Animal cell bioreactors*. C.S. Ho and D.I.C. Wang, Eds., Butterworth-Heinemann, Boston.
- Griffiths, B. 1991. Cultural revolutions. *Chem. & Industry (London)* **18**: 682-684.
- Hirtenstein, M.D., Clark, J.M., and Gebb, C. 1982. A comparison of various laboratory scale culture configurations for microcarrier culture of animal cells. *Dev. Biol. Stand.* **50**: 73-80.

Chapter 8

Conclusions and Recommendations

Physical damage of animal cells in suspension cultures, due to stirring and sparging, is coupled with complex metabolic responses. Nylon microcapsules, therefore, were used as a physical model to study the mechanisms of damage in a stirred bioreactor and in a bubble column. Microcapsule breakage followed first-order kinetics in all experiments. Entrainment of bubbles into the liquid phase in the stirred bioreactor gave more microcapsule breakage. In the bubble column, the bubble bursting zone at the gas-liquid interface was primarily responsible for microcapsule breakage. The forces on the microcapsules were equivalent to an external pressure of approximately $4 \times 10^4 \text{ N}\cdot\text{m}^{-2}$, based on the critical microcapsule diameter for survival of $190 \mu\text{m}$. A stable foam layer, however, was found to be effective in protecting microcapsules from damage. The microcapsule transport to the gas-liquid interface and entrainment into the foam phase was consistent with flotation by air bubbles.

In order to test a novel bioreactor design for shear-sensitive cells, a murine hybridoma cell line was grown in an inclined bubble column that was inclined up to 45° . Maximum viable cell count and exponential growth of the cells were not affected by inclination, but an inclination of 30° gave an antibody titer of 42 mg/L which more than doubled the yield of 17 mg/L in the vertical position. By comparison, the culture gave yields of 30 mg/L when grown in spinner flasks. The enhanced antibody production in the inclined bioreactor corresponded to a prolonged stationary phase of 45 h.

A rectangular bubble column was used to study the hydrodynamics and mixing in an inclined bubble column. The inclination angle was varied in the range of $0 - 45^\circ$; and the sparging rate from 0.001 to 0.06 vvm. The hydrogen bubble technique was used to find the liquid velocity and its profile. The liquid circulation was significantly enhanced by inclination, but little additional effect was found when the inclination angle was greater than 10° . CFD using the FLOW3D package was attempted to have obtained agreement with experimental

results in the order of magnitude. Mixing in the inclined bubble column was investigated by a pulse injection method. Compared to the vertical column, mixing time was significantly reduced by inclining the column. But the largest reduction in mixing time was found within 10° inclination. A recycle-cross-flow model was proposed to investigate mixing in the inclined bubble column. The adjustable parameter K , which reflected the cross mixing between the downward flow and the upward flow, was potentially useful as a guiding parameter for scale-up.

Further research is recommended along the following lines:

1. CFD using multiphase models are required to better simulate the liquid flow in the inclined bioreactor. The recycle-cross-flow model can be used to further investigate mixing in light of scale-up based on mixing models. To better describe mixing in the inclined bioreactor, axial dispersion will have to be included in the mixing model. Mixing time can be derived from this mixing model, and then compared to experimental data.
2. In terms of design, the plate spacing and aspect ratio have to be varied to optimize the Inclined-plate Bioreactor. Bottom design is important for the bioreactor. Mass transfer study, such as K_La measurements, in the inclined bioreactor remained to be investigated.
3. In general, flotation of other cell types, such as insect cells, may be more serious than hybridoma cells. This new bioreactor design, therefore, should be tested with these cell types. The Inclined-plate Bioreactor may find application for microcarrier cultures for which direct sparging has always be problematic.
4. Due to cell segregation in the inclined bioreactor, perfusion type of operation may be possible. This needs to be investigated with real cell cultures; and hydrodynamic characterization will be necessary.

APPENDIX A

ELISA PROCEDURE FOR DETERMINATION OF IgG ANTIBODY

- (1) Dissolve HSA (Sigma, St. Louis, Missouri) to 1mg/mL in PBS.
- (2) Dispense 50 µl/well on 96-wells ELISA plates, cover with parafilm, and leave overnight at 4° in a refrigerator.
- (3) Wash wells twice with PBS, dispense 100 µl/well blocking solution, 1% Bovine Serum Albumin (BSA, Miles Inc., Kankakee, Illinois) in PBS, and incubate at 37°C for 30 min.
- (4) Flick off blocking solution, dispense 1° antibody in triplicate, i.e. diluted cell supernatants and purified antibody of 1.5 mg/mL (kindly provided by Biomira Inc., Edmonton, Alberta, Canada) as standards. Standards were double diluted in cell culture medium so that there were 8 concentrations for a standard curve, i.e. 75 ng/well, 37.5 ng/well, 18.75 ng/well, ..., and straight medium.
- (5) Incubate at 37°C for 2 h.
- (6) Wash three times with PBS, dispense 2° antibody (goat anti mouse IgG-HRPO, Southern Biotechnology Associates, Inc., Birmingham, Alabama) 50 µl/well, and incubate at 37°C for 1 h.
- (7) Wash three times with PBS, and dispense substrate solution 50 µl/well. Substrate solution was made from 1:1 solution A (ABTS peroxidase substrate solution A, Kirkegaard & Perry Laboratory, Inc., Gaithersburg, Maryland) and solution B (peroxidase solution B, Kirkegaard & Perry Laboratory, Inc., Gaithersburg, Maryland).
- (8) Read OD at a test wavelength of 405 nm and a reference wavelength of 490 nm in a ELISA plate reader after the color was developed for 10 - 15 min.
- (9) Linear regression was carried out on the linear part of the standard curve, and the repression equation was used to calculate the antibody concentration of the supernatants which was then multiplied by the dilution factor to obtain the actual IgG concentration of the cell supernatants. Figure A-1 is a representative ELISA standard curve.

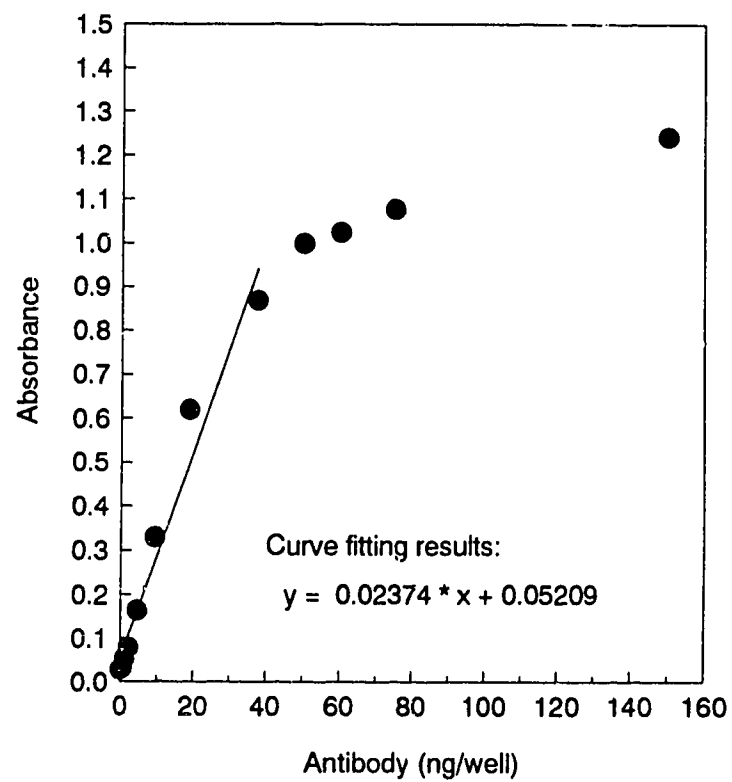


Figure A-1. A standard curve for ELISA assay from Experiment #4.

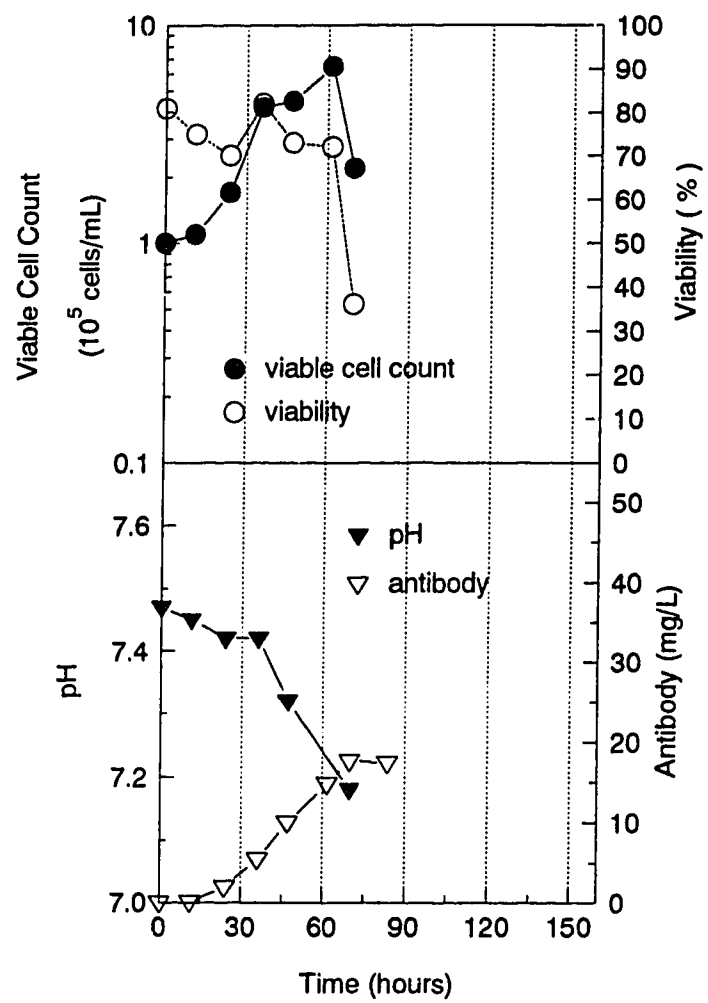


Figure A-2. Cell growth and antibody production for the repeated vertical experiment.

Table A-1. Amino acid concentrations (μM) in the fresh medium and in the spent medium at the end of experiment #1.

	fresh medium	bioreactor	dish control	spinner control
Aspartic acid	133.61	112.69	87.63	90.68
Glutamic acid	179.50	253.99	214.40	226.44
Asparagine	284.32	229.53	200.48	207.29
Serine	270.06	198.96	189.78	231.18
Glutamine	772.75	252.23	257.85	16.98
Histidine	124.04	49.82	37.58	46.95
Glycine	150.10	152.66	153.34	169.48
Threonine	170.27	51.27	21.69	45.76
Citrulline	13.51	5.72	5.20	0.00
Arginine	408.58	380.83	281.00	322.57
Taurine	12.20	9.08	8.84	8.38
Alanine	72.96	283.11	281.01	281.05
Tyrosine	115.60	46.66	31.00	38.39
Tryptophan	26.51	2.92	3.01	2.29
Methionine	95.39	32.93	17.16	26.07
Valine	166.06	41.73	7.45	21.67
Phenylalanine	199.05	55.00	22.55	41.15
Isoleucine	231.01	156.35	120.47	106.19
Leucine	248.06	131.74	92.57	85.85
Ornithine	54.50	197.30		109.41
Lysine	219.87	60.78	75.11	67.72

Appendix B

Command File Used for FLOW3D Simulation

```
/******  
/*SOLVE THE INCLINED CHANNEL PROBLEM WITH THE */  
/*FOLLOWING ASSUMPTIONS: */  
/*          CLOSE BOTTOM */  
/*          MASS FLOW BOUNDARY AT OPEN END */  
/*          MOVING UPPER PLATE */  
/*          TURBULENT FLOW */  
/******  
>> FLOW3D  
  >> SET LIMITS  
    TOTAL REAL WORK SPACE 2000000  
    TOTAL INTEGER WORK SPACE 800000  
    MAXIMUM NUMBER OF BLOCKS 1  
    MAXIMUM NUMBER OF PATCHES 20  
    MAXIMUM NUMBER OF INTER BLOCK BOUNDARIES 0  
    END  
  >> OPTIONS  
    TWO DIMENSIONS  
    TURBULENT FLOW  
    RECTANGULAR GRID  
    END  
>> MODEL TOPOLOGY  
  >> INPUT TOPOLOGY  
    READ GEOMETRY FILE  
    END  
  >> CREATE PATCH  
    PATCH TYPE 'WALL'  
    PATCH NAME 'UPPER PLATE'  
    BLOCK NAME 'BLOCK-NUMBER-1'  
    HIGH J
```

```

END
>> CREATE PATCH
  PATCH NAME 'EXIT'
  PATCH TYPE 'MASS FLOW BOUNDARY'
  BLOCK NAME 'BLOCK-NUMBER-1'
  HIGH I
  END
>> MODEL DATA
  >> PHYSICAL PROPERTIES
    >> STANDARD FLUID
      FLUID 'WATER'
      STANDARD FLUID REFERENCE TEMPERATURE 294.65
    END
  >> TITLE
    PROBLEM TITLE 'TURBULENT FLOW IN THE INCLINED CHANNEL'
  END
>> SOLVER DATA
  >> PROGRAM CONTROL
    MAXIMUM NUMBER OF ITERATIONS 200
    OUTPUT MONITOR POINT 3 10 1
    MASS SOURCE TOLERANCE 5.0E-10
  END
>> CREATE GRID
  >> INPUT GRID
    READ GRID FILE
  END
>> MODEL BOUNDARY CONDITIONS
  >> WALL BOUNDARY CONDITIONS
    PATCH NAME 'UPPER PLATE'
    U VELOCITY 0.2586
  END
  >> MASS FLOW BOUNDARY CONDITIONS
    MASS FLOW SPECIFIED
    FLUXES 0.0
  END
>> STOP

```

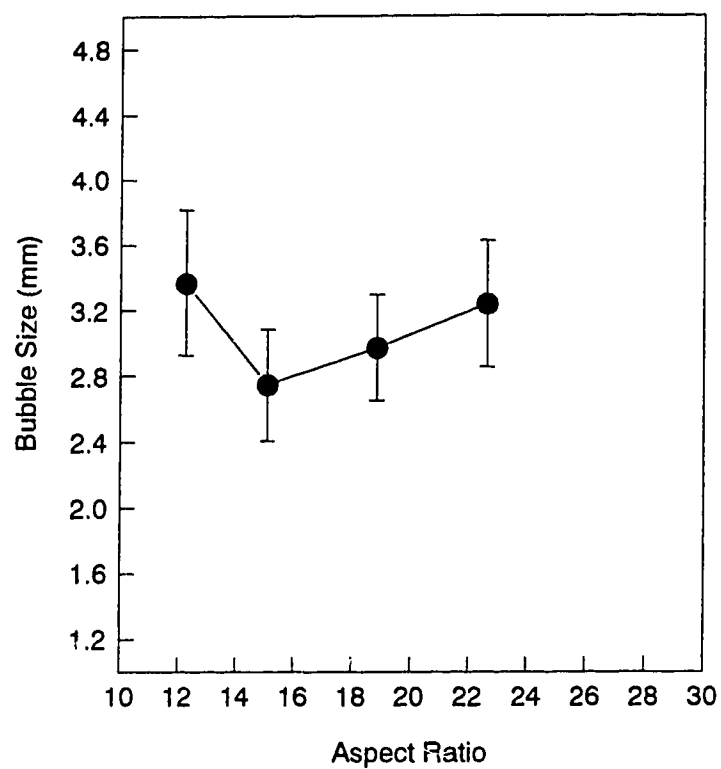


Figure B-1. Bubble size as a function of the aspect ratio for a sparging rate of 33.7 mL/min and 30° inclination.

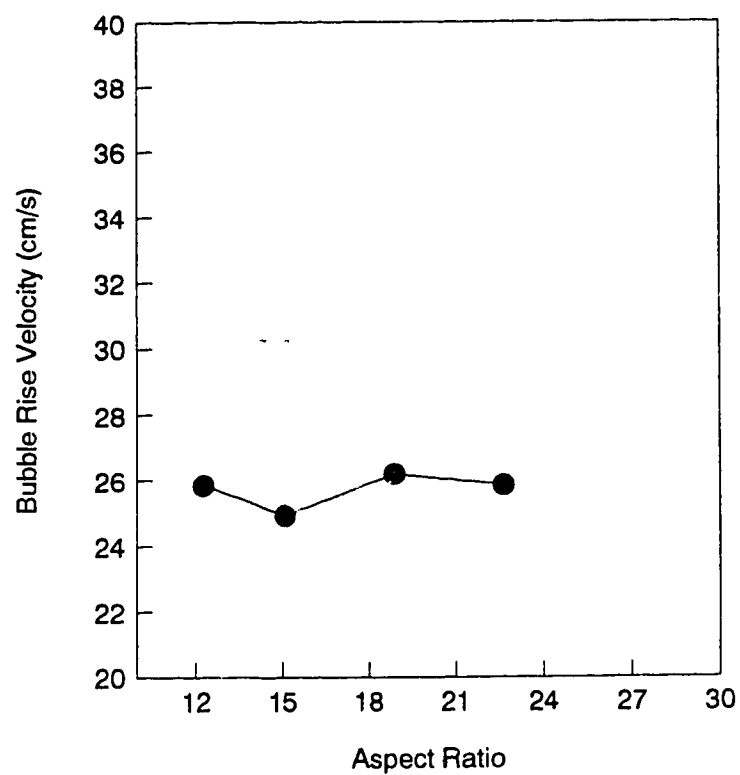


Figure B-2. Bubble rise velocity as a function of the aspect ratio for a sparging rate of 33.7 mL/min and 30° inclination.

Appendix C

Seven bioreactor experiments were carried out in the Inclined-tube Bioreactor for the study reported as Chapter 4. The inclination angles and aeration rates used in these experiments were summarized in Table 4-2, except for experiment #7 which repeated 45° inclination with varied aeration rate. Experiment #7 was actually the first bioreactor run to have been carried out in this series for the purpose of selecting a reasonable aeration rate for the bioreactor cultures.

All raw data from these bioreactor experiments including cell growth, antibody production, and formation of other metabolites are summarized in this appendix.

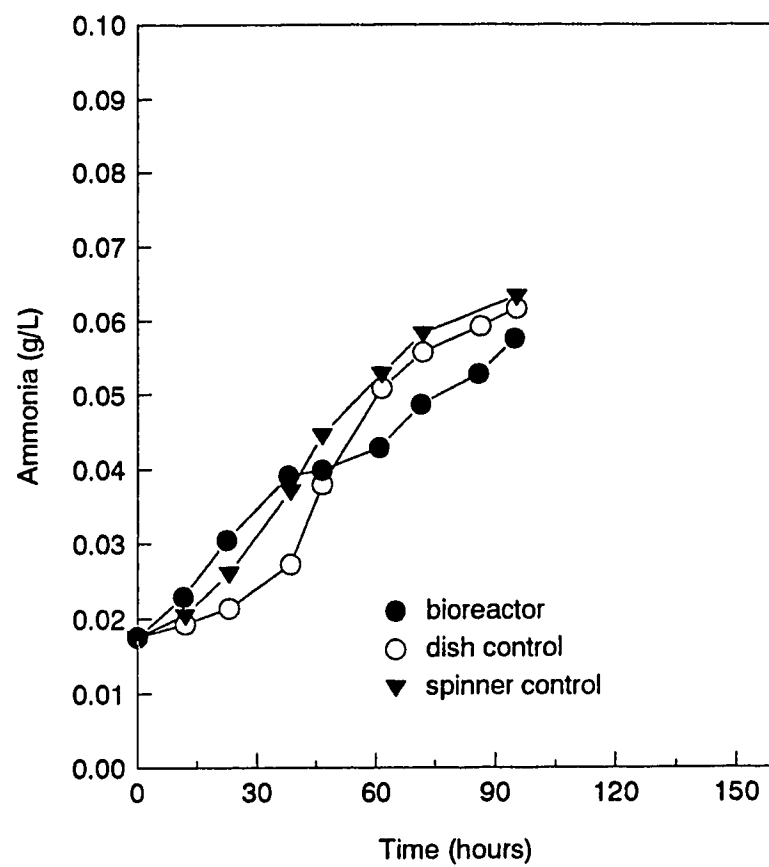


Figure C-1. Ammonia formation in bioreactor experiment #1.

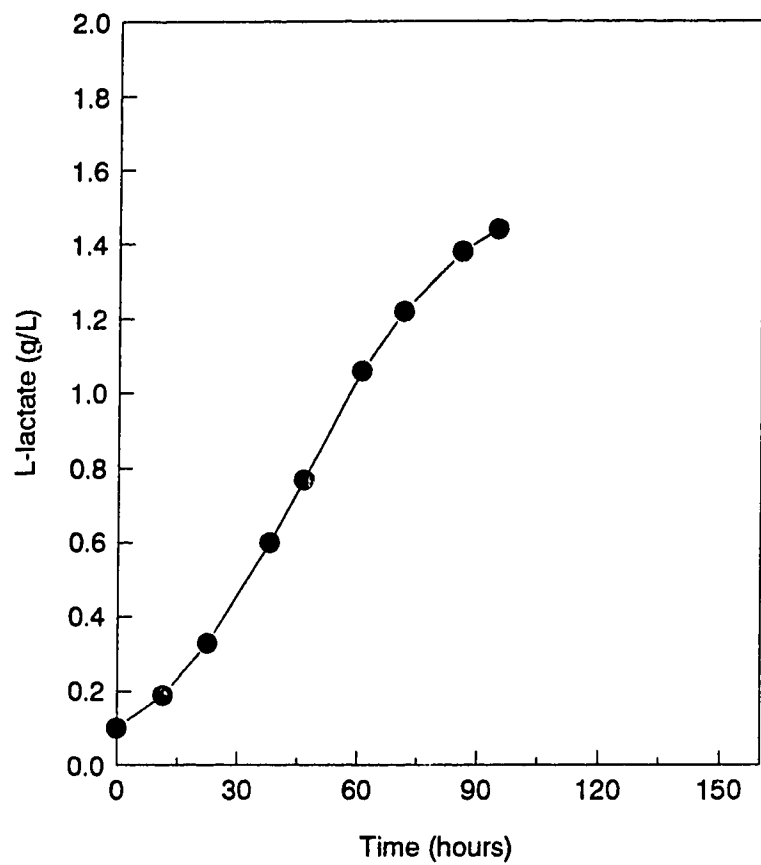


Figure C-2. Lactate formation in bioreactor experiment #1.

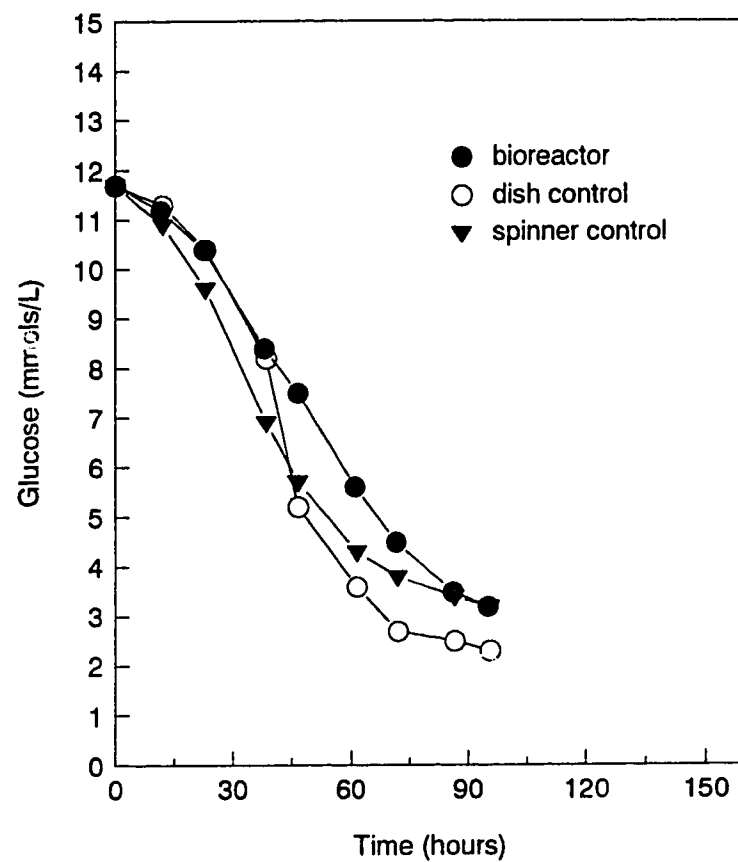


Figure C-3. Glucose consumption in bioreactor experiment #1.

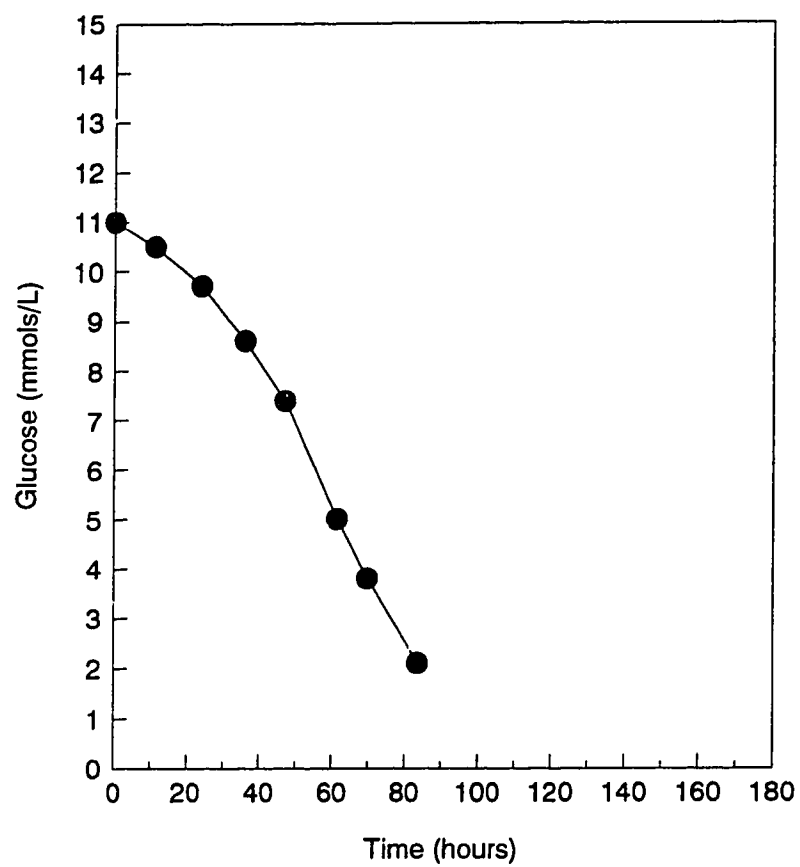


Figure C-4. Glucose consumption in bioreactor experiment #2.

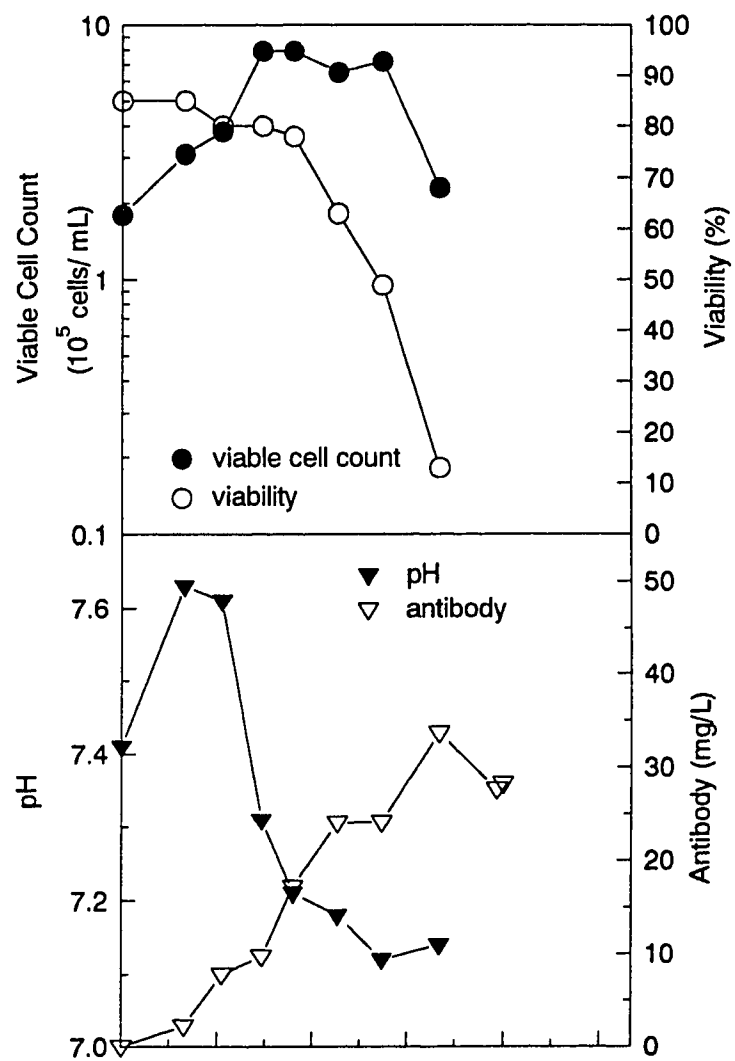


Figure C-5. Cell growth and antibody production for bioreactor experiment #3.

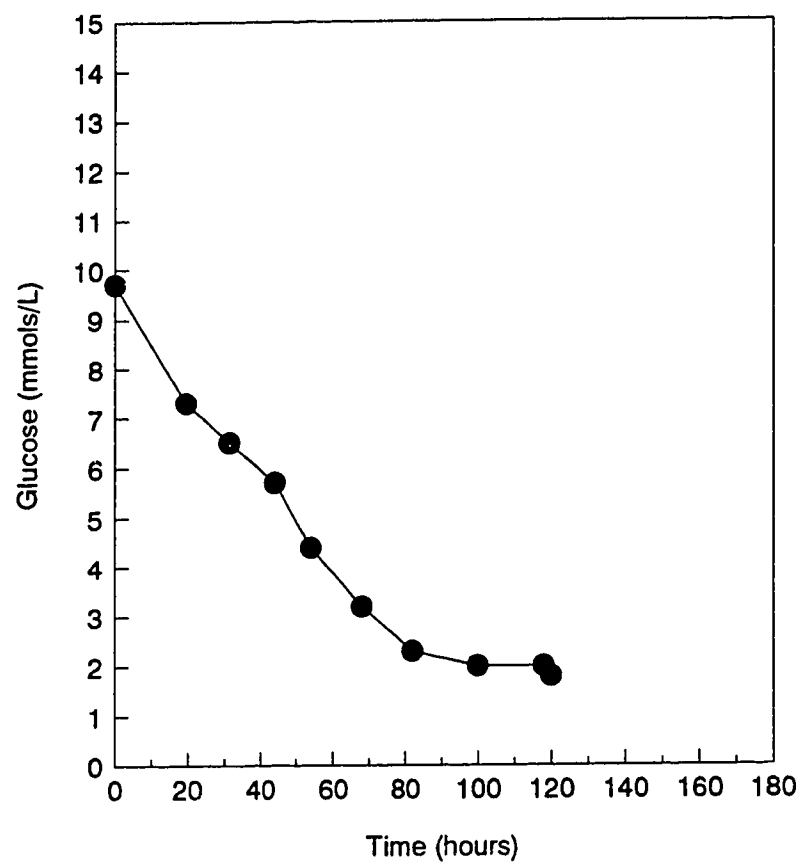


Figure C-6. Glucose consumption in bioreactor experiment #3.

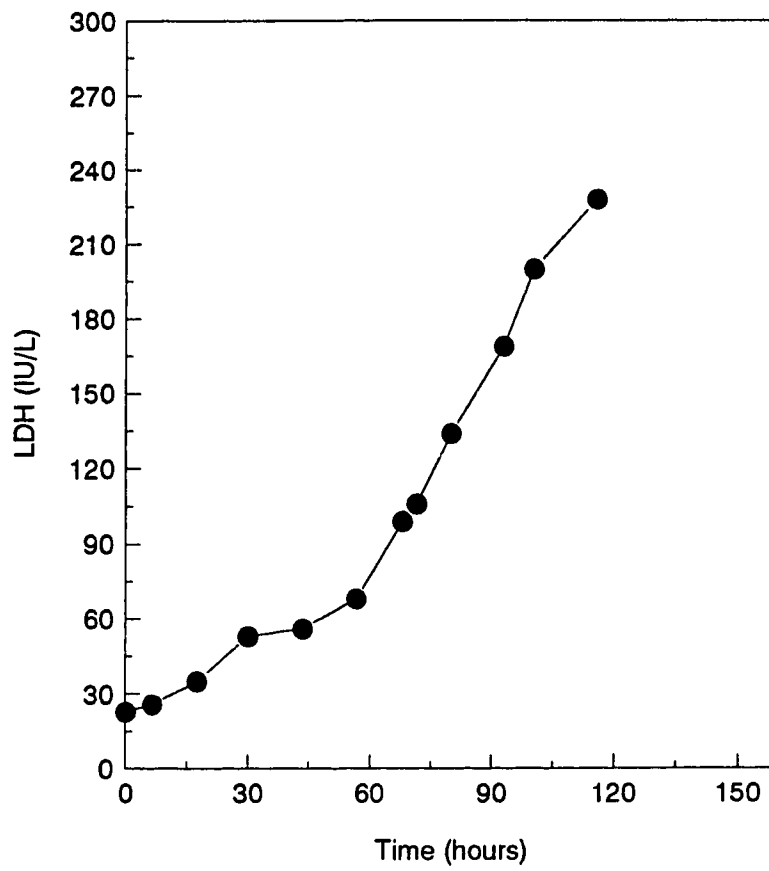


Figure C-7. LDH release in bioreactor experiment #4.

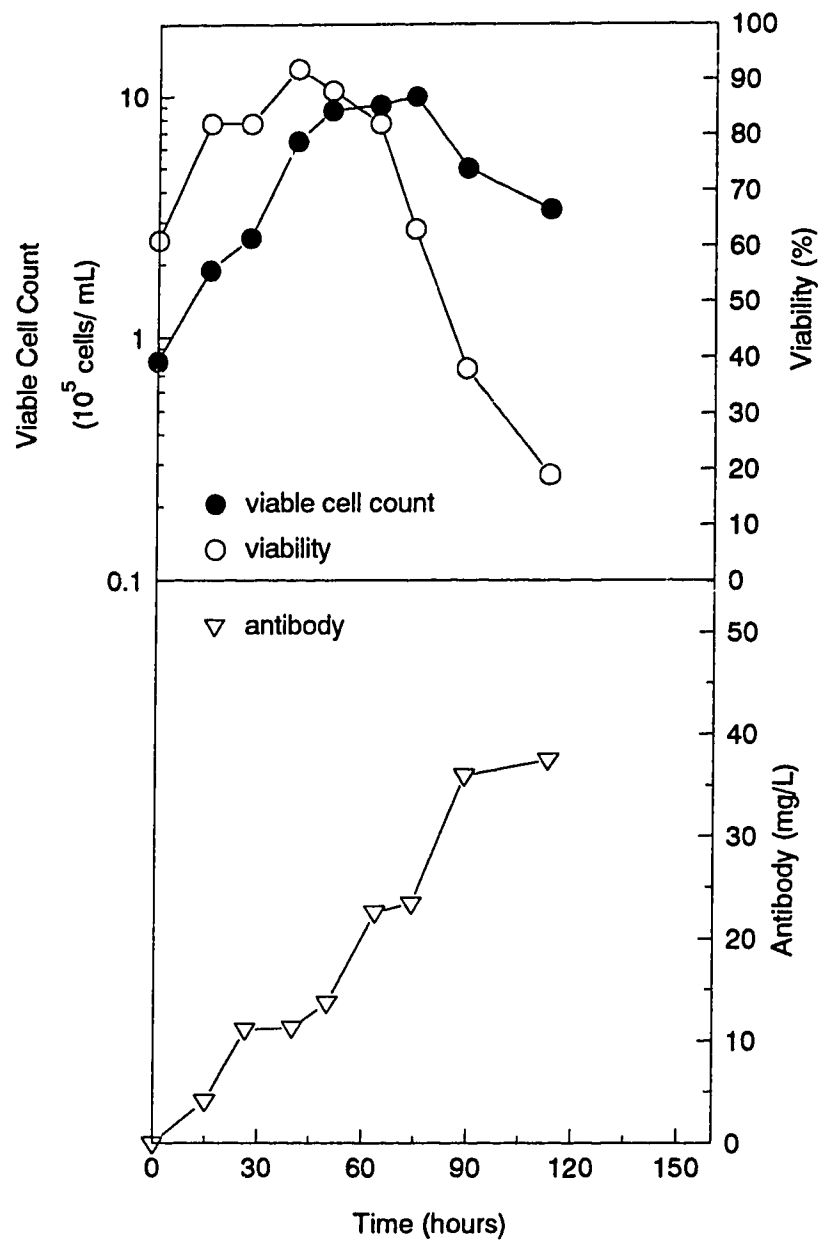


Figure C-8. Dish control for bioreactor experiment #5.

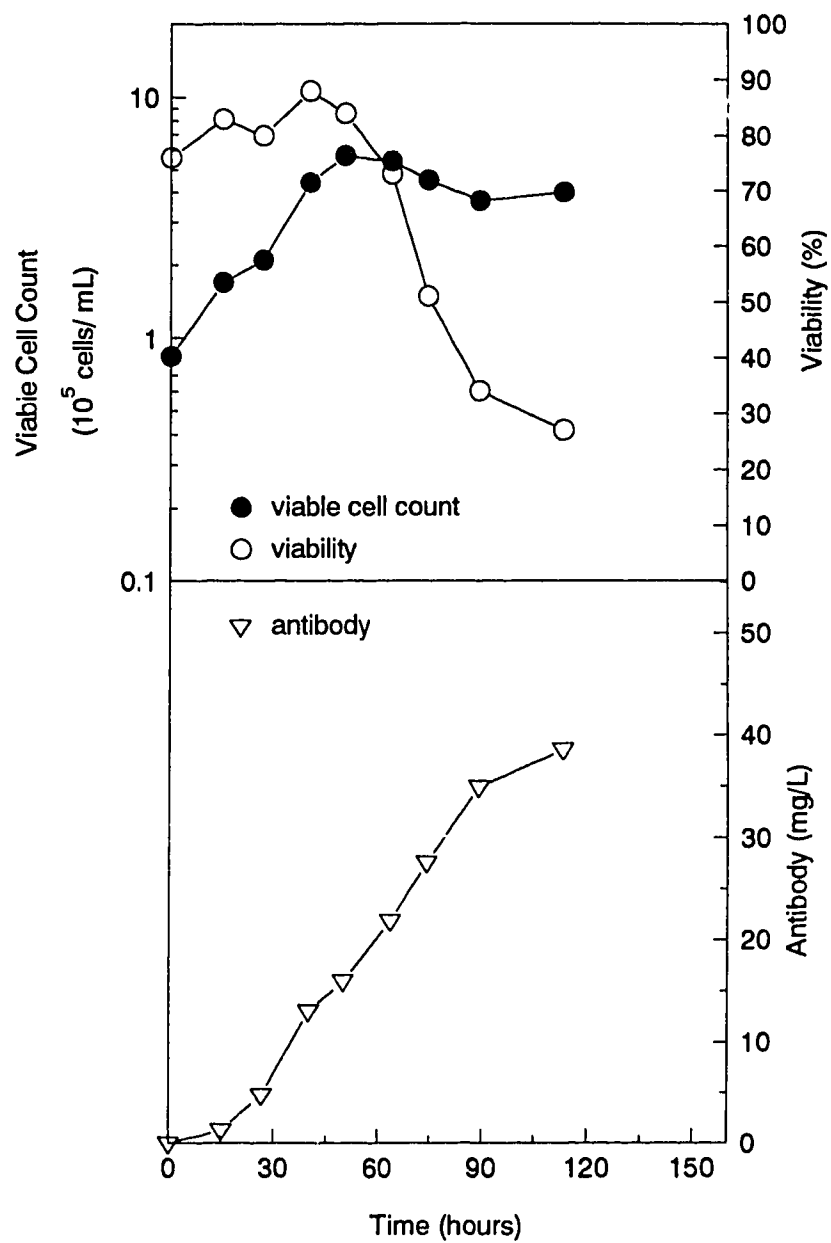


Figure C-9. Spinner control for bioreactor experiment #5.

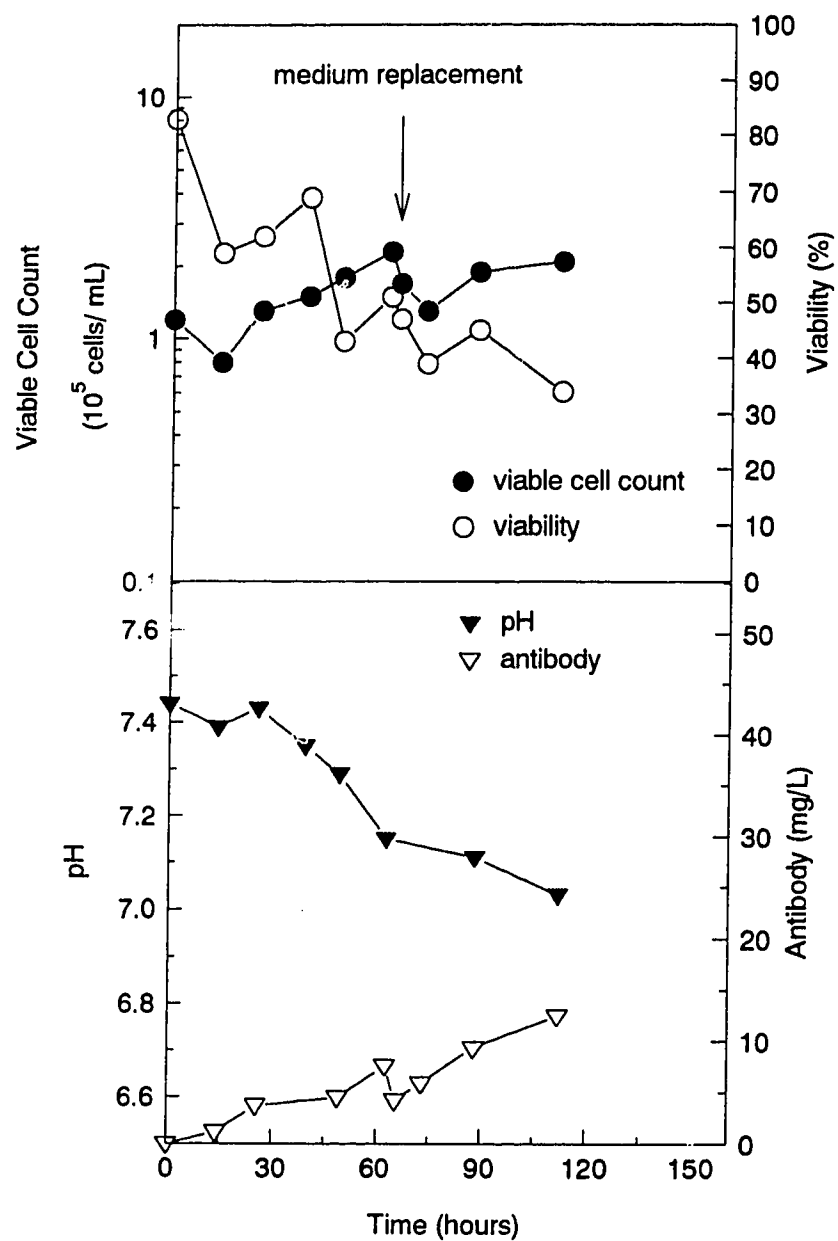


Figure C-10. Cell growth and antibody production in bioreactor experiment #5.

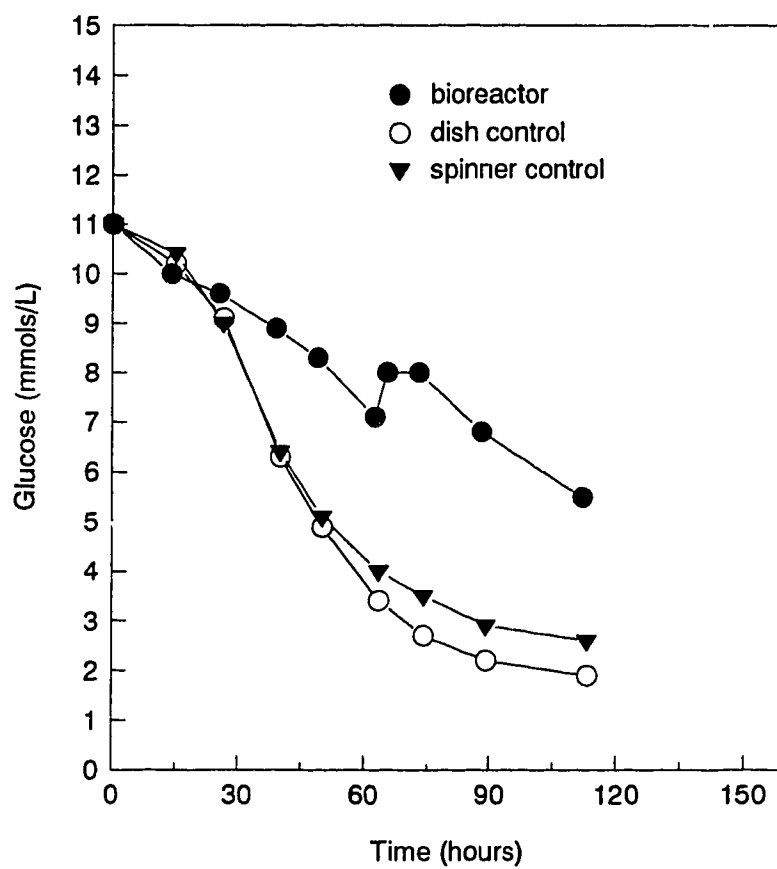


Figure C-11. Glucose consumption in bioreactor experiment #5.

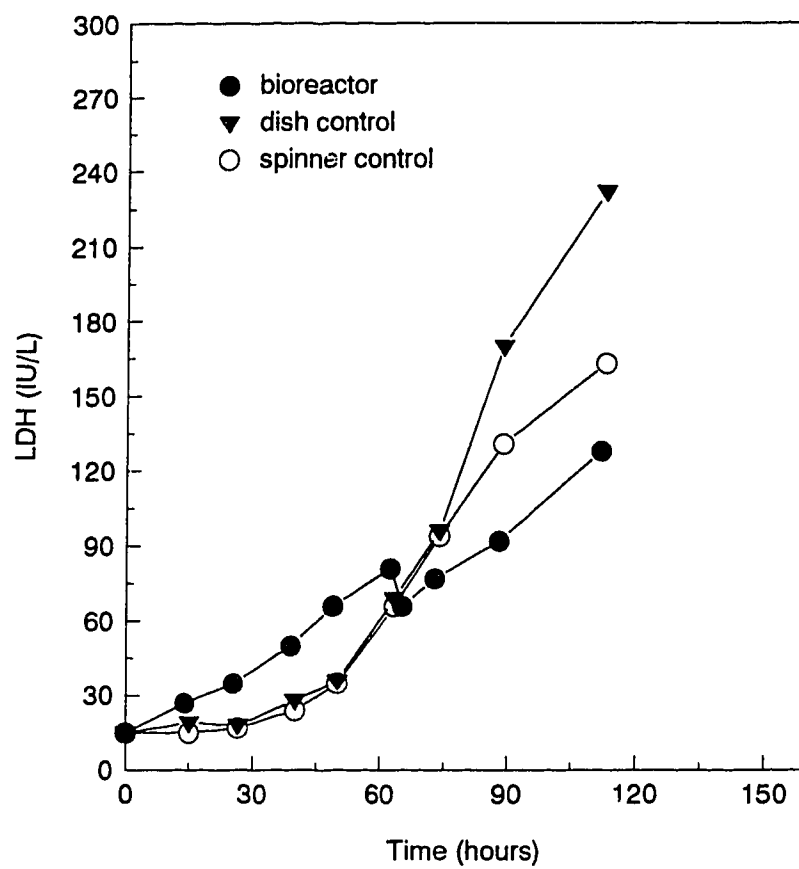


Figure C-12. LDH release in bioreactor experiment #5.

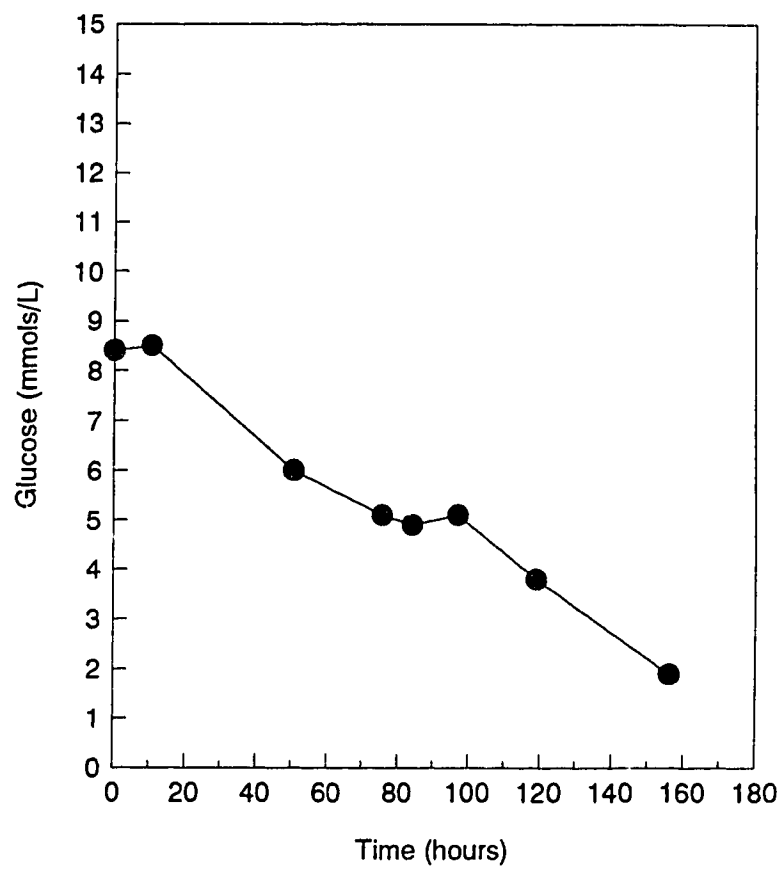


Figure C-13. Glucose consumption in bioreactor experiment #6.

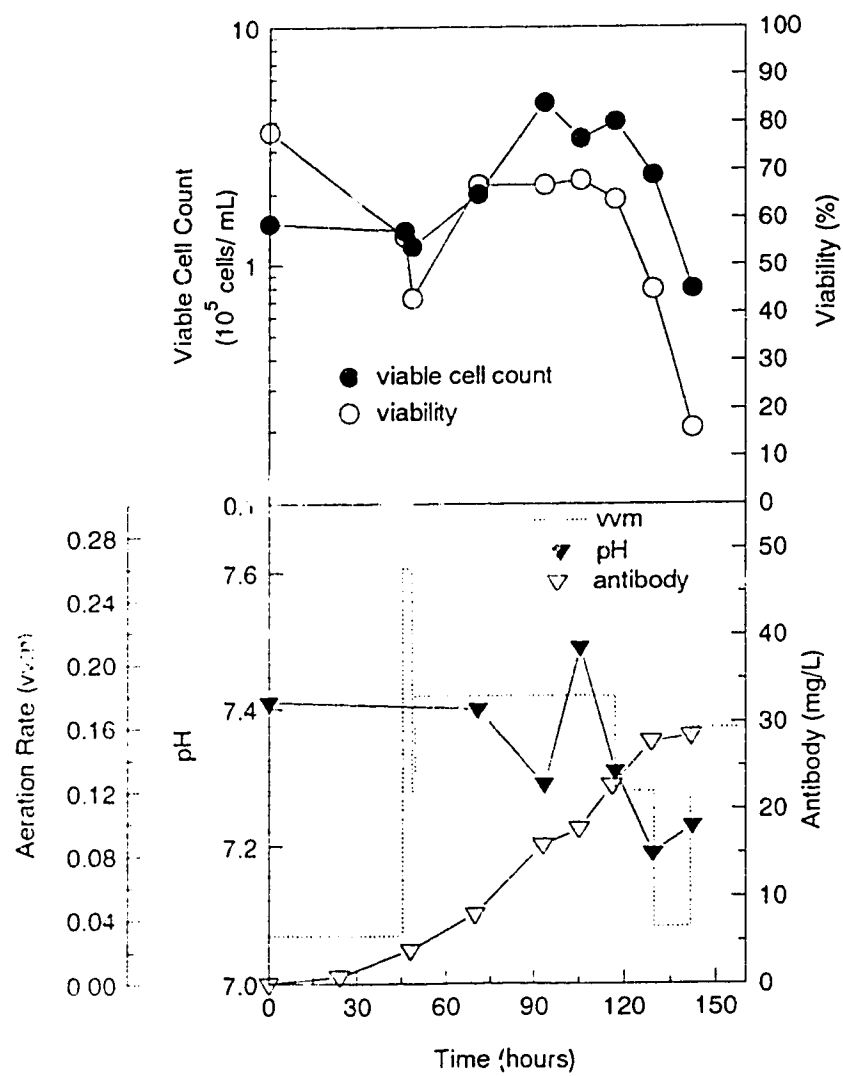


Figure C-14. Cell growth and antibody production in bioreactor experiment #7.

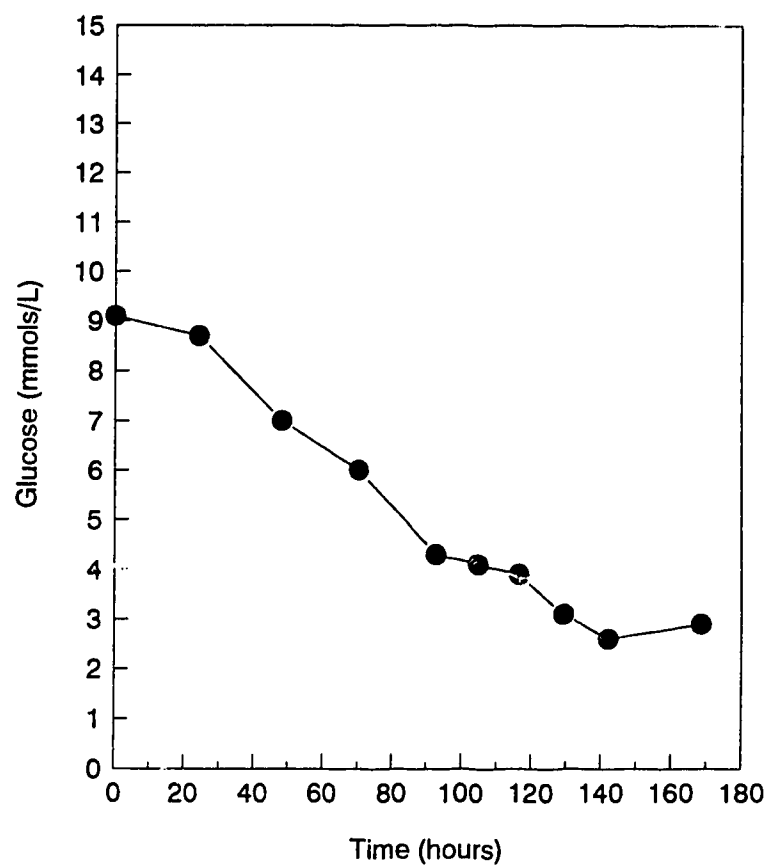


Figure C-15. Glucose consumption in bioreactor experiment #7.

Appendix D

Four bioreactor experiments were carried out in the Inclined-tube Bioreactor for the study reported as Chapter 5. The inclination angles and aeration rates used in these experiments were summarized in Table 5-1.

All raw data from these bioreactor experiments including cell growth, antibody production, and formation of other metabolites are summarized in this appendix.

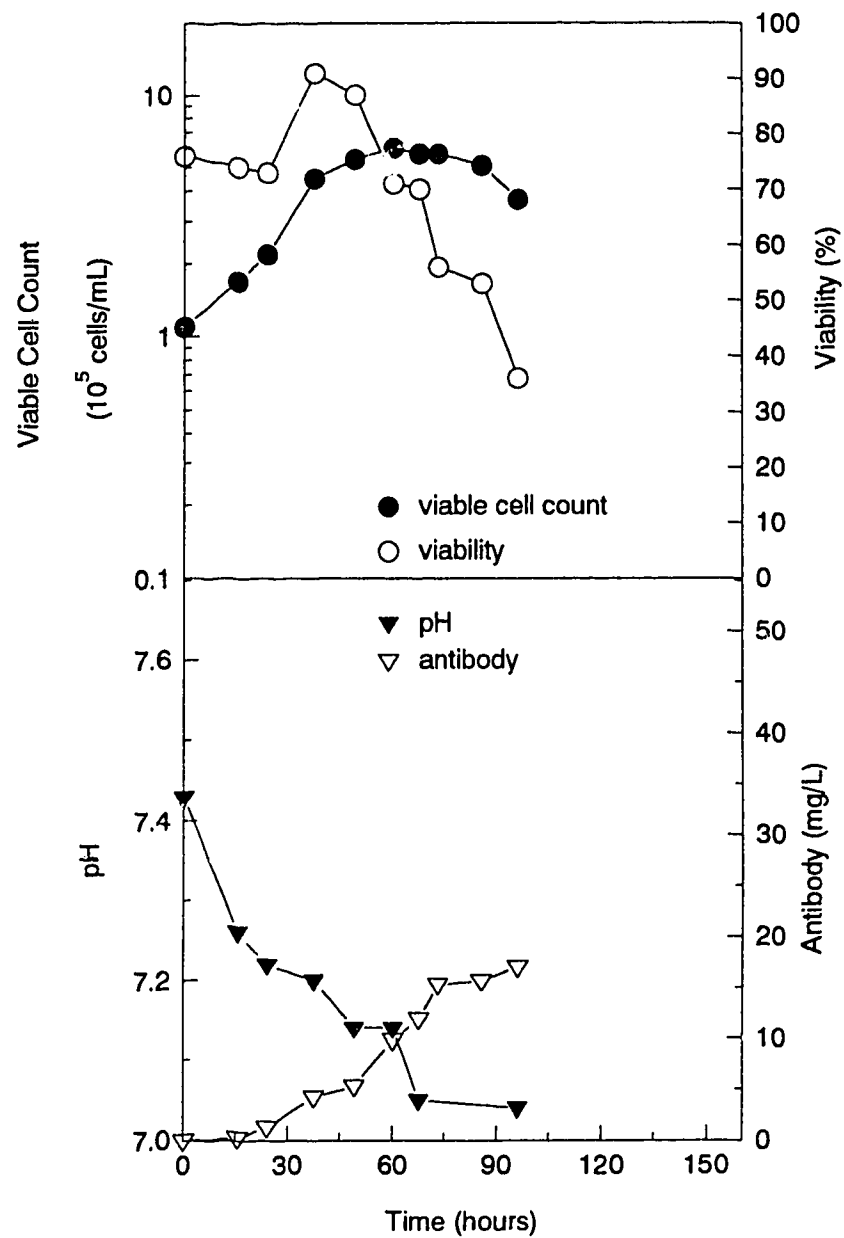


Figure D-1. Cell growth and antibody production in bioreactor experiment #1.

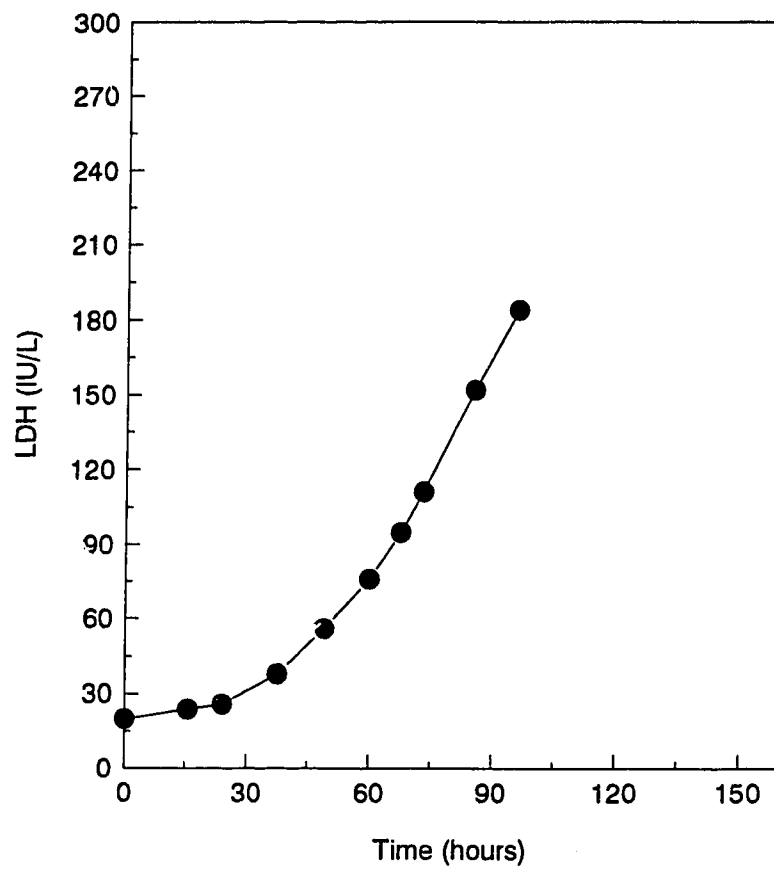


Figure D-2. LDH release in bioreactor experiment #1.

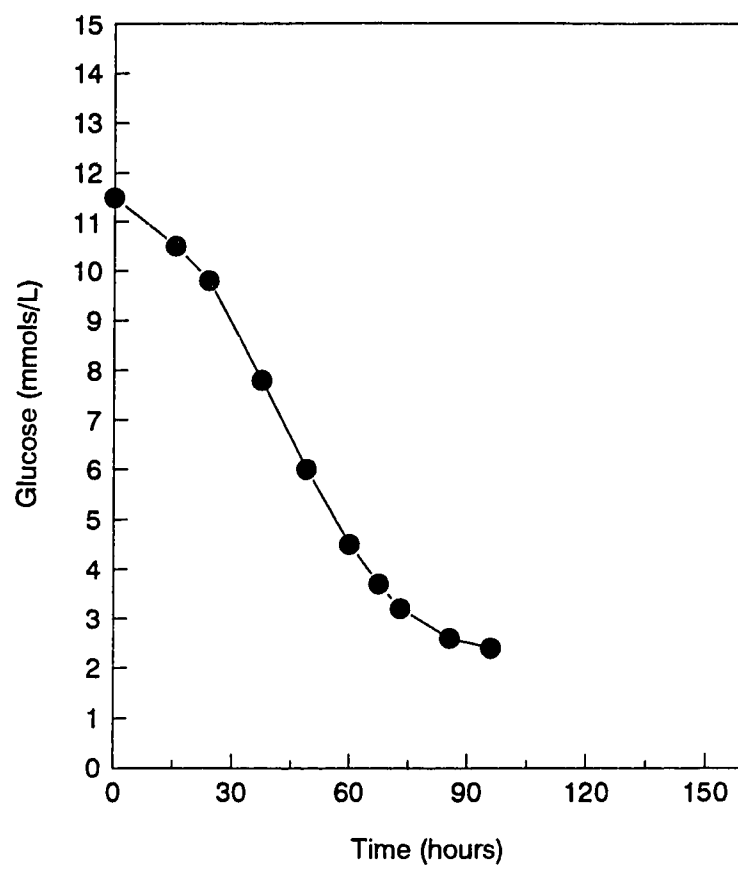


Figure D-3. Glucose consumption in bioreactor experiment #1.

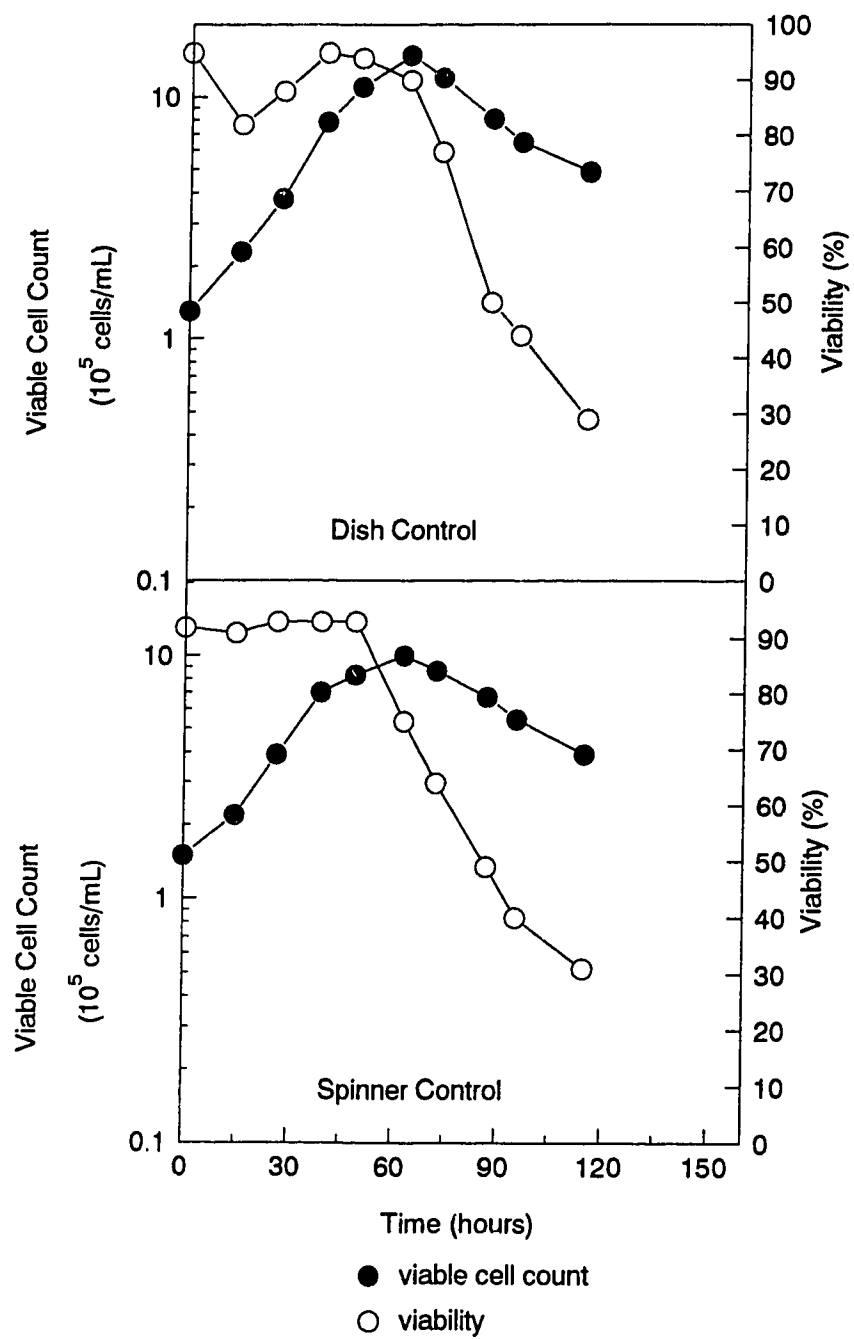


Figure D-4. Controls for bioreactor experiment #2.

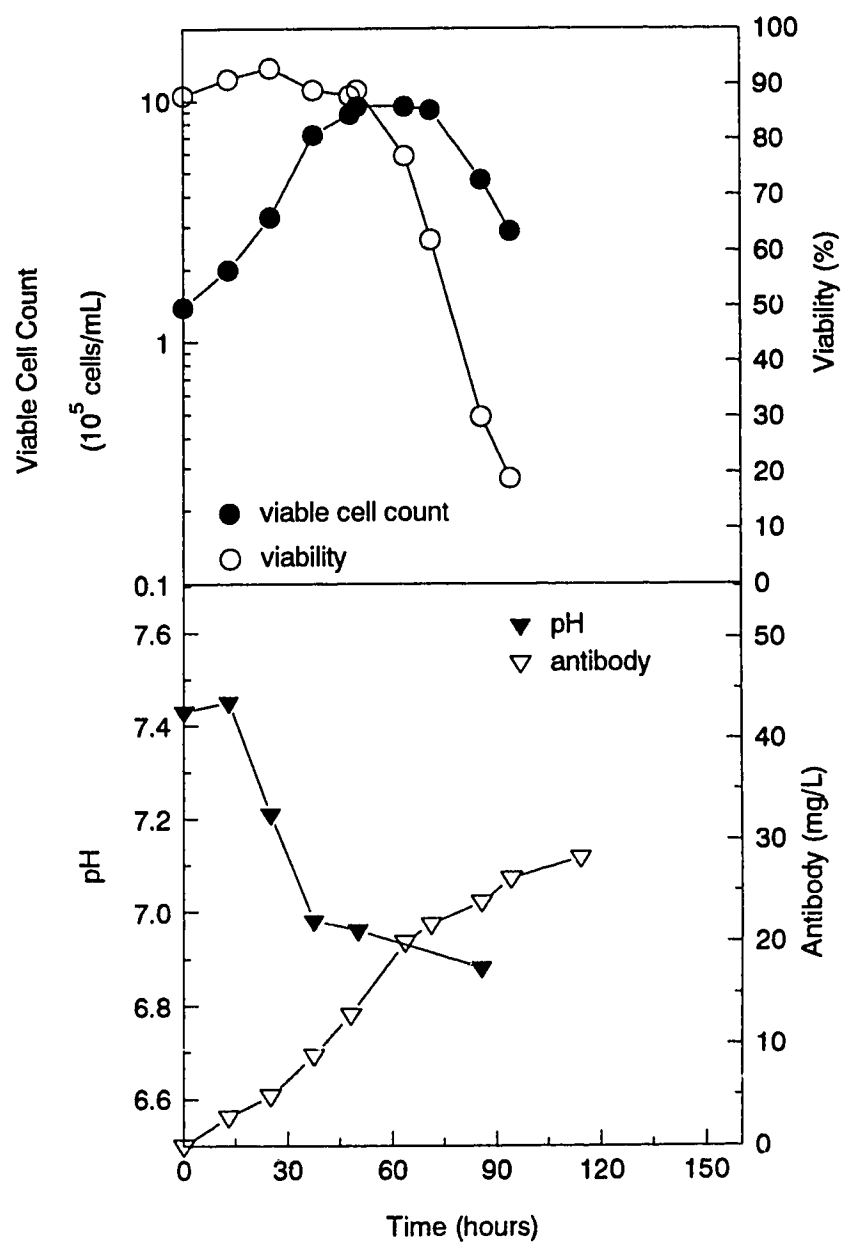


Figure D-5. Cell growth and antibody production in bioreactor experiment #2.

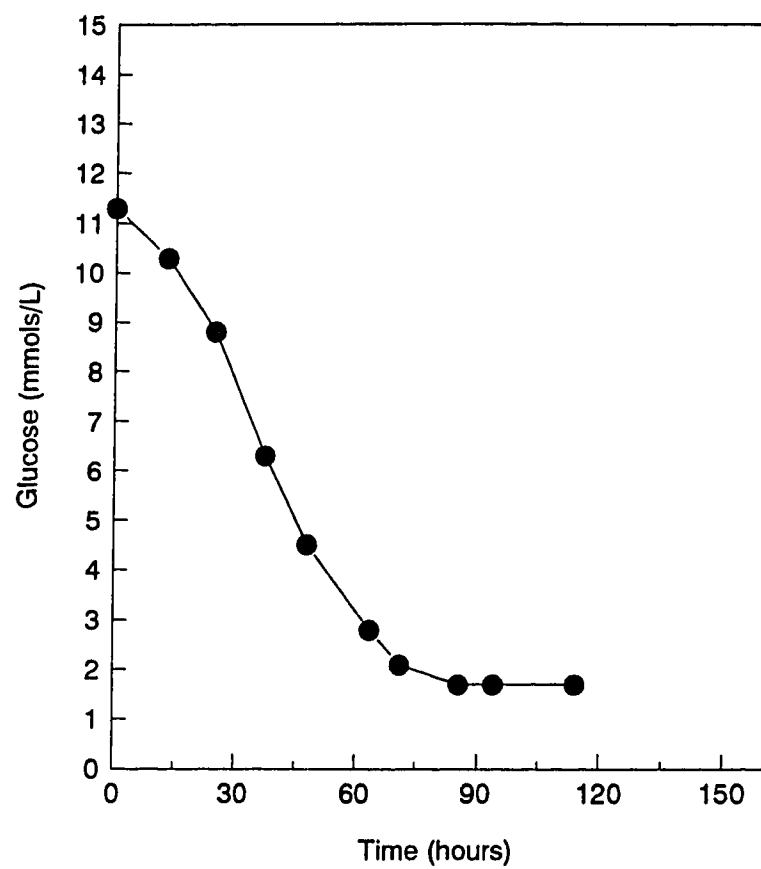


Figure D-6. Glucose consumption in bioreactor experiment #2.

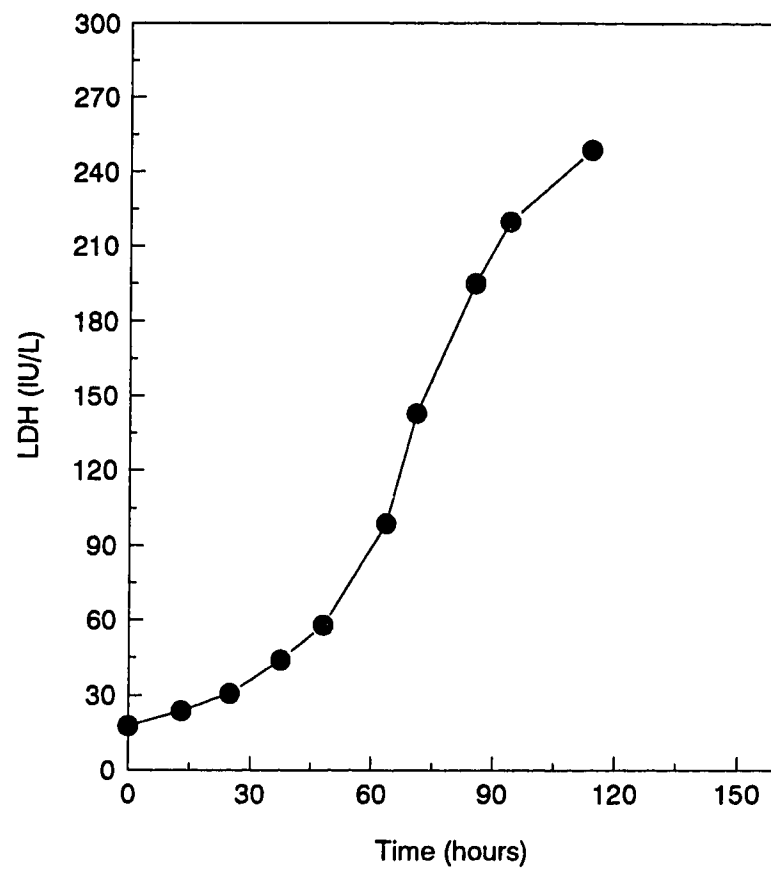


Figure D-7. LDH release in bioreactor experiment #2.

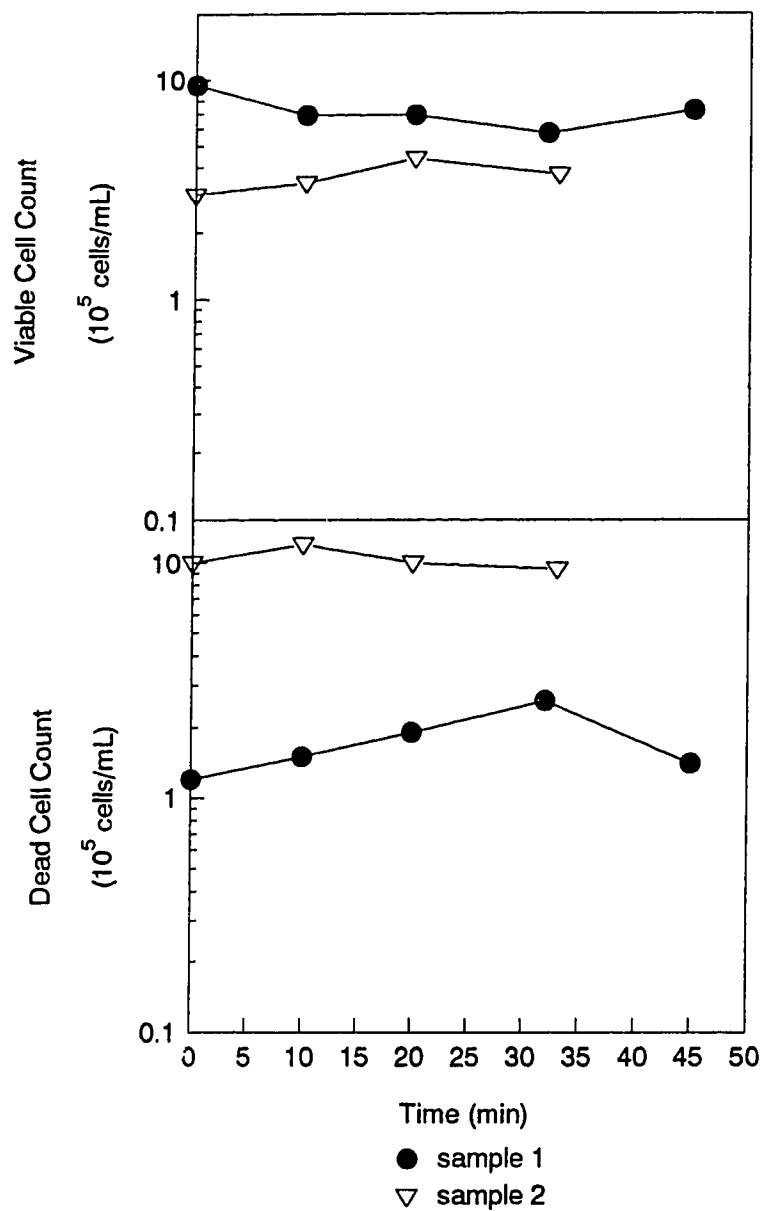


Figure D-8. Flotation study #2 used cells from the bioreactor culture (experiment #2). Sample 1 was taken at 50 hr, and sample 2 at 86.5 hr. The flotation study was discussed in Chapter 4.

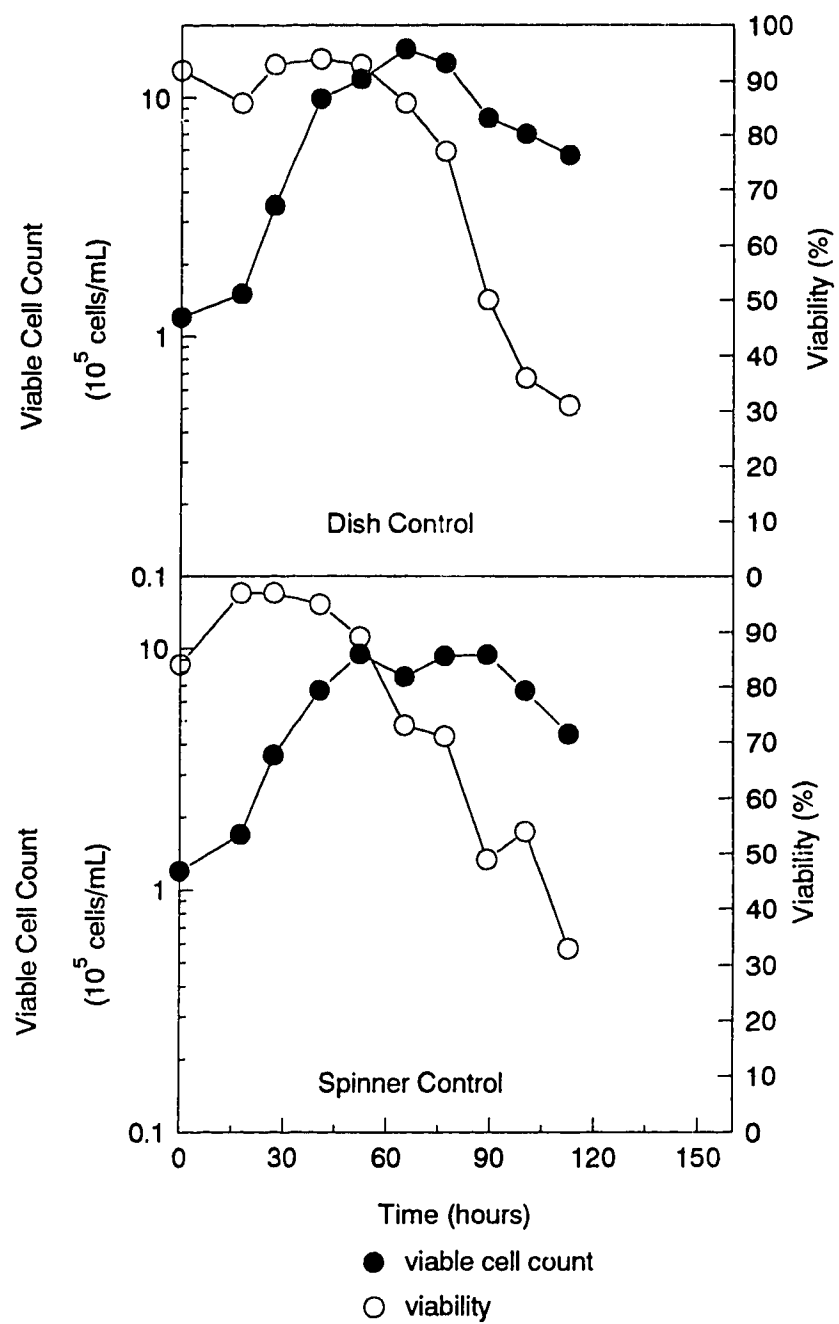


Figure D-9. Controls for bioreactor experiment #3.

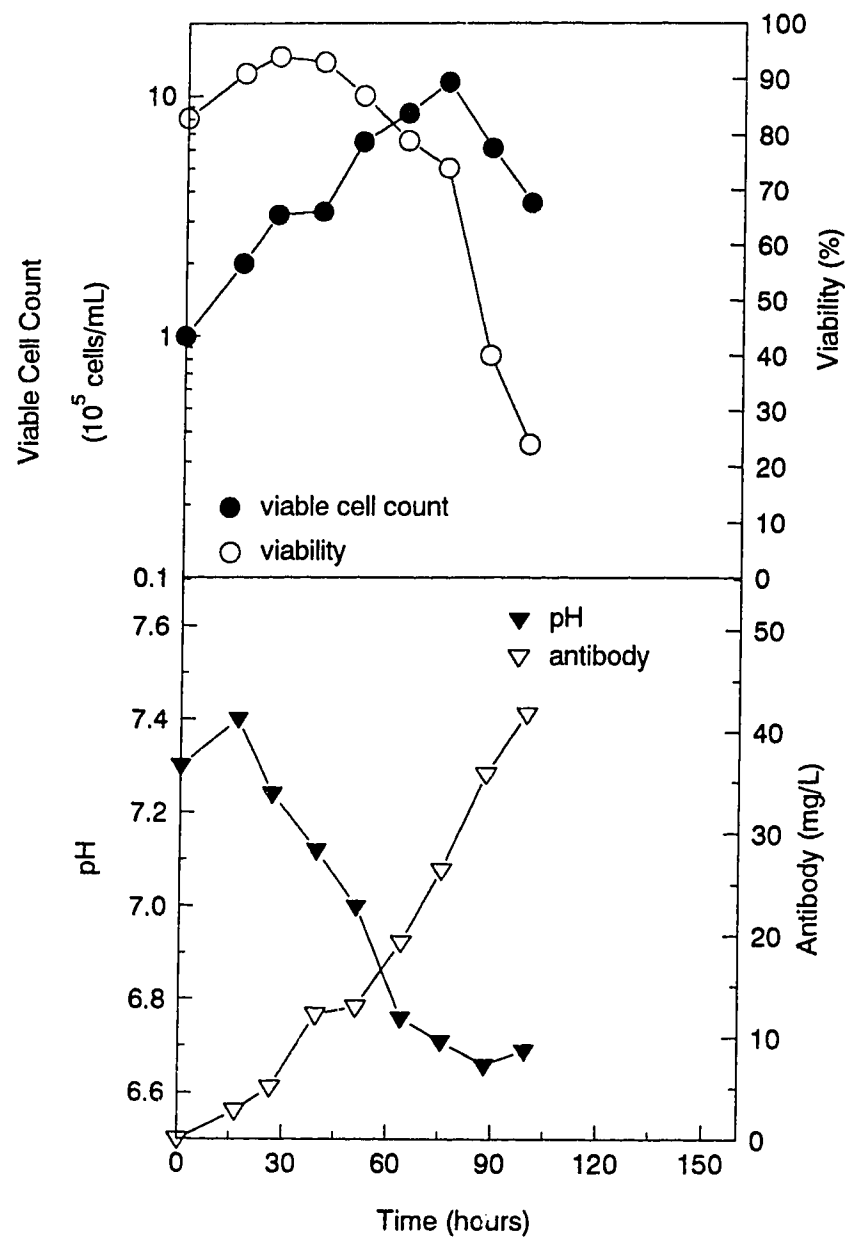


Figure D-10. Cell growth and antibody production in bioreactor experiment #3.

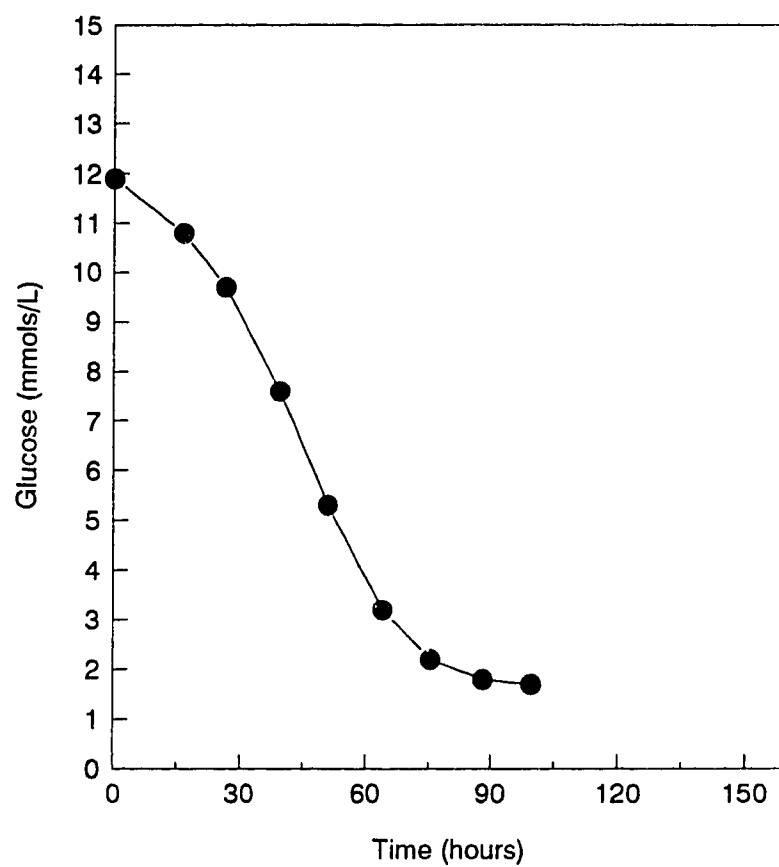


Figure D-11. Glucose consumption in bioreactor experiment #3.

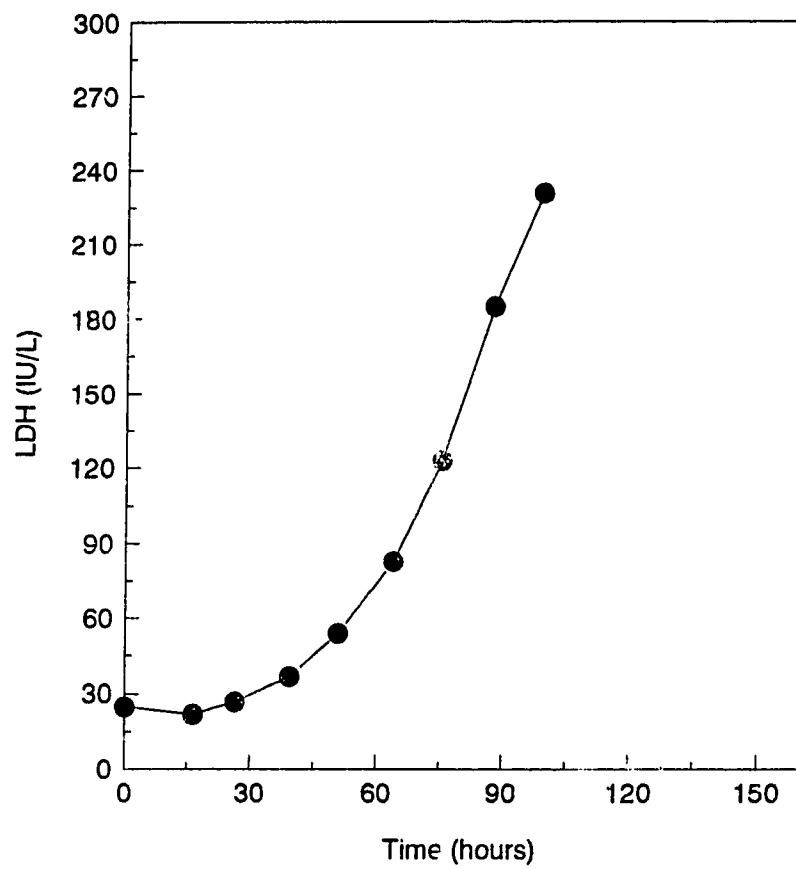


Figure D-12. LDH release in bioreactor experiment #3.

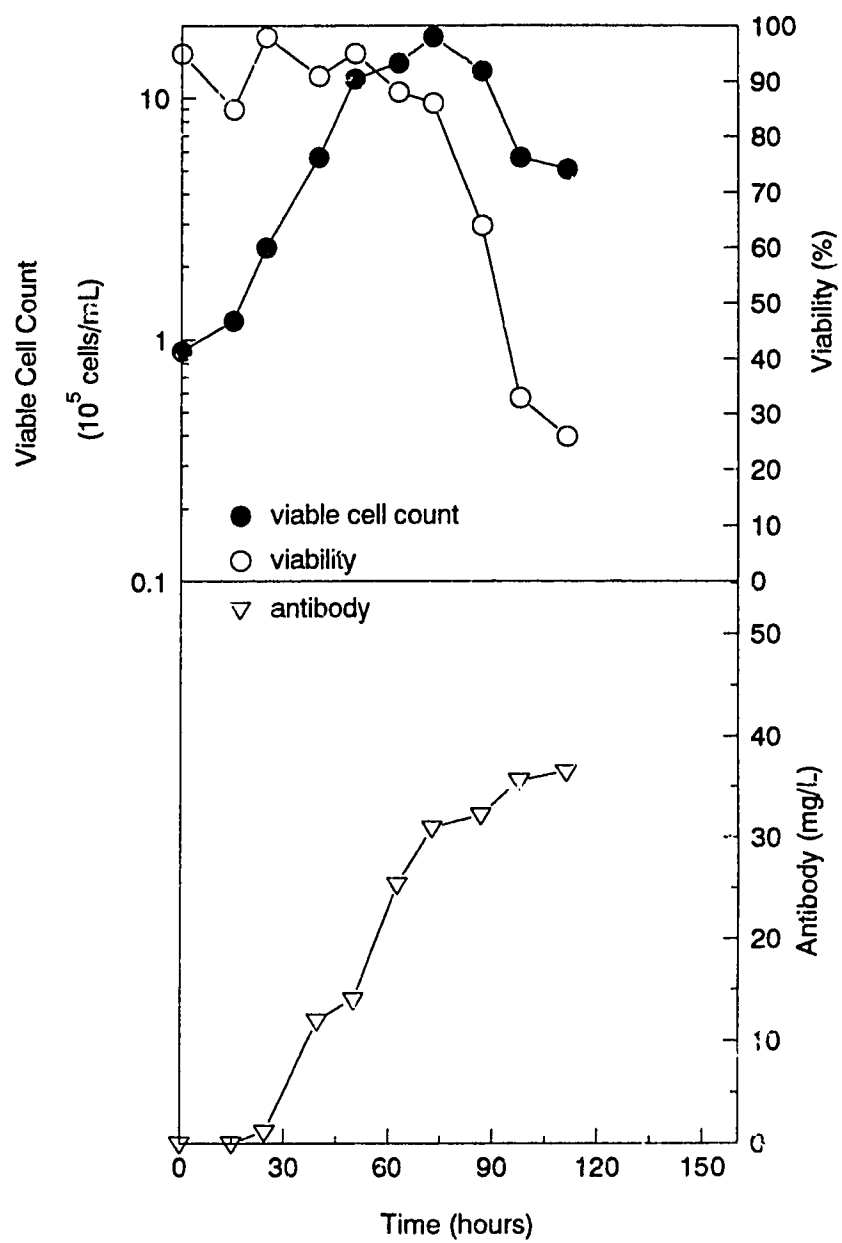


Figure D-13. Dish control for bioreactor experiment #4.

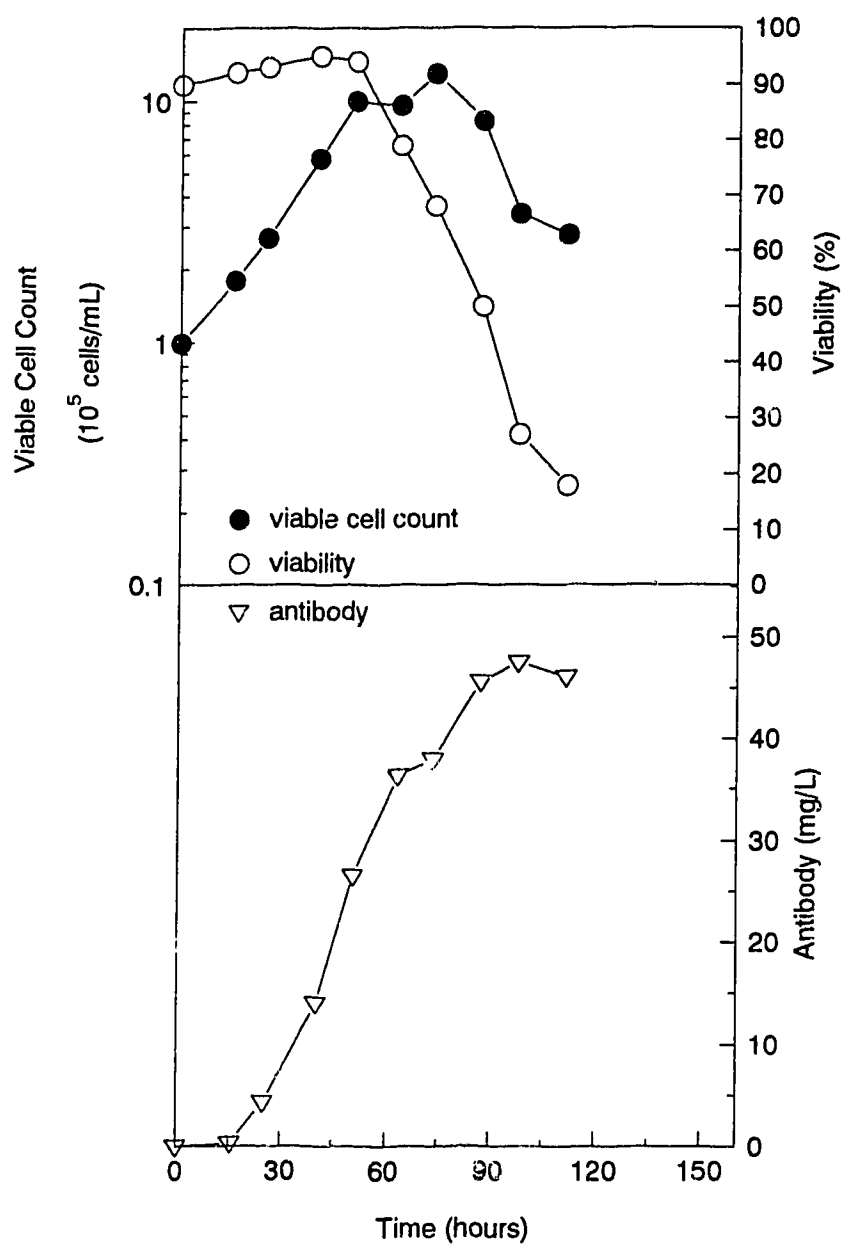


Figure D-14. Spinner control for bioreactor experiment #4.

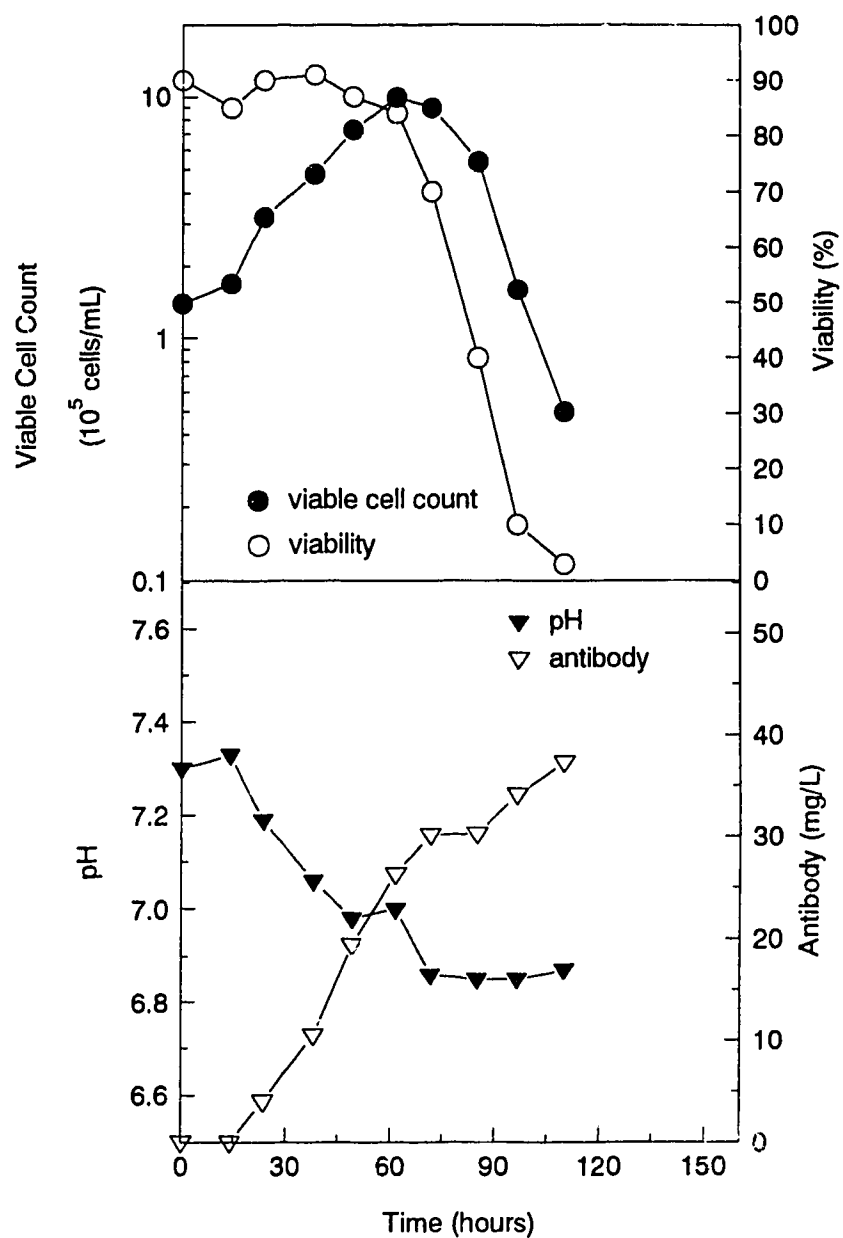


Figure D-15. Cell growth and antibody production in bioreactor experiment #4.

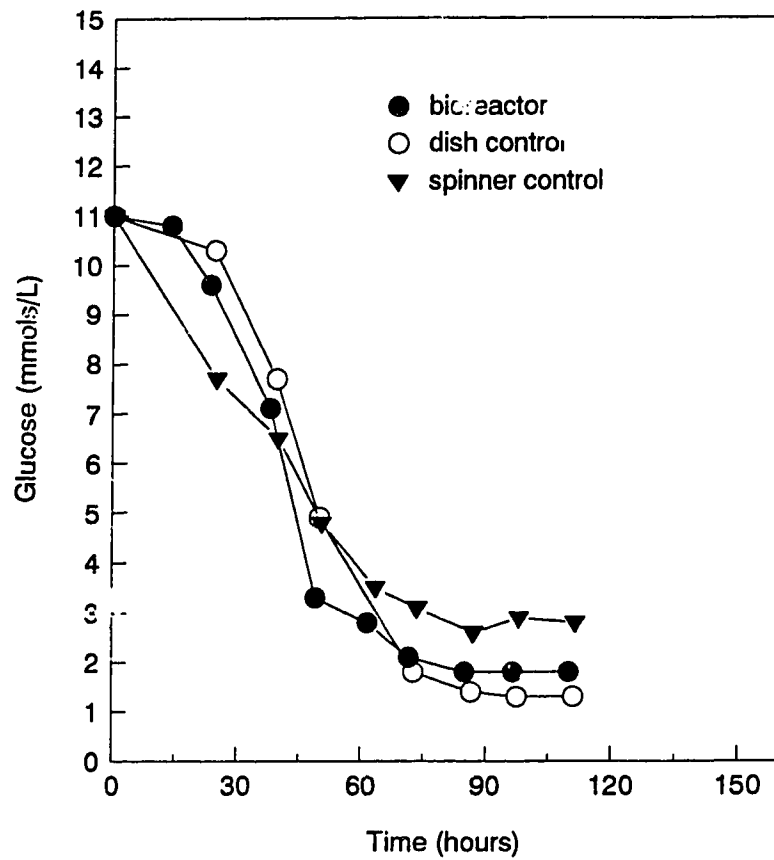


Figure D-16. Glucose consumption in bioreactor experiment #4.

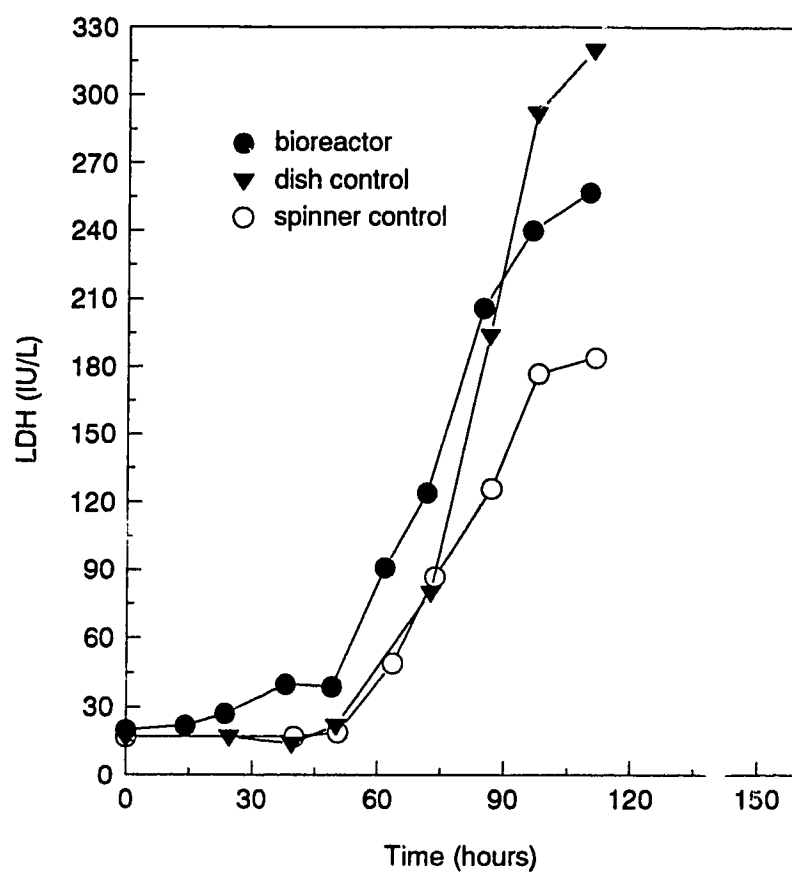


Figure D-17. LDH release in bioreactor experiment #4.